Polymer vs. Surfactant

competitive adsorption at the solid-liquid interface

Promotoren:

prof. dr. M. A. Cohen Stuart
hoogleraar fysische chemie met bijzondere aandacht voor de kolloïdkunde
Wageningen Universiteit

prof. dr. ir. F. A. M. Leermakers
persoonlijk hoogleraar bij de leerstoelgroep Fysische chemie en kolloïdkunde
Wageningen Universiteit

Promotiecommissie:

dr. E. M. Blokhuis	Universiteit Leiden
prof. dr. J. H. van Esch	TU Delft
dr. H. J. W. van den Haak	Akzo Nobel, Sassenheim
prof. dr. W. H. van Riemsdijk	Wageningen Universiteit

Dit onderzoek is uitgevoerd binnen de onderzoeksschool Vlag

Polymer vs. Surfactant

competitive adsorption at the solid-liquid interface

B. R. Postmus

Proefschrift
ter verkrijging van de graad van doctor
op gezag van de rector magnificus
van Wageningen Universiteit,
prof. dr. M. J. Kropff,
in het openbaar te verdedigen
op dinsdag 10 juni 2008
des namiddags te vier uur in de Aula.

Postmus, B. R.
Polymer vs. Surfactant: competitive adsorption at the solid-liquid interface
Ph.D. Thesis, Wageningen University, The Netherlands, 2008

ISBN: 978-90-8504-928-9

Voor mijn ouders
Voor Mariska

Voorwoord

Het boekje dat u nu aan het lezen bent, is het resultaat van 4 jaar en 9 dagen werk van een fysicus in een chemisch lab. Het is wonderlijk, hoe je van technische natuurkunde, via biomedische technologie en milieukunde bij de vakgroep fysische chemie en kolloïdkunde terecht kan komen zonder een grote overstap te maken. Een buitenstaander zou hier zomaar een random walk in kunnen zien (of misschien wel chaos). Echter, 'insiders' weten dat het wetenschappelijke wereldje klein is, en dat er vele raakvlakken en overeenkomsten zijn tussen de verschillende disciplines.
Als u al stiekem een stukje van het proefschrift heeft gelezen, dan heeft u wellicht opgemerkt dat het werk voornamelijk in de eerste persoon meervoud (wij-form) is geschreven. De reden hiervoor is simpel: ondanks dat er maar één naam op de kaft van dit boekje staat, hebben vele mensen een bijdrage geleverd. Een paar van deze vrienden wil ik graag noemen.
Zonder twijfel is Frans diegene van wie ik het meeste geleerd heb tijdens mijn promotietijd. Frans, niet alleen heb ik kunnen profiteren van jouw kennis op het gebied van van surfactants, polymeren en modelleren, maar ook bij het helder opschrijven van de resultaten en het juist verwoorden van de conclusies heb jij een enorme bijdrage geleverd. Ondanks dat je vaak geketend was door andere verplichtingen, wist je steeds weer tijd vrij te maken als ik weer eens in de knoop zat. Zonder jouw bevlogenheid en stortvloed aan ideeën was dit boekje zeker een stuk dunner geweest. Verder heeft Martien een grote invloed gehad. Martien, niet alleen heb je het project bedacht en het voorstel geschreven, maar ook je frisse kijk op de resultaten was zeer waardevol. Verder ben je de eerste die echt enthousiast werd over mijn experimentele resultaten met mengsels (Figuur 3.5a). Dit moment is cruciaal geweest en heeft de richting van mijn proefschrift in grote mate bepaald. Bedankt promotoren voor jullie geweldige inzet voor mijn onderzoek.
Wetenschappelijk onderzoek kent pieken en dalen. Soms, als een resultaat tegenvalt of een berekening niet het gewenste antwoord oplevert, kan een motiverend gesprek met een begeleider, waar de technische of wetenschappelijke details nog eens stevig doorgenomen worden, soelaas bieden. Soms, echter, is een persoonlijk gesprek belangrijker. Anita, ik wil je graag bedanken voor je begrip en je hulp met alles wat niet direct met wetenschap te maken heeft.
Nagenoeg alle experimenten beschreven in dit proefschrift zijn gedaan met een reflectometer. Remco, bedankt dat je ervoor gezorgd hebt dat mijn reflectometer altijd goed werkte. Verder is bij het interpreteren van de reflectometer resultaten en bij het doen van de SCF berekeningen veelvuldig gebruik gemaakt van de software "Professor Huijgens" en "Houston" van het illustere bedrijf Dullware. Mijn dank gaat dan ook uit naar de CEO en

hoofdprogrammeur van dit bedrijf (bedankt Peter!).
I have had the privilege to receive Philip Karlsson as a guest in our lab in Wageningen. Thanks Phil, for a stimulating collaboration that has resulted in a very good article with surprising dissolution results.
De sfeer by Fysko was (bijna) altijd erg goed. De koffiepauzes waren altijd veel te gezellig en duurden veel te lang. Ook de borrels en uitjes waren steeds weer buitengewoon leuk. Marijn en Saskia, ik vond het leuk om met jullie een kamer te delen. Ik heb alleen maar goede herinneringen aan de Student Conference, welke ik samen met Henk en Wout mocht organiseren. Al het voorbereidende werk ging plezierig en in harmonie, de conferentie was een groot succes, en het natafelen in "het Koetshuis" was heerlijk. Ook koester ik bijzonder leuke herinneringen aan de "zoek de puma" fietstocht, die ik samen met Bas, Wiebe en Henk georganiseerd heb. Verder wil ik graag Guido, Pascal, Ilja, Diane, Josie en Jerry (gaan we nog een keer met de brommer de dijk op?) bedanken voor de leuke gesprekken en de vriendschap.
Sander en Arjan, ik ben ontzettend blij dat jullie als paranimfen mij terzijde willen staan tijdens mijn promotie.
Tenslotte, diegenen aan wie dit boekje is opgedragen. Bertus en Geertje, pa en ma, bedankt voor al jullie steun door de jaren heen. En Mariska, bedankt voor alles. Ik hoop dat wij nog vele korte en lange reizen met de fiets, motor, auto of met het vliegtuig mogen maken.

- Bart

Contents

Chapter 1

Introduction

Waterborne mixtures play a prominent role in modern technologies. Key examples include foods, paints, cosmetics, herbicides, drug delivery, medical imaging, etcetera.[1,2] Typically, these systems contain - besides water - a multitude of different components, such as polymers, surfactants, proteins, and also small ions such as salts. The reasons for adding these components to technological products are diverse. For example, in a chocolate mousse proteins are used to strengthen the small air bubbles in the product,[3,4] paints contain polymers to obtain a proper viscosity so that the paint will not drip from the wall after application,[5] cosmetics contain surfactants to facilitate the mixing of the watery and oily components,[6] herbicide formulations contain surfactants to ensure that the product covers the whole leaf after application,[7] and in the biomedical setting surfactants are used as vehicles to deliver drugs or contrast agents.[2,8] However, when a solution contains different components, these components may influence each others' behaviour. It is possible that component A can only fulfill its technological role in the presence of component B, or the other way around, that component A cannot fulfill its role because it is hindered by component B.

An example of a complex water based mixture is a modern paint. In such a paint, large numbers of pigment particles are present to give colour to the resulting film. Polymers are added to give the solution a high viscosity. Surfactants are present to stabilise the particles and to provide the property that the paint wets the surface. All compounds should work together in concert. Problems may arise when e.g. the polymer adsorbs preferentially on the pigment particles such that the particles aggregate in clusters. This loss in "stability" leads to loss in colour appearance and inferior adhesion properties of the dried film (blisters).

It is clear that it is necessary to better understand the behaviour of

mixtures, so that we learn how to tune their properties to meet our increasing demands. This may lead, in the long term, to product innovations such as better paints, more environmentally friendly herbicides, etcetera.

In science, solutions containing multiple components that show intricate behaviour are often called complex mixtures. The body of literature on the adsorption from complex mixtures is currently growing rapidly.[9–14] My thesis deals with the bulk behaviour and the adsorption properties of an aqueous mixture containing the nonionic polymer "poly (ethylene oxide)" or PEO and the nonionic surfactant "alkyl poly (ethylene oxide)" or C_nE_m. PEO is a flexible homopolymer (vide infra) which consists entirely of EO groups (we neglect the end groups here). Figure 1.1 gives the skeletal formula of a PEO chain of length N and an artistic impression of a small section of chain in solution. The length N of the polymers used varies from 100 to 4000, which corresponds roughly to a molecular mass of 4 to 170 kg/mol. Figure 1.1 also shows an impression of a C_nE_m surfactant. The C_n part of this surfactant is an alkyl section consisting of n CH_2 groups, and the E_m part is similar to (a short section of) PEO. For the research described in this thesis, we typically used surfactants that have $10 < n < 18$ and $3 < m < 9$.

For studying the adsorption behaviour of these molecules, we have used a silica surface. Silica is a technologically relevant surface,[5,15] and it is easy to use in an experimental setting due to its reflectivity (in the case of a silicon/silica wafer) and its availability. To study the behaviour of this system, we have used an experimental technique called reflectometry and a theoretical self-consistent field model.[16,17] Furthermore, we have paid extra attention to the effect of the ionic strength and the pH.

In the remainder of this introduction, I will first go into somewhat more detail about polymers, surfactants and their mixtures. Also, at the end of this section, I will give an outline for the rest of this thesis.

1.1 Polymers

Polymers are long, chain-like molecules. The word polymer comes from the Greek language, and means many parts. Hence, a polymer is a long string consisting of many equal parts or monomers. One can safely say that polymers are everywhere. Almost all technological products contain polymers, which can either be plastics such as computer monitors or car tires, but also many liquid products contain polymers. Not all polymers are synthetic, or man-made. There are many biological molecules, such as DNA, RNA, and collagen, that fit well within the definition of a polymer. Hence, whether we are working in our office or taking a relaxing walk in a beautiful forest,

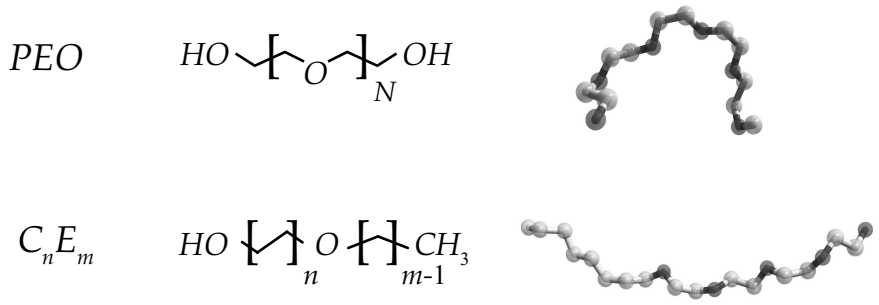

Figure 1.1: *The chemical and skeletal formula (left and middle respectively) and an artistic impression (right) of the most important chemicals used for the research described in this thesis, e.g. PEO and C_nE_m. The CH_2 groups (and also the CH_3 groups) are are drawn as white spheres and the oxygen groups are depicted as dark spheres.*

polymers are really all around us.

A polymer that is entirely made from one type of monomer is called a homopolymer.[18] It is also possible that a polymer consists of multiple types of monomers. In this case the polymer is called a copolymer, and depending on the distribution of the monomers, there are alternating copolymers, block copolymers, random copolymers, etcetera. Sometimes (some of) the monomers have a charge. These molecules are referred to as polyelectrolytes.

Similar to the case of small molecules, polymers may or may not dissolve in a solvent. In this thesis, the solvent is always water. In the case that a polymer can dissolve in such an aqueous environment, we call the polymer hydrophilic, or water loving. If a polymer does not like to be in an aqueous environment, we call it hydrophobic, or water hating. Alternatively, we may say that when a polymer dissolves well, the solvent is good. If we then change the system a bit, the solvent conditions may change. An example is the case of PEO dissolved in water at room temperature.[19] Adding some salt, or increasing the temperature, will cause the interactions between the PEO and the water to become less favourable. In this case, we say that the solvent quality deteriorates. When, at a certain temperature or salt concentration, the polymer starts to phase separate, we call the solvent a poor solvent.

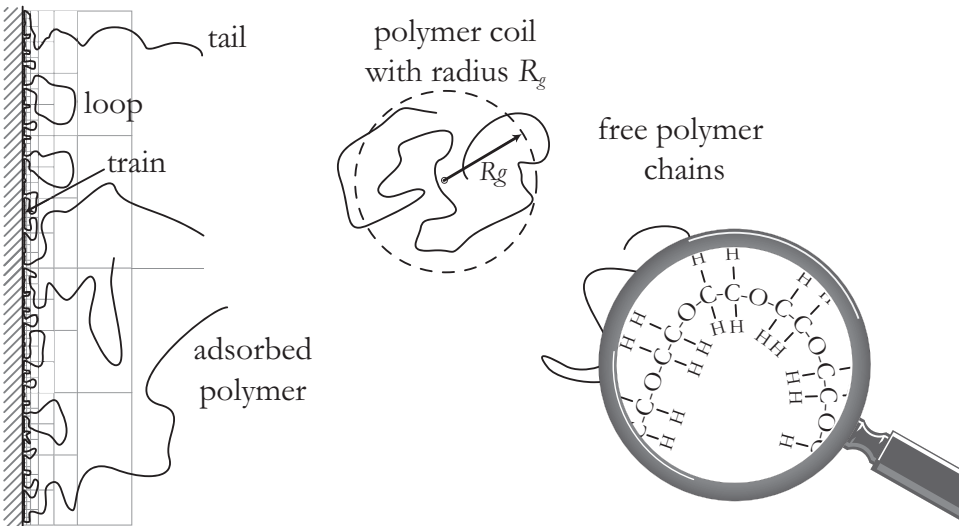

Figure 1.2: *Impression of a polymer adsorbed onto a surface (left) and a polymer coil in a good solvent (right). The grid on the surface is a so-called self similar grid, which can be used to illustrate the scaling of the central part of a polymer layer (see text for details).*[20] *A polymer coil in solution is a dynamic object. Averaged over time, the coil will have a spherical shape, where its radius R_g is the characteristic length.*

1.1.1 Polymers in bulk

In the case of a polymer in an aqueous environment, the polymer concentration is an important parameter. Based on this, we can define three regimes:[20,21] (i) the dilute regime where the polymer chains are far apart and isolated from each other. In this case, the average polymer shape will be a sphere with radius R_g. This radius is called the radius of gyration and it is the characteristic length scale here. (ii) Above the so-called overlap concentration, the semidilute regime is found, where the polymer chains start to overlap and interpenetrate. In this regime, the characteristic length scale is the spacing between the overlaps in the chains also called the mesh size, ξ. The mesh size is a function of only the polymer concentration, c_{pol}, and these two properties are, in good solvents, related through a scaling law: $\xi \propto c^{-3/4}$. (iii) The concentrated regime where all the excluded volume effects are screened and the chains have a random coil size, i.e. $R_g \propto \sqrt{M_{\mathrm{w}}}$ where M_{w} is the molecular mass.

Even though the scope of the research described here is the adsorption from dilute solutions, we should keep in mind that in the adsorbed layer the local polymer concentration will often be in the semidilute or concentrated region (see the left side of Figure 1.2). Moreover, polymers in poor solvent

conditions can and will phase separate into a polymer-rich phase, and a phase rich in solvent even if the overall polymer concentration is relatively low.

1.1.2 Polymer adsorption

If a polymer solution is in contact with a solid surface, then the polymers may or may not adsorb and the concentration of polymers near the surface will respectively be higher or lower compared to the bulk.[17,20,21] When a polymer chain adsorbs, it looses some conformational and some translational entropy. Because a large chain has little translational entropy, the loss in conformational entropy is most important. This entropy loss is easily estimated in a lattice model. Taking an isotropically interacting segment on a simple cubic lattice in the bulk, that is, the part of the system far from the surface, there are six different directions for bonds between two segments. However, in the immediate vicinity of an impermeable surface, there are only five possible bond directions. Hence, the entropy loss per adsorbed segment (or, more precisely, per bond lying in the surface plane) is $\Delta S = k_B \ln(5/6) \approx -0.18 k_B$, where k_B is the Boltzmann constant.

For a polymer chain to adsorb, it needs a gain in adsorption energy that exceeds (overcompensates for) this loss in conformational entropy. This energy gain should arise from removing a solvent molecule from the surface and replacing it by a polymer segment. In effect, this means that a polymer chain adsorbs only if the change in energy per adsorbed segment obeys $\Delta E_{\text{ads}} < -\chi_s^{cr} \approx -0.18 k_B T$, where χ_s^{cr} is the critical interaction energy between a polymer segment and the surface (Here we have ignored the fact that there is one more segment in the chain than the number of bonds). Upon the variation of the adsorption energy, one thus can witness an adsorption transition, below which the polymer does not adsorb, and above which the polymer does adsorb. We note that some interactions (e.g. hydrogen bonds) have a distinct orientational character, so that the adsorption process also involves changes in orientational entropy. Therefore, the adsorption strength of a segment is characterised by a free energy. For long chains, this adsorption transition displays high intrachain cooperativity (i.e., different monomers in one chain help each other to adsorb) but it remains a smooth second-order transition. This means that no hysteresis is expected in the transition region. For the case of PEO adsorption onto silica, i.e. the system studied in this thesis, it is known that an adsorption/desorption transition can be induced upon changing the pH. This transition is examined in detail in Chapter 5.

A layer of physisorbed polymer molecules can be seen as a collection of trains, tails and loops.[17] A train is a sequence of monomers that are all in close contact with the surface, loops are strings of polymer segments not

bound to the surface, but restricted on both sides by at least one bound segment and tails are free chain ends (see also Figure 1.2). Another way to describe an adsorbed polymer layer is in terms of the polymer density profile $\varphi(z)$, i.e. the volume fraction of segments as a function of distance z from the surface.[21] In this profile there are three zones: i) a proximal zone close to the surface, where the volume fraction of polymer is close to the concentrated regime (trains). This part should be highly dependent on the chemistry of the chain, that is, the exact density near the surface may depend on the adsorption mechanism, number of adsorption sites, etcetera. ii) A central region with loops and tails, where volume fractions of polymer have semi-dilute values. De Gennes showed that as the distance from the surface increases, the volume fraction drops as a power law with an exponent that depends on the solvent quality. iii) A distal region where the volume fraction decreases exponentially with the distance (tails).

One can integrate the (excess) volume fraction profiles and obtain the adsorbed amount. Relevant for experimental situations is an adsorption isotherm. In such an isotherm, the adsorbed amount is given as a function of the polymer concentration in the bulk. Typically high affinity isotherms must be expected, meaning that the polymer starts adsorbing from very dilute solutions and that the plateau in the isotherm is found for any experimentally measurable bulk concentration. In good solvent conditions and for strong adsorption, we find that the plateau value of the isotherm is a very weak function of the chain length and essentially remains limited to order one equivalent monolayer. For theta conditions however, the adsorbed amount grows logarithmically with the chain length. In the case of a poor solvent, the adsorbed amount may grow to arbitrary large values if the bulk concentration is increased towards the bulk binodal (provided that the polymer rich phase accumulates near the surface and not in the bulk).

1.2 Surfactants

Surfactants or amphiphiles are relatively small molecules that combine a hydrophillic and a hydrophobic moiety in one molecule. It is general practice to refer to the hydrophilic moiety as the head, and to the hydrophobic moiety as the tail. The name surfactant comes from the term **surf**ace **act**ive **a**ge**nt**, which immediately refers to the distinctive property that a surfactant molecule has an affinity to virtually all types of surfaces. For instance, on an air-water interface, a surfactant will adsorb with its hydrophobic moiety such that the contact area between the hydrophobic segments and the water will decrease.[22] On a hydrophilic surface, such as silica, it will adsorb using

its head groups which triggers the adsorption of a secondary layer to from a bilayer.[23] This type of behaviour will be described further below in section 1.2.2.

Surfactants can be classified based on their head group charge. There are nonionics, anionics, cationics, and zwitterionics. Nonionics are surfactants that do not carry any charged groups. Anionic surfactants have a negatively charged head group, and cationics have a positively charged head group[a]. Zwitterionic surfactants have a head group with two oppositely charged groups. These groups usually have a charge depending on the solution pH, and hence, the charge on the surfactant can be controlled by choosing the proper pH. It is also possible to have surfactants with more than one head or tail group. For example, there is a class of surfactants called gemini surfactants that have two tail groups and two head groups, which are connected by a short spacer.

Although, most paragraphs of this introduction are valid for any type of surfactants, the larger part of this thesis only covers nonionic surfactants. The advantage of using this type of surfactant is that it is easy to change the surfactant architecture by changing the head group size or the tail group size. Furthermore, this type of surfactant is often used in technology because it is relatively insensitive to surface charge and salt concentration. However, even nonionics are responsive to charged surfaces and the salt concentration. This effect, which is often overlooked, is described in detail in Chapter 6.

1.2.1 Surfactants in bulk

In bulk solution, surfactants form aggregates above a certain threshold concentration. These aggregates, first mentioned by McBain in 1913,[24] are commonly called micelles and the concentration where they start to form is denoted as the **c**ritical **m**icelle **c**oncentration or CMC. Individual surfactant molecules – i.e. molecules not part of a micelle – are referred to as surfactant monomers or unimers. In this thesis, I will reserve the word monomer for one unit of a polymer molecule, and refer to individual surfactant molecules as unimers. The number of unimers in a micelle is called the aggregation number, g, and, for nonionics in an aqueous solution, g is typically of order 100.[25]

At low concentrations, the unimers have a translational entropy that is large enough to compensate for the unfavourable interactions between the tail groups and the solvent. However, as the concentration of unimers increases,

[a]The nomenclature for anionic and cationic surfactants is a bit confusing because the names are derived from oppositely charged electrodes. Anionics are attracted by an (positively charged) anode and cationics are attracted by a (negatively charged) cathode.

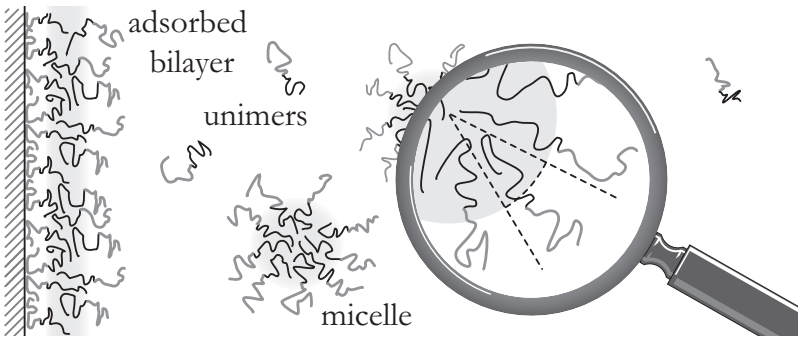

Figure 1.3: *Artistic impression of surfactants adsorbed onto a hydrophillic surface (left) and in solution (right). The magnifying glass inset gives an idea about the core and corona of the micelle, and the dashed triangle (2D pyramid) gives the average unimer shape in a micelle. Surfactant head groups are represented by gray lines, and the tail groups by black lines. Hydrophobic areas have a gray background colour.*

the translational entropy per unimer decreases, and at some concentration it will become favourable to form micelles. When a micelle is formed, its core consists almost entirely of hydrophobic tail groups, whereas the micellar corona consist of hydrophillic head groups mixed with solvent molecules (see Figure 1.3).

So, the driving force for the formation of a micelle comes from the tail group, that prefers the interior of the micelle above the water. The reason that the tail groups do not aggregate to form a separate phase, is that there is also a stopping mechanism on the growth of a micelle. This stopping mechanism is the accommodation of the head groups. For a spherical micelle, the volume of the core V_{core} can be approximated by $V_{\text{core}} = 4/3\pi r_{\text{core}}^3 = g \times n_{\text{tail}} \times V_{\text{segment}}$, where r_{core} is the core radius, n_{tail} is the number of segments in the tail and V_{segment} is the volume of a single segment. Thus, the volume of the core increases linearly with g, i.e. $V_{\text{core}} \sim g^1$, and $r_{\text{core}} \sim g^{1/3}$. However, the surface of the core, a_{core}, grows faster, i.e. $a_{\text{core}} = 3\pi r_{\text{core}}^2 \sim g^{2/3}$. When g is low, the head groups are too small to shield all tail groups from the surrounding water. As g increases, the shielding of the micellar core will improve. That is, until the head groups cover the entire surface of the micellar core. If we add another unimer to this micelle, the head groups will have to make room (i.e. a_{head} decreases), and this is entropically unfavourable. Hence, at this point, the head groups are stopping the growth of this micelle, and it will be more favourable to form a new micelle.

The **c**ritical **p**acking **p**arameter or CPP defined by Israelachvili in 1976 combines V_{tail}, L_{tail} and a_{head} into one convenient parameter.[26,27] This pa-

CPP	preferred aggregate	unimer shape
< 0.33	spherical or ellipsoidal micelles	pyramid or cone
$0.33 - 0.5$	rod-like micelles	pyramid-like
$0.5 - 1$	vesicles	pyramid to cylinder
1	planar bilayer	cylinder
> 1	inverted micelles	topped off cone

Table 1.1: *The critical packing parameter for a number of micellar shapes and an approximation of their corresponding unimer shape.*

rameter is defined as:

$$CPP = \frac{V_{\text{tail}}}{a_{\text{head}} L_{\text{tail}}} \tag{1.1}$$

Based upon the CPP, which roughly describes the shape of a surfactant unimer, one can get an idea about the shape of the aggregate that the unimer preferably forms. For instance, in the case of the spherical micelle in Figure 1.3, all the unimers resemble a cone with a square base, also called a pyramid[b]. The base of this pyramid is equal to the head group area at the core surface, and the apex is in the center of the micelle. The volume of this cone is described by $V_{\text{tail}} = 1/3 \times L_{\text{tail}} \times b_{\text{head}}^2$, where b_{head} describes one side of the square base of the cone. The head group area is represented as the base area and can be calculated using $a_{\text{head}} \approx b_{\text{head}}^2$. Now we can calculate the $CCP = 1/3 \times L_{\text{tail}}/L_{\text{tail}} \times b_{\text{head}}^2/b_{\text{head}}^2 = 1/3$ for a spherical micelle. Other aggregate shapes and their corresponding CPP are listed in table 1.1.

One might intuitively expect that when an unimer is part of a micelle, and its head group is pointing towards the solution, the tail group will be pointing towards the center of the micelle, with its last segment positioned right in the micellar center. This is also the idea that most artist impressions of micelles transfer. However, at least for spherical micelles, there is very little space in the center of a micelle. Hence, there can only be a few tail segments in the center, and the remainder of the segments need to find space more to the edge of the core ($V_{\text{sphere}} \sim r^3$). It has been shown by self-consistent field theory on a spherical lattice (vide infra) that the distributions of all tail segments are approximately equal.[28] Also, for the case of nonionic surfactants that lack a strong repulsion between the head and tail groups, the separation between the core and the corona is rather diffuse.

The micellar model described above, where micelles of a fixed size only occur above the CMC, and the unimer concentration is always smaller than

[b]Of course, the base of this shape is actually a polygon on a curved surface. However, we approximate this complicated shape by an easy-to-handle square. Alternatively, one can also use a cone with a round base.

or equal to the CMC, adequately describes most experiments. However, it has some simplifications that are flawed from a physical point of view. A more sophisticated model would describe the micelles in equilibrium with the unimers. One could assign a chemical potential to a micelle consisting of g surfactants which has to be in equilibrium with the unimer chemical potential and micelles of other sizes. If we - just to keep things simple - assume that all micelles are of size g, the equilibrium can be expressed by the reaction

$$gX_1 \rightleftarrows X_g \tag{1.2}$$

and, according to the mass-action law, the equilibrium constant should obey

$$K_g = \frac{[X_g]}{[X_1]^g} \tag{1.3}$$

In this model we can calculate that for micelles of size $g = 100$, a three-fold increase in micelle concentration, leads to just a 1% increase in unimer concentration. Hence, above the CMC the unimer concentration, and also the chemical potential, is hardly a function of the total amount of surfactant anymore. This argument can be extended to a distribution of micelles by applying the mass-action law for all micellar sizes. This leads to a large set of coupled equations, that also include how the (average) aggregation number changes as the unimer concentration changes. Of course, you need a large set of K_g values for this. These parameters are not easily available and the analytical theory has its problems. One possible solution is to turn on the computer, and solve the large set of equations with numerical techniques.

1.2.2 Surfactant adsorption

Surfactants have special surface properties, i.e. they adsorb onto interfaces and they can modify the interfacial properties. As told above, a polymer typically only adsorbs onto a surface if it has some favourable interaction with the surface. Interestingly, the surfactant has two groups that behave differently – i.e. a head group and a tail group – that it can use to adsorb. Hence, surfactants can adsorb onto all kinds of hydrophobic and hydrophilic interfaces, such as liquid-air, liquid-liquid, or solid-liquid.

Figure 1.4 gives an artistic impression of the different structures that a surfactant can form on a surface. The surfactant unimers are represented as lines consisting of two colours. The dark section represents the tail group, and the grayish section represents the head group. In the case of a hydrophilic surface, the surfactants will adsorb with their head groups. Since it is energetically unfavourable for the tails of the adsorbed surfactant molecules to

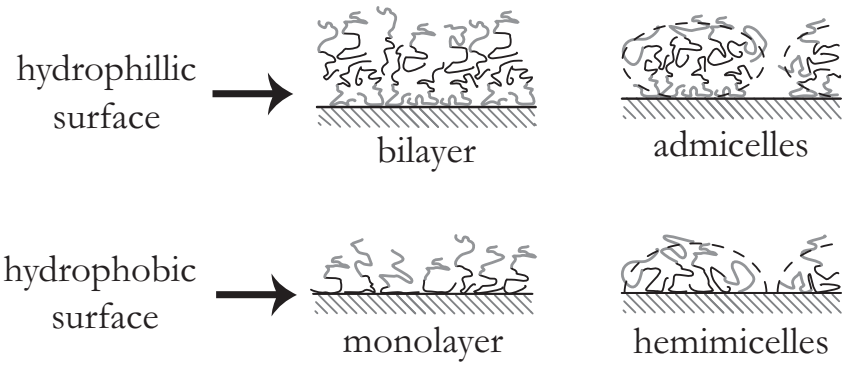

Figure 1.4: *Artistic impression of an adsorbed surfactant layer. The surfactants are represented as line segments, where the gray sections represent the head groups, and the black sections the tails. On a hydrophillic surface, the surfactants adsorb with their heads to form either a bilayer, or some sort of fragmented structure (which is depicted here as an admicelle). In the case of a hydrophobic surface, the surfactants adsorb with their tails, to form a full monolayer, or a fragmented structure (such as a hemimicelle).*

be surrounded by water, another surfactant layer will adsorb onto the layer of tails, and therefore, a bilayer will be formed. In the case of a hydrophobic surface, surfactants will adsorb with their tails, and hence, a monolayer where the tails are pointing towards the surface and the head are pointing toward the solution will be formed. Similar to the formation of aggregates in the bulk, the adsorbed unimers also have a preferred aggregate shape on the surface. Hence, some unimers, for instance those that have $CPP = 0.33$, might prefer a curved surface structure instead of a flat layer. In Figure 1.4 we have plotted an admicelle and a hemimicelle to illustrate this behaviour.

Surfactant adsorption is, just like the case of polymer adsorption, often described by an adsorption isotherm. This is a graph where the adsorbed amount is plotted versus the bulk concentration. In the case of nonionic surfactants that adsorb onto a silica surface, the adsorbed amount is typically very low at low bulk concentrations.[29–32] At some bulk concentration the adsorbed amount increases rapidly until it reaches a plateau value that corresponds to a saturated surface (for an example isotherm see Figure 3.4). The concentration where the adsorbed layer goes from almost non-existing to almost completely developed is called the **c**ritical **s**urface **a**ggregation **c**oncentration, or $CSAC$.[32] There is evidence that, in the case of an equilibrium adsorbed layer, some surfactants only cover about 70% of the surface and that 30% of the surface is still in direct contact with the solvent.[33,34]

1.3 Mixtures

As mentioned above, this thesis deals with the adsorption of polymers and surfactants from complex mixtures, i.e. solutions that contain at least one type of polymer and one type of surfactant. Adsorption in such systems will be strongly affected by the interactions between the components, both in solution and at the surface. In some mixtures, not all components adsorb onto the surface from individual solution. In this case, the surface is called a selective surface.

Polymer/surfactant mixtures can display a wide variety of behaviours. In the bulk solution, it is possible that polymers and surfactants form mixed aggregates. This effect has been studied quite extensively. Typically, both polymer molecules and surfactant unimers exist as free solution species at low surfactant concentrations. If the surfactant concentration is increased, there will be a point where the surfactants will start to aggregate on the polymer. The polymer acts as a nucleation core for the surfactant unimers. That concentration where the first aggregates start to form is denoted as the **c**ritical **a**ggregation **c**oncentration, or CAC. When the surfactant concentration is increased further, more aggregates on the polymer will form, and the unimer concentration will essentially be constant. Typically, the surfactants will form spherical micelles at fixed distances around a polymer chain. These types of structures are referred to as strings of pearls. At some surfactant concentration, c_{sat}, the polymer will be saturated. This is very dependant on the total amount of polymer, i.e. its concentration, but also on its length when the concentration is expressed in moles/L. As the surfactant concentration is increased even further above c_{sat}, the concentration of polymer/surfactant aggregates will be fixed and the concentration of unimers will increase until it reaches the CMC. From here, normal micelles will be formed and the unimer concentration will again be fixed.

By considering the interaction between the species (a bulk property) and the adsorption behaviour from individual solutions (a surface property), a schematic overview of different scenarios in mixed polymer/surfactant adsorption studies can be given.[35,36] This overview gives four cases:

Type I	mixed bulk aggregates & selective surface
Type II	mixed bulk aggregates & non-selective surface
Type III	no mixed bulk aggregates & selective surface
Type IV	no mixed bulk aggregates & non-selective surface

Typically, a type I system is a charged system, where the component that is oppositely charged to the charged (and hydrophilic) surface does not adsorb. In the case that the polymer and the surfactant have an opposite charge,

the bulk aggregation is electrostatically driven. What component adsorbs depends on the surface charge. It is also possible to have a nonionic surfactant and a polyelectrolyte that repels the equally charged surface, or a charged surfactant that does not adsorb and a nonionic polymer. The equilibrium layer that adsorbs from a mixture depends on the relative strength of the competing effects. For instance, it is possible that an adsorbing component does not adsorb because of the nonadsorbing component. Or, in the opposite case, it is also possible to have a positive surface excess of an otherwise nonadsorbing component. This process is termed 'shuttling'.[35] For some systems, it is possible to make a non-equilibrium layer that remains off-equilibrium for at least six hours. Braem *et al.* adsorbed the pluronic $F108$ (a nonionic polymeric surfactant) onto (negatively charged) silica from either a solution containing only $F108$, and a solution containing both $F108$ and the anionic surfactant SDS. The normally nonadsorbing SDS would coadsorb with the $F108$. When the SDS was subsequently rinsed away, the remaining $F108$ layer turned out to be denser than the layer adsorbed from a $F108$ solution.

Type II systems are typically similar to type I systems, with the exception that the surface is hydrophobic (and not charged). In this type of systems, there is also a form of shuttling, i.e. the adsorbed amount of component A is higher when it is co-adsorbed with component B than when it is just adsorbed from a solution containing only component A.

Systems of the type III case are not so interesting. The different components of the mixture do not interact, and only one component adsorbs. Hence, the behaviour of the mixture will be determined by the adsorbing component and adding or removing the nonadsorbing component will not change the properties of the system.

In type IV systems the components do not form aggregates in the bulk, and both components adsorb onto the surface. Hence, there will be a competition for adsorption. Such a system can be charged, for instance the adsorption of the cationic surfactant $CTAB$ mixed with the cationic polyelectrolyte poly-L-lysine hydrobromide onto negatively charged silica.[37,38] Another type IV system is the adsorption of nonionic PEO mixed with nonionic triton surfactants onto colloidal silica.[36,39]

A particularly interesting type IV situation, is when the polymer and the surfactant interact with the substrate by way of the same adsorption mechanism. Then, bond energies are not decisive, but the layer structure, and other species specific issues become decisive factors. The focus in this work is on the nonionic surfactants C_nE_m and the corresponding nonionic polymer PEO. Both the polymer and the surfactant bind to hydrophilic silica by the formation of H-bonds, but in bulk solution the polymers and

surfactants do not form complexes.

1.4 Outline of this thesis

The scope of this thesis concerns the competitive adsorption from solutions containing both polymers and surfactants. We have chosen to restrict our research to the $PEO/C_nE_m/SiO_2$ model system. In the first part of my thesis, I describe the most important features of the reflectometer, which is the main experimental technique (chapter 2) and the results of a systematic set of experiments performed to unravel the competitive adsorption behaviour of our system (chapter 3). The second part of my thesis mainly deals with the detailed modelling of our system. In chapter 4, I describe the basics of the SCF theory and the parameter set that we have used. Subsequently, the results of this model on the PEO/SiO_2 system are evaluated in chapter 5 and in chapter 6 the use of the model on the C_nE_m/SiO_2 system is discussed. Chapters 5 and 6 also contain some experimental results, which are needed to validated the model. In chapter 7, the SCF results for the $PEO/C_nE_m/SiO_2$ system are addressed. And finally, the work described in this thesis is discussed in chapter 8.

Chapter 2

Reflectometry

Most of the experimental data described in this theses is obtained using a technique called near brewster angle reflectometry. This is an optical technique that is very similar to ellipsometry. The main advantage of ellipsometry is that it measures two physical properties, whereas a reflectometer typically measures only one property. Reflectometry, on the other hand, is simpler. Data can be recorded very rapidly, so that one can do more measurements per unit of time, making this technique more suitable for kinetic studies. Both techniques measure changes in the reflectivity of a surface. This immediately reveals a requirement for the surface that is being used: it must be reflecting. Using a model consisting of a stack of layers, it is possible to relate the change in reflection of the surface, to an increase or decrease of the surface excess.

Figure 2.1 shows a detailed drawing of our reflectometer. Basically, this apparatus consists of two independent parts. There is a hydrodynamic part, where a solution is led in a well defined manner through the stagnation point flow cell (SPF), and there is an optical part that, eventually, measures the adsorbed amount. This chapter will first describe the optical part, and then the hydrodynamics of our SPF. To conclude this chapter, there are some details of our apparatus and a few practical tips.

2.1 Optical description

Light is a form of electromagnetic radiation, which means that it is a combination of an electric and magnetic wave. Usually when we consider light, we typically do not recall that it is an electromagnetic wave, but rather notice the colour or the brightness (intensity) of the light. These two properties of

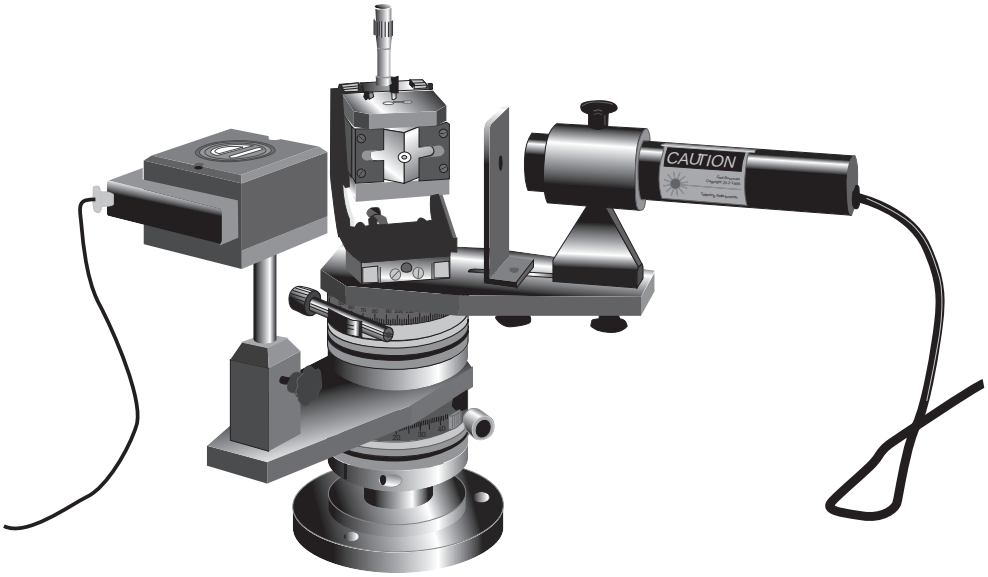

Figure 2.1: *Sketch of the reflectometer used for part of the research described in this thesis. The cylinder on the right is the laser. The beam from the laser passes through a polariser, and enters the flowcell. In the flowcell, there is a surface on which the laser beam reflects. This reflected beam is "caught" by the detector, which is the box on the left. The detector measures the change in light intensity, which can, using the theory from this chapter, be used to obtain the adsorbed amount on the reflecting surface.*

light, together with many other properties are mathematically described by a field of physics that is generally referred to as optics. The paragraph below explains how to describe the properties of light starting from the Maxwell equations. At the end of this paragraph, we want to understand the optics of our reflectometer, so the argumentation is directed towards understanding the reflection of a polymer/surfactant covered surface.

In the second half of the 19^{th} century, the Scottish mathematician and theoretical physicist James Clark Maxwell formulated a set of eight differential equations that described the relation between electric and magnetic fields. Twenty years later, Oliver Heaviside and Josiah Willard Gibbs reformulated these equations into four new equations. These four equations are now generally known as the Maxwell equations. For the case of electromagnetic waves *in vacuo*, these equations can be written as:

$$\nabla \cdot E = 0 \tag{2.1}$$

$$\nabla \times E = -\dot{B} \tag{2.2}$$

$$\nabla \cdot B = 0 \tag{2.3}$$

$$\nabla \times B = \varepsilon_0 \mu_0 \dot{E} \tag{2.4}$$

In these equations, E is the electric field, B is the magnetic flux density, ε_0 is the permittivity of free space (electric constant) and μ_0 is the permeability of free space (the degree of magnetisation). The magnetic field, H, can be calculated using $H = B/\mu_0$. We can eliminate B by taking the curl on both sides of Eqn. 2.2

$$\nabla \times (\nabla \times E) = -\nabla \times \dot{B} = -\partial/\partial t(\nabla \times B) = -\varepsilon_0 \mu_0 \ddot{E} \tag{2.5}$$

Using the mathematical identity $\nabla \times \nabla E = \nabla(\nabla \cdot E) - \nabla^2 E$ and Eqn. 2.1, we can now write

$$\nabla^2 E - \varepsilon_0 \mu_0 \ddot{E} = 0 \tag{2.6}$$

One can recognise Eqn. 2.6 as a three-dimensional wave equation, where the wave velocity $c = 1/\varepsilon_0 \mu_0$ (which is the speed of light *in vacuo*). We can also write down Eqns. 2.5 and 2.6 for B which would show that B also is a 3-dimensional wave with velocity c. Furthermore, it is also possible to prove from the Maxwell equations that B is always perpendicular to E, and that both waves travel in the direction $E \times B$ (which is orthogonal to both E and B). However, it is general practice to describe electromagnetic waves using only E, and here we will conform to this practice.

Now that we have established that electromagnetic radiation behaves like a wave, we would like to write the function describing this wave in a simpler

form, so that it is easier to manipulate. We therefore focus on waves with some set frequency, λ, which we refer to as monochromatic waves. There is no loss of generality in this, because according to Fourier's theorem, we can describe any wave as a superposition of a number of monochromatic waves with appropriate amplitudes, frequencies and phases. Suppose that our monochromatic wave travels in the x-direction. Then we could write:

$$E_y = E_{y0} \sin(kx - \omega t + \phi_y) \tag{2.7}$$

Here E_{y0} is the maximum displacement or amplitude, ω is the angular frequency defined as $\omega = 2\pi\lambda$, $k = 2\pi/\lambda$ is the wave number, and ϕ_y is the phase difference. In Eqn. 2.7, we only have a displacement in the y-direction. These waves are called linearly polarised waves, and the light described by these waves is called polarised light. However, typically, a light wave travelling in the x-direction vibrates in all directions in the y-z plane. This type of light is called unpolarised light. It is possible to decompose the unpolarised light into two mutually orthogonal vectors E_y and E_z in the y-z plane. Typically, $E_y \neq E_z$ and $\phi_y \neq \phi_z$. The case where two orthogonal monochromatic waves have a different amplitude and phase is called elliptically polarised. For the special case that the phase difference is $1/4^{\text{th}}$ of a wavelength, or $\phi_y = \pi/2$ in radians, and the amplitudes are equal, we call the light circularly polarised.

The intensity of a light beam, which is a time-averaged measure for the energy flux, is a function of the amplitudes of the two mutually orthogonal waves

$$I = k(|E_y|^2 + |E_z|^2) \propto E_{y0}^2 + E_{z0}^2 \tag{2.8}$$

where k is a proportionality constant.

2.1.1 Reflection

We want to describe how a wave that obeys Eqn. 2.7 reflects off a surface. All equations derived so far are applicable *in vacuo* only, but it is easy to extend these equations to a dielectric medium, i.e. a non-conductive, isotropic and homogeneous medium. We can simply account for the properties of the medium by replacing the speed of the wave *in vacuo*, c, by the appropriate speed in the medium c_m

$$c_m = 1/\sqrt{\varepsilon_0 \varepsilon_r \mu_0 \mu_r} = c/\sqrt{\varepsilon_r \mu_r} \tag{2.9}$$

We can now define the refractive index n of a medium using

$$n = \frac{c}{c_m} \tag{2.10}$$

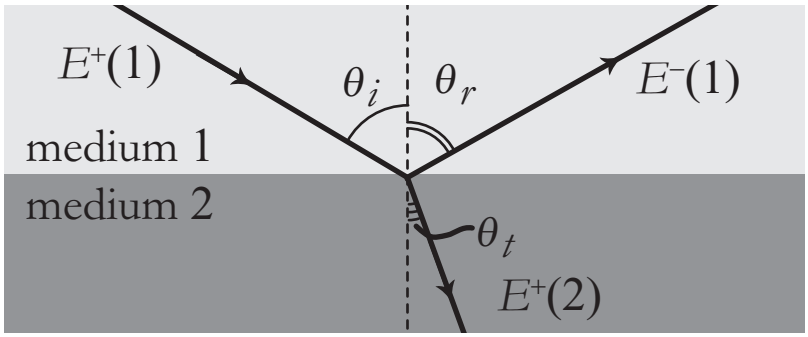

Figure 2.2: *Reflection and transmission of a light beam on the interface between medium a and medium b. The angle between the incoming beam and the surface normal, θ_i, is equal to the angle between the normal and the reflecting beam, θ_r. Typically, also a part of the beam is transmitted. The angle between the normal and the transmitted beam is denoted with θ_t. The variables $E^+(1)$, $E^-(1)$ and $E^+(2)$ are used in the Abeles matrix formalism to describe the forward ($^+$) and backward ($^-$) travelling wave in the medium 1 or 2.*

It is also possible to describe the interaction between a wave and a medium more thoroughly, by also accounting for the extinction. In this case we must introduce the complex refractive index $\tilde{N}$ as

$$\tilde{N} = n - j\tilde{k} \tag{2.11}$$

where $\tilde{k}$ is the extinction coefficient. For the sake of simplicity, we assume for the remainder of this text that $\tilde{k} = 0$, and we only use the real part of the refractive index.

When an electromagnetic wave travels from a medium with refractive index n_1 to a medium with refractive index n_2, part of the wave is reflected and part of the wave is transmitted, which is indicated in Figure 2.2. The angles between the incident beam, θ_i and the reflected beam, θ_r, are always equal (with respect to the surface normal). The angles of the incident beam and the transmitted beam, θ_t, obey Snell's law or Fermat's principle (principle of least time).

$$n_1 \sin\theta_i = n_2 \sin\theta_t \tag{2.12}$$

By matching the field strength of the E and H fields on both sides of the interface, it is possible to determine the amount of light, or more accurately the energy, that is reflected and that is transmitted. This exercise yields the so-called Fresnel coefficients. Typically, the Fresnel equations are calculated separately for E_y and E_z, where one component, say y, is in the same plane as the surface, and the other component, z, is perpendicular to the surface.

This gives a reflection coefficient for light that is polarised parallel to the interface $r_{\parallel}$, and also a transmission coefficient for parallel polarised light $t_{\parallel}$.

$$r_{\parallel} = \frac{E_{\parallel,r}}{E_{\parallel,i}} = \frac{(n_2/n_1)\cos\theta_i - \cos\theta_t}{(n_2/n_1)\cos\theta_i + \cos\theta_t} \tag{2.13}$$

$$t_{\parallel} = \frac{E_{\parallel,t}}{E_{\parallel,t}} = \frac{2\cos\theta_i}{(n_2/n_1)\cos\theta_i + \cos\theta_t} \tag{2.14}$$

In a similar manner, we can also formulate the transmission $t_{\perp}$ and reflection coefficient $r_{\perp}$ for waves that are polarized perpendicular to the surface.

$$r_{\perp} = \frac{\cos\theta_i - (n_2/n_1)\cos\theta_t}{\cos\theta_i + (n_2/n_1)\cos\theta_t} \tag{2.15}$$

$$t_{\perp} = \frac{2\cos\theta_i}{\cos\theta_i + (n_2/n_1)\cos\theta_t} \tag{2.16}$$

Hence, we can describe the reflection of light on an interface using Eqns. 2.13 and 2.15, and the transmission is described by Eqns. 2.14 and 2.16. To calculate the reflected and transmitted intensities, one has to use Eqn. 2.8. This gives another set of reflection and transmission coefficients, $\mathcal{R}_{\parallel} = r_{\parallel}^2$, $\mathcal{R}_{\perp} = r_{\perp}^2$,$\mathcal{T}_{\parallel} = t_{\parallel}^2$, and $\mathcal{T}_{\perp} = t_{\perp}^2$.

For the case that a light wave hits an interface between two optical media, it can be shown using Eqns. 2.13 and 2.15, that there is a special angle of incidence where $r_{\parallel} = 0$ and $r_{\perp} \neq 0$. This angle is called the Brewster angle, θ_B, and it can easily be found using

$$\tan\theta_B = \frac{n_1}{n_0} \tag{2.17}$$

If the index of refraction of the incoming medium is higher than the index of refraction of the outgoing medium, e.g. $n_0 > n_1$, it is possible to show using Eqns. 2.13 and 2.15 that there is another special angle of incidence where $r_{\parallel} = r_{\perp} = 1$. This angle is called the critical angle, θ_c, and it can be calculated using

$$\sin\theta_c = \frac{n_1}{n_0} \tag{2.18}$$

At $\theta \geq \theta_c$ all the incoming light is reflected, and hence, this is often called total internal reflection. However, the transmission coefficients do not go to zero. It can be shown that, besides the reflected wave, there will be another wave, travelling along the interface. This wave is called an evanescent wave, and because is decays very rapidly in the direction perpendicular to the surface, it can be used to excite adsorbed species with fluorescent properties. Once an evanescent wave is established, it does not 'use' any energy, and hence it is possible to simultaneously have a nonzero t and $r = 1$.

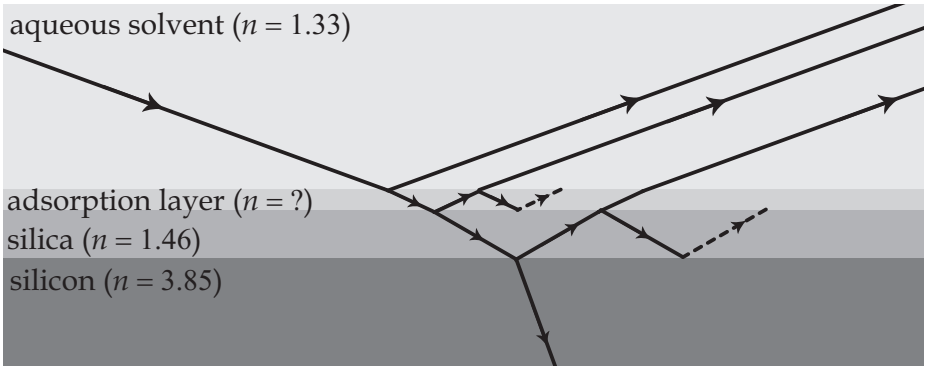

Figure 2.3: *Schematic image of a two layer structure sandwiched between two semi-infinite media. The two layers, defined by a thickness d and an index of refraction n, are bounded on either side by a semi-infinite medium, that is only characterised by its index of refraction. The solid line is an illustration of some reflections and transitions that an incoming ray of light might experience. All experiments described in this thesis were modelled using a set of layers similar to this image.*

2.1.2 Isotropic stratified structures

The goal in this paragraph is to understand the reflection of a light beam on a surface covered with a polymer or a surfactant layer. To do this, we assume that the surface consists of parallel layers, stacked onto each other. These layers are bounded on either side of the stack by a semi-infinite media. To keep things simple, we neglect any structure in these layers, and we assume that they are homogeneous and isotropic. In the case of our experiments, the bottom semi-infinite medium is the silicon of the wafer. On top of the silicon, there is a layer of silica. However, this layer can also be a polymeric layer, or some other inorganic oxide. It is even possible to have an arbitrary number of stacked inorganic and/or polymer layers here. When such a surface comes into contact with a solution containing some adsorbing species, the adsorbing species will form another layer, and, also to keep things simple, we model this layer as a flat slab. To complete the system, there is the solution from which the polymer/surfactant adsorbs. This solution is modelled as another semi-infinite medium. We want to describe the entire system of stacked layers by means of a set of mathematical equations.

To generalise the model, we take a stack of m layers that we call L_1 to L_m. These layers are sandwiched between two semi-infinite media L_0 and L_{m+1}. All media are described by their index of reflection, n_L, and their thickness d_L (note that $d_0 = d_{m+1} = \infty$). In this text we will only use the word 'layer' for those media that have a properly defined thickness.

A convenient method to calculate the reflectivity of such a stack of layers is the 2 × 2-matrix formalism by Abeles. This formalism uses the property that all equations describing the propagation of a monochromatic wave are linear and then matches the tangential fields across interfaces – similar to the case of the Fresnel equations – using matrix transformations.

Generally, if a wave hits an interface, part of the wave is reflected and part of the wave is transmitted (see also the previous section). This means that there will be a forward travelling wave (the initial wave and the transmitted wave) and a backward travelling wave (the reflected wave). These waves are denoted by, respectively, $E^+(z)$ and $E^-(z)$, which is also illustrated in Figure 2.2. We will describe the field at every point z as:

$$E(z) = \begin{bmatrix} E^+(z) \\ E^-(z) \end{bmatrix} \tag{2.19}$$

The reflection and the transmission depend on the polarisation of the light. All equations in this paragraph are valid for parallel and perpendicular polarised light. To keep things general, we will not specify the direction of polarisation. The next step, is to describe every layer, or interface between layers, or even a set of layers, by a scattering matrix S such that

$$E(z') = \begin{bmatrix} E^+(z') \\ E^-(z') \end{bmatrix} = \begin{bmatrix} S_{1,1} & S_{1,2} \\ S_{2,1} & S_{2,2} \end{bmatrix} \begin{bmatrix} E^+(z'') \\ E^-(z'') \end{bmatrix} = SE(z'') \tag{2.20}$$

where z' and z'' are on either side of a layer, or on either side of an interface, or, more general, on either side of a (sub)system consisting of layers and interfaces. In the case of an interface, we call the scattering matrix I, and it can be shown that I should look like[40]

$$I_{ab} = \frac{1}{t_a b} \begin{bmatrix} 1 & r_{ab} \\ r_{ab} & 1 \end{bmatrix} \tag{2.21}$$

where the subscripts a and b refer to the layers on either side of the interface. A layer can be described by a 2×2 matrix L that can be written as

$$L_a = \begin{bmatrix} e^{j\beta} & 0 \\ 0 & e^{-j\beta} \end{bmatrix} \tag{2.22}$$

where β is the phase shift of the electromagnetic wave which is defined as

$$\beta = 2\pi d n \lambda^{-1} \cos\phi \tag{2.23}$$

The goal is to calculate the overall reflectivity of a stack of dielectric layers. So, we want to calculate the scattering matrix S that relates the incoming waves from medium 0 to the outgoing waves in medium $m + 1$

$$E(0) = SE(m + 1) \tag{2.24}$$

Because the whole system is linear, we can calculate S quite easily by just applying Eqn. 2.20 repeatedly for all interfaces and for all layers

$$S = I_{01}L_1I_{12}L_2...L_mI_{m(m+1)} \tag{2.25}$$

Hence, the whole layer system can be described by combining Eqn. 2.24 and 2.25. Finally, we can use S to calculate a coefficient of reflection R and a coefficient of transmission T that describes the behaviour of the whole stacked layer system. By comparing Eqn. 2.20 with Figure 2.2, we can find that

$$R = \frac{E_a^-}{E_a^+} = \frac{S_{21}}{S_{11}} \tag{2.26}$$

$$T = \frac{E_b^+}{E_a^+} = \frac{1}{S_{11}} \tag{2.27}$$

Hence we can find overall reflection and transmission coefficients for isotropic stratified structures, that are very similar to the Fresnel coefficient. It is possible to extent this theory to apply for anisotropic materials, or for density gradients in the layers. For these types of complications and many others, we refer to the excellent book by Azzam and Bashara.[40]

2.1.3 The 2-layer system

The reflectometer experiments described in this thesis are modelled by a system consisting of two layers and two semi-infinite media (see Figure 2.3). The adsorbent is semi-infinite silicon with a silica layer. An adsorption layer is formed on top of the silica, and the adsorption layer is bounded by the semi-infinite solution. The total scattering matrix for such a system should look like

$$\begin{aligned} S &= I_{01}L_1I_{12}L_2I_{23} \\ &= \frac{1}{t_{01}t_{12}t_{23}} \begin{bmatrix} 1 & r_{01} \\ r_{01} & 1 \end{bmatrix} \begin{bmatrix} e^{j\beta_1} & 0 \\ 0 & e^{-j\beta_1} \end{bmatrix} \begin{bmatrix} 1 & r_{12} \\ r_{12} & 1 \end{bmatrix} \begin{bmatrix} e^{j\beta_2} & 0 \\ 0 & e^{-j\beta_2} \end{bmatrix} \begin{bmatrix} 1 & r_{23} \\ r_{23} & 1 \end{bmatrix} \end{aligned} \tag{2.28}$$

By performing all the matrix multiplications and applying Eqns. 2.26 and 2.27, it is straight forward to find

$$R = \frac{(r_{01} + r_{12}e^{-j2\beta_1}) + (r_{01}r_{12} + e^{-j2\beta_1})r_{23}e^{-j2\beta_2}}{(1 + r_{01}r_{12}e^{-j2\beta_1}) + (r_{12} + r_{01}e^{-j2\beta_1})r_{23}e^{-j2\beta_2}} \tag{2.29}$$

$$T = \frac{t_{01}t_{12}t_{23}e^{-j(\beta_1+\beta_2)}}{(1 + r_{01}r_{12}e^{-j2\beta_1}) + (r_{12} + r_{01}e^{-j2\beta_1})r_{23}e^{-j2\beta_2}} \tag{2.30}$$

These equations can easily be solved using basic spreadsheet software. Using a bit more sophisticated software, it is possible to implement the Abeles matrix approach for a more general system consisting of an arbitrary number of layers.

2.1.4 Near brewster angle reflectometry

Using the method described above, it is possible to calculate the reflectivity of a stratified layer structure. Our reflectometer measures the ratio $I_{\parallel}/I_{\perp} \propto \mathcal{R}_{\parallel}/\mathcal{R}_{\perp} = R_{\parallel}^2/R_{\perp}^2$. Most of the parameters of the stratified layer structure described above are known. Typically, our system is similar to the system as in Figure 2.3. For this system, we know that $n_{\text{solvent}} = 1.333$, $n_{SiO_2} = 1.46$, and $n_{Si} = 3.8$. Furthermore, we measure the thickness of the silica layer, d_{SiO_2} beforehand using an ellipsometer. This means that there are only two unknowns, which are n_{ads} and d_{ads}.

Typically, a reflectometer experiment is done to determine the adsorbed amount of some species. In such an experiment, it is assumed that there is a layer of the species near the surface. The index of refraction of this layer, n_{ads}, is equal to the index of refraction of the solvent plus some term describing the adsorbed material. Mathematically, de Feijter showed that[41]

$$n_{\text{ads}} = n_w + \frac{(\mathrm{d}n/\mathrm{d}c)\,\Gamma}{d_{\text{ads}}} \tag{2.31}$$

Here, $\mathrm{d}n/\mathrm{d}c$ is the refractive index increment, which is a species dependant parameter, and Γ is the adsorbed amount.

The reflectometer used for the research described in this thesis is a so-called near brewster angle reflectometer. This implies that the angle between the laser beam and the normal of the adsorbent is equal to the brewster angle ($\approx 71^\circ$ here) and that we do not vary this angle during the experiments. For this setup, it can be shown that the thickness of the adsorption layer shows very convenient behaviour. This thickness appears in the equations on many different places, but effectively it cancels.[16] Hence we only have to provide the order of magnitude for the adsorption layer thickness, i.e. $d_{\text{ads}} \approx 5\text{nm}$.

A convenient method to relate the change in reflectivity to the adsorbed amount in near brewster angle reflectometry is the use of the Q-factor.

$$\Gamma = \frac{(R_p/R_s)_\Gamma - (R_p/R_s)_0}{(R_p/R_s)_0} \times Q \tag{2.32}$$

Where the Q-factor is defined as

$$Q = \frac{R_p}{R_s}\frac{\mathrm{d}\Gamma}{\mathrm{d}(R_p/R_s)} \tag{2.33}$$

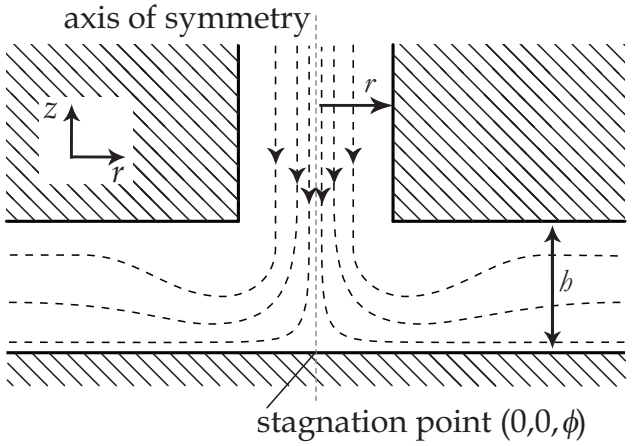

Figure 2.4: *Schematic representation of a stagnation point flow chamber. The solution enters the chamber from the top and spreads equally over the r-ϕ plane due to the solid surface that is placed perpendicular to the flow. This is indicated by the dashed flow lines. The cell is characterised by the radius of the circular inlet tube r and the distance between the end of the inlet tube and the solid surface surface, h.*

The trick with this method is that Q is hardly a function of the adsorbed amount (maximum error $\approx 10\%$). However, for increased precision one can routinely solve the Abeles equations for every experimental datapoint. This yields more accurate results.

By routinely solving the Abeles equation one can also try to find the thickness of one of the layers instead of n_{ads}. A possible application of such a method is to follow the dissolution of a layer, where n is fixed during the experiment and d decreases. For such a situation, it is not possible to use the Q-factor, since n_{ads} is fixed and $(\mathrm{d}n/\mathrm{d}c)$ is undefined.

2.2 Hydrodynamics in the SPF

Our reflectometer is equipped with a stagnation point flow chamber (SPF). This type of flow system is also known as an impinging jet. The advantage of such a system is that the hydrodynamic flow pattern is well defined. Hence, the experimental conditions are easy to control, and it is possible to model the particle flux at the surface. In figure 2.4 a schematic picture of a SPF is presented. The dashed lines in the Figure are streamlines. These indicate the flow pattern of the liquid. At the inlet, the streamlines are perpendicular to the (flat) surface, and hence, they have to bend when they approach the

surface. The system has radial symmetry, and therefore, the fluid spreads out over the surface in equal amounts in all radial directions. The point on the surface which is exactly in the middle of the jet, is called the stagnation point. In this paragraph, we will use cylindrical coordinates to describe our system. The radial coordinate r gives the distance from the axis of symmetry, ϕ will define the angle around the axis of symmetry, and z gives the distance perpendicular to the surface, where a positive value corresponds to a point in the solution (see also Figure 2.4).

The flowfield in such a SPF has been carefully looked at by Dabros and van der Ven and they found that, close to the axis of symmetry, the flowfield can be approximated by:[42]

$$\vec{v} = \begin{pmatrix} v_r \\ v_z \\ v_\phi \end{pmatrix} = \begin{pmatrix} \alpha z r \\ -\alpha z^2 \\ \beta r z \end{pmatrix} \tag{2.34}$$

Since the SPF has an axis of symmetry, around which it is cylindrically symmetric, $v_\phi = 0$. Hence $\beta = 0$. It is possible to make an approximate calculation of the amount of particles arriving at the surface per unit of time. To do this, we use an Eulerian method. Eulerian methods are used to calculate the particle distribution in space, as opposed to Lagrangian methods, which are focussed on single-particle trajectories.[43]

In all our experiments, we use quite low polymer (or surfactant) bulk concentrations. We can therefore assume that there are no interactions between our particles. In this case, it is possible to formulate the convective-diffusion (CD) equation as[44]

$$\frac{\partial c}{\partial t} + \nabla \cdot \mathbf{J} = Q \tag{2.35}$$

Here, the flux of particles entering a volume element is defined as:

$$\mathbf{J} = -\mathbf{D} \cdot \nabla c + vc \tag{2.36}$$

In these Equations, $\partial c/\partial t$ is the change of the number of particles in a volume element per unit of time, Q is a source term, $\mathbf{D}$ is the diffusion tensor, and v is the fluid velocity (∇ is the gradient operator). An approximation that can be used to solve Eqn. 2.35 is the Smoluchowski-Levich approach. In this approach it is assumed that the polymers or surfactants do not interact with the substrate and that they are point-like, e.g. their volume is zero. Hence, the particles do not experience hydrodynamic drag, they exactly follow the streamlines, and interception (when the center of the particle follows the streamline and the particle edge hits the surface) does not occur. Furthermore, we assume that the fluid is incompressible ($\nabla \cdot v = 0$), that

a steady state situation has been achieved ($\partial c/\partial t = 0$) and that the source term is zero. Using this we obtain:

$$D\nabla^2 c = v \cdot \nabla c \tag{2.37}$$

Here D is the diffusion coefficient, which is equal in the bulk and near the surface. Next, we want to combine Eqns. 2.37 and 2.34. Performing the matrix multiplication gives

$$D\left(\frac{\partial^2 c}{\partial r^2} + \frac{1}{r}\frac{\partial c}{\partial r} + \frac{\partial^2 c}{\partial z^2} + \frac{1}{r^2}\frac{\partial^2 c}{\partial \phi^2}\right) = \alpha z r \frac{\partial c}{\partial r} - \alpha z^2 \frac{\partial c}{\partial z} + \frac{\beta r z}{r}\frac{\partial c}{\partial \phi} \tag{2.38}$$

Since the systems has cylindrical symmetry, we can neglect the variation in the ϕ-direction. Also, since we measure only in the stagnation point, we neglect the variation in the r-direction. This leaves:

$$D\frac{\partial^2 c}{\partial z^2} = -\alpha z^2 \frac{\partial c}{\partial z} \tag{2.39}$$

We can solve Eqn. 2.39 using a mathematical trick. We define: $l \equiv \frac{\partial c}{\partial z}$, and we can rewrite (2.38) into

$$-\frac{\alpha z^2}{D}\partial z = \frac{\partial l}{l} \tag{2.40}$$

This expression has separated variables. We can integrate this equation and obtain

$$-\frac{\alpha}{3D}z^3 + C_1 = \ln l \tag{2.41}$$

Using the definition of l, we can now write

$$\frac{\partial c}{\partial z} = l = C_2 \exp\left[-\frac{\alpha}{3Dz^3}\right] \tag{2.42}$$

Next it is important to determine the constant C_2. We realise that c far from the surface is equal to the bulk concentration c_b and very close to the surface we call the concentration c_0

$$\begin{aligned}
\int_0^\infty \frac{\partial c}{\partial z}\mathrm{d}z &= c_b - c_0 \\
&= C_2 \int_0^\infty \exp\left[-\frac{\alpha z^3}{3D}\right]\mathrm{d}z \\
&= C_2 \int_0^\infty \exp\left[\frac{\alpha z^3}{3D}\right]\mathrm{d}\left(\frac{\alpha z^3}{3D}\right)^{1/3} \cdot \left(\frac{\alpha}{3D}\right)^{-1/3} \\
&= C_2 \left(\frac{\alpha}{3D}\right)^{-1/3} \int_0^\infty e^{-l^3}\mathrm{d}l \\
&= C_2 \left(\frac{\alpha}{3D}\right)^{-1/3} \frac{\Gamma(1/3)}{3}
\end{aligned} \tag{2.43}$$

So

$$\begin{aligned} C(2) &= (c_b - c_0)\left(\frac{\alpha}{3D}\right)^{1/3}\frac{3}{\Gamma(1/3)} \\ &\approx 0.776\left(\frac{\alpha}{D}\right)^{1/3}(c_b - c_0) \end{aligned} \tag{2.44}$$

With this result, we can calculate the flux at the collector surface using

$$J = D\frac{\partial c}{\partial z}\Big|_{z=0} \tag{2.45}$$

The parameter α is still a function of the flowfield, e.g. the characteristic sizes of the flowcell, the fluid viscosity and the flow rate. Using $\alpha = \bar{\alpha}Re\nu R^{-3}$ where Re is the Reynolds number, ν is the kinematic viscosity, r is the radius of the SPF inlet (see Figure 2.4), and $\bar{\alpha}$ is a new constant that depends only on the cell geometry and its value can be found in literature.[42] The Reynolds number is defined as $Re = vr/\nu$ where v is the fluid velocity. Using this definition, Eqn. 2.45 can be rewritten to

$$J_L = 0.776(\bar{\alpha}Re)^{1/3}\frac{D^{2/3}}{r}(c_b - c_0) \tag{2.46}$$

2.3 Miscellaneous

The reflectometer used for the research described in this thesis is equipped with syringe pumps. The big advantage of working with these type of pumps, is that they can be accurately set to deliver a certain flow rate without any fluctuations. As their name suggests, these pumps work with syringes. In order for the plunger to move freely, it is necessary to use a bit of lubricant, which typically is some fatty substance. When we work with solutions containing surfactants, the fat from the syringe can be solubilised. Hence we used the syringe pump to collect the waste instead of delivering the polymer or surfactant solution.

A flask containing the aqueous polymer or surfactant solution was placed at some high place. The solution in this flask was allowed to flow through a tube to the flowcell inlet, then pass the flowcell and finally go to the waste. Typically, the flowrate of this setup was 5 ml/min. Subsequently, the waste is connected to the syringe pump, which is typically set to 1 ml/min. Hence, the flux is controlled by the pump, and the pressure inside the tube is slightly higher than it is outside the tube. Setting the flask containing the solution at the same height as the pump, will result in the formation of small bubbles

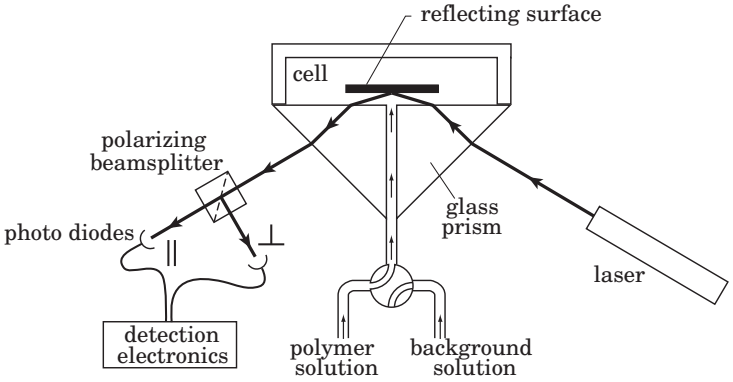

Figure 2.5: *Schematic representation of how the optical and hydrodynamic part of the reflectometer combine. The laser light coming from the right reflects on the surface, and the detector on the left measures the intensity of the reflected light ($I_{\parallel}$ and $I_{\perp}$). The valve at the bottom of the image is the fluid inlet. It can be used to switch between different solutions.*

in the solution that scatter light. This is thought to be due to the relatively low pressure inside the tubing, which promotes the bubble formation.

For the experiments with the syringe pumps, a special flow cell was made that entirely closes the system. The two major advantages of this flow cell are that it is virtually leak proof, and that the distance between the surface and the prism (h in Figure 2.4) is very constant (which in turn implies that the kinetics are very reproducible).

The silica surfaces used to study the adsorption of PEO or C_nE_m are cut from silica wafers. These wafers are subsequently baked and cleaned with a very aggressive solution called piranha solution, which is described in more detail in chapter 3.1. To get reproducible results, the cleaning of the silica is very important. Different cleaning methods may give different results. Furthermore, even if every silica surface is cleaned in the same manner, the experimental results may depend on the surface. The cleaning method used in this thesis is very thorough, and with this method it is possible to re-use the surfaces. By re-using the silica surface, it is possible to minimise the experimental error between measurements. Often is is also possible to clean the surface without taking the cell apart. Sometimes, in the case of surfactant adsorption, simply rinsing with solvent will result in a clean surface. In the case of polymer adsorption, it might be possible to displace the polymer using a surfactant (see chapter 3), or by changing the pH and/or the ionic strength (see chapter 5).

Chapter 3

Competitive adsorption

This chapter describes experimental findings on the competitive adsorption of nonionic PEO and the nonionic surfactant C_nE_m from aqueous solutions onto a silica surface. From one-component solutions, both species readily adsorb onto silica and, in the bulk of mixed (two-component) solutions, polymer-surfactant complexes are not observed. Because both species bind by the same mechanism to silica, subtle differences in layer structure, or other species specific parameters, determine whether one or both of the species will adsorb. It is found that various surfactants can displace PEO up to a certain critical molecular weight. Surfactants with a high aggregation number, in bulk and possibly also on the surface, can displace PEO with a higher molar mass than surfactants with a low aggregation number. As the molar mass of the polymer increases, the time a surfactant needs to completely displace the polymer also increases. We can explain both the existence of the critical molar mass and the decrease in adsorption kinetics with a shift in the $CSAC$.

3.1 Materials

A number of monodisperse poly(oxyethylene oxide) alkyl ethers ($C_{12}E_3$, $C_{12}E_5$, $C_{12}E_6$, $C_{12}E_7$, $C_{14}E_7$ and $C_{16}E_7$) were purchased from Nikko chemicals (Japan) and used without further purification. Typically, these surfactants are produced by the addition of $1,2-$epoxyethane (or ethylene oxide) to a fatty alcohol such as $1-$dodecanol. The end group on the fatty alcohol side of the

Part of this chapter has been published as: Bart R. Postmus, Frans A. M. Leermakers, Luuk K. Koopal, and Martien A. Cohen Stuart. Competitive adsorption of nonionic surfactant and nonionic polymer on silica. *Langmuir*, 23:5532-5540, 2007.

Surfactant	M_w(g/mol)	CMC(mol/l)	dn/dc (g/ml)
$C_{12}E_3$	318	3.0×10^{-5}	0.120
$C_{12}E_5$	406	6.5×10^{-5}	0.131
$C_{12}E_6$	450	8.7×10^{-5}	0.136
$C_{12}E_7$	494	1.0×10^{-4}	0.142
$C_{14}E_7$	522	2.0×10^{-5}	0.136
$C_{16}E_7$	550	9.0×10^{-7}	0.133

Table 3.1: *Properties of the surfactants used in this study. M_w is the molar mass, CMC the critical micel concentration and dn/dc the refractive index increment. The CMC and dn/dc were determined by fitting a straight line through a plot of literature data[45,46] versus the number of EO-groups.*

surfactant is a methyl group, and the other end group is a hydroxyl group. Important properties of these surfactants are summarised in Table 3.1. A series of well-defined, nearly homodisperse PEO samples was obtained from Polymer Laboratories and was used as received. This PEO was prepared by anionic addition polymerization of $1,2-$epoxyethane, and its end groups are $t-$butyl from the initiator and hydroxyl from the termination with alcohol. A stock solution was prepared for every surfactant and polymer used in this study. All solutions needed for the experiments were freshly prepared by dilution of the stock solutions and the stock solutions were never older than two weeks. DI water was obtained by purifying tapwater using a Barnstead Easypure apparatus (resistivity 18.3 MΩcm).

Polished silicon wafers (Boron doped, orientation {1,0,0} and resistivity 12-18 Ωcm) were purchased from Wacker Siltronic. These wafers were cut to fit our flowcell, and, on these strips, an oxide layer of approximately 50 nm was thermally grown. This procedure yields surfaces with a water contact angle of $\approx 47°$. Washing was performed by soaking in piranha solution, which is a mixture of 33% hydrogen peroxide (Lamers en Pleuger) and 67% Sulfuric Acid (Fluxa) for 5 minutes followed by thorough rinsing with DI water. This yields surfaces with a water contact angle of $\approx 21°$. To further hydrophilise these surfaces, they were soaked in a sodium hydroxide solution (Aldrich, p$H \approx 11$) for 5 minutes[a], giving surfaces with a water contact angle of $\approx 8°$, then thoroughly rinsed with DI water and ethanol, subsequently dried in a stream of nitrogen and put in a plasma cleaner (Harrick Scientific Corp., model PDC-32G) for 5 minutes at medium power. This produces surfaces

[a]There is evidence in the literature that silica dissolves at high pH.[47] However, we checked the solubility of the silica layer in a p$H = 11$ solution, and we could not measure a change in silica thickness after 24 h of exposure.

with a contact angle smaller than 5°. Surfaces were stored in DI water and were never allowed to dry after the cleaning procedure.

The teflon flowcell and glass prism used for the reflectometry experiments (see chapter 2) were cleaned using the plasma cleaner for 10 minutes at medium power and thoroughly rinsed with DI water. All glassware needed for the experiments was also cleaned using piranha solution, and subsequently rinsed thoroughly with copious amounts of water.

3.2 Bulk behavior

In order to obtain the size of the surfactant micelles, we performed dynamic light scattering (DLS). DLS was performed using an ALV setup featuring an argon laser tuned at a wavelength of 514.5 nm with a typical output intensity of 500 mW and an ALV-5000 correlator card. For our measurements, we used a pinhole with an opening radius of 600 μm. To analyze the autocorrelation data we used the method of cumulants. This method assumes spherical particles and that only the translational diffusion coefficient contributes to the decay of the autocorrelation function. The hydrodynamic radius was calculated using the Einstein-Stokes relation.

To get a reasonable signal from this setup, we were forced to use quite high surfactant concentrations. For this reason the concentration used for our DLS measurements is 3.00×10^{-3} M, which is 30 times higher than the concentration used in our displacement experiments. The results of the DLS experiments are presented in Table 3.2. We find that $C_{12}E_5$ and $C_{16}E_7$ form larger micelles than the other surfactants. We could not measure the micellar size of $C_{12}E_3$, because this surfactant has a cloudpoint which lies much lower than the concentration necessary to get a proper scattering signal.

We have also performed DLS experiments on a number of polymer/ surfactant mixtures. It was found that in all cases, the micellar size was not altered by the addition of polymer. From these results we conclude that surfactants and polymers do not associate in bulk solution.

3.3 Adsorption results

Figure 3.1 shows the evolution of the surface excess in time for a typical PEO adsorption experiment. Every experiment starts with flowing solvent through the cell until a stable signal is obtained. At $t \approx 1$ minute, the flow is switched to a PEO solution (indicated by the gray background colour) and at $t \approx 3$ minutes the flow is switched back to the solvent. Shortly after

Surfactant	R_{h} (nm)	$\mathrm{d}\Gamma/\mathrm{d}t$ (μmol/m^{2}s)	Γ (μmol/m^2)	σ (nm^2/molec.)	$\rho_{EO,\mathrm{bilayer}}$ (EO/nm^2)
$C_{12}E_3$	NA	0.17	7.55	0.22	6.82
$C_{12}E_5$	14.5	0.38	4.68	0.36	7.04
$C_{12}E_6$	4.3	0.37	3.33	0.50	6.02
$C_{12}E_7$	3.7	0.49	2.83	0.59	5.97
$C_{14}E_7$	4.2	0.48	2.87	0.58	6.05
$C_{16}E_7$	6.9	0.37	3.45	0.48	7.28

Table 3.2: *Properties of surfactants used in this study. R_h is the hydrodynamic radius of the surfactant micelles as found by dynamic light scattering, $d\Gamma/dt$ is the rate of adsorption from a solution with a bulk concentration of 6.00×10^{-5} M for $C_{12}E_3$ and 1.00×10^{-4} M for the other surfactants, Γ is the surface excess above the CMC, σ is the area one molecule occupies on the adsorption plateau, and $\rho_{EO,bilayer}$ is the density of EO-groups near the surface if we assume that the surfactant adsorbs as a bilayer.*

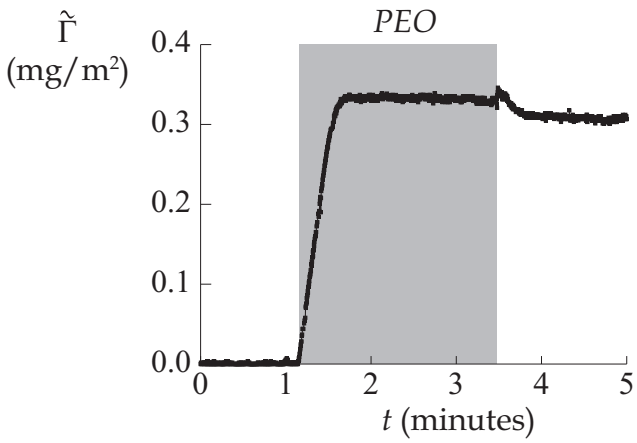

Figure 3.1: *Adsorbed amount in mg/m^2, $\tilde{\Gamma}$, of PEO (M_w = 26840 g/mol) on silica plotted versus time in minutes. The gray background colour indicates a nonzero polymer bulk concentration.*

M_w (g/mol)	N (EO/molec.)	M_w/M_n	$\tilde{\Gamma}$ (mg/m^2)	Γ (μmol/m^2)
4250	97	1.03	0.17	0.040
12600	286	1.04	0.24	0.019
20360	463	1.03	0.30	0.015
26840	610	1.05	0.35	0.013
43520	989	1.03	0.30	0.007
82250	1869	1.02	0.40	0.005
167700	3811	1.02	0.50	0.003

Table 3.3: *Properties of the polymers used in this study. M_w is the molar mass, N is the number of monomers per polymer, M_w/M_n is a measure for the monodispersity of the polymer, $\tilde{\Gamma}$ is the surface excess on the plateau of the isotherm in mg/m^2 and Γ the surface excess on the plateau of the isotherm in μmol/m^2.*

the PEO solution is introduced in the cell, the surface excess, $\tilde{\Gamma}$, starts to increase linearly in time. As the surface approaches saturation, the rate of adsorption decreases until it reaches zero in the plateau. When the flow is switched back to solvent for a rinsing step, it can be seen that PEO hardly desorbs. The shape of $\tilde{\Gamma}(t)$ curves like that in Figure 3.1 has been discussed by Dijt *et alia*.[48]

By performing a series of the experiments such as the one described by Figure 3.1, one can construct an adsorption isotherm. An example of such an isotherm for PEO with $M_\mathrm{w} = 26840$ g/mol, is presented in Figure 3.2. Because even the lowest experimentally feasible PEO bulk concentration corresponds to a high surface coverage, this isotherm is called a high-affinity-isotherm. In Table 3.3, some properties of the polymers used in this study are presented.

Polymer adsorption is generally thought of as a two stage process. To adsorb onto a surface, the polymer first needs to be transported to the surface, and subsequently it needs to attach to the surface. To model these two stages, a thin layer, called subsurface layer, close to the surface, is assumed. In order for a polymer to adsorb, it needs to be transported to the subsurface (transport step), and subsequently it needs to migrate from the subsurface to the surface (attachment step). For the stagnation point flow, that we use in our setup, the transport step can be described by:

$$J = k_\mathrm{tr}(c_\mathrm{b} - c_\mathrm{s}) \tag{3.1}$$

where c_b and c_s are respectively the bulk and subsurface concentrations, and k_tr is the transport coefficient, which is described in Chapter 2.2.

Sometimes the lateral spreading of the polymer on the surface is described as a third adsorption step.[49] However, with our experimental setup, we

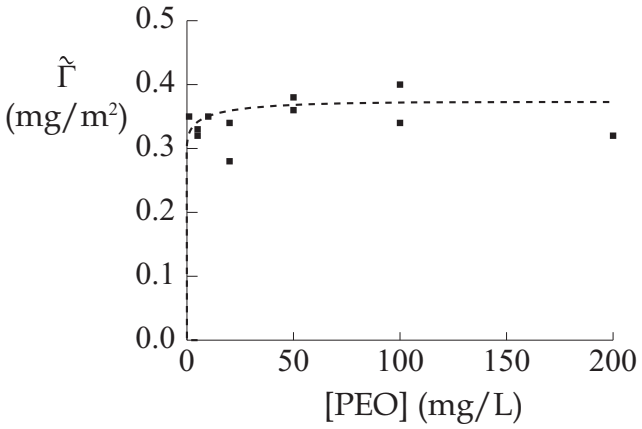

Figure 3.2: *Adsorbed mass in mg/m^2 of PEO M_w = 26840 g/mol on silica as a function of polymer bulk concentration (adsorption isotherm). The dotted line is only to guide the eye.*

cannot measure the amount of spreading or reconformation of polymer on the surface if there is no accompanying change in surface excess.

Dijt *et al.* have found that adsorption of *PEO* is transport dominated, or in other words, that the attachment step is very fast compared to the transport step. Furthermore, they concluded that a local equilibrium must hold. This implies that the value of c_s can be found as the bulk concentration that corresponds to the current surface excess in the equilibrium isotherm (Figure 3.2). Of course, when the system is in equilibrium, you will find $c_\mathrm{s} = c_\mathrm{b}$. But, if this is not the case, there is a concentration gradient that can be used in Eqn. 3.1 to calculate the adsorption rate, J. Using this concept, it can be understood that J is constant during most of the adsorption process, because $c_s \ll c_b$. Hence, the concentration gradient is constant and Γ increases linearly in time. Also, *PEO* hardly desorbs upon rinsing. The concentration gradient ($c_\mathrm{b} - c_\mathrm{s} = -c_\mathrm{s}$ for this case) is too small to observe desorption on laboratory timescales.[16,48,50]

With respect to the polymer, surfactants display a number of important differences in adsorption behaviour. An example of a surfactant adsorption experiment is given in Figure 3.3. In this figure the surface excess is plotted as a function of time. The three adsorption/desorption cycles represent respectively $C_{16}E_7$, $C_{14}E_7$ and $C_{12}E_7$. The period where the surfactant bulk concentration is nonzero is marked with gray shading. When compared with polymer, the first difference is the magnitude of the surface excess at equilibrium. For the surfactants and polymers used here, the surfactants adsorb to a surface excess $\tilde{\Gamma}$ at least three times higher than the polymer. The second difference is that surfactants readily desorb upon rinsing with solvent.

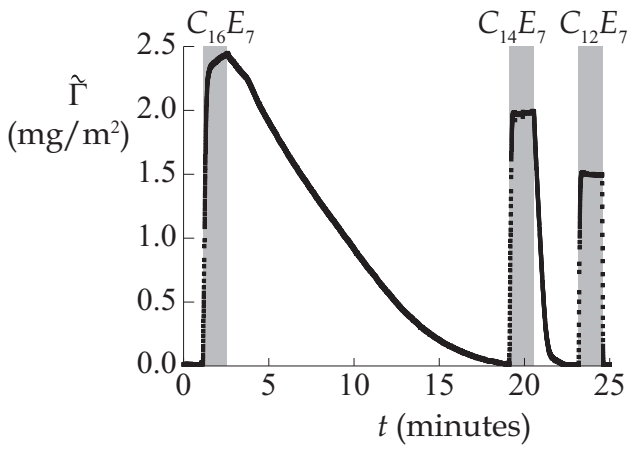

Figure 3.3: *The adsorbed amounts in mg/m^2 of $C_{16}E_7$, $C_{14}E_7$ and $C_{12}E_7$ as a function of time in minutes. The gray shaded areas indicate a nonzero bulk surfactant concentration (type of surfactant is indicated). As mentioned before, to calculate the surface excess we used $dn/dc = 0.136$, which implies a minimal error.*

In Figure 3.4, the surface excess of a surfactant as a function of the bulk concentration is shown. This type of sigmoidal shaped isotherm is characteristic for nonionic surfactant adsorption. The concentration where adsorption increases steeply is called **c**ritical **s**urface **a**ssociation **c**oncentration or $CSAC$ after Tiberg *et alia*.[32]

As a rule of thumb, the $CSAC$ is approximately equal to $0.7\times CMC$.[32] Tiberg *et al*. assumed that surfactant adsorption is transport limited.[51] If this assumption is made, the adsorption kinetics can be understood by the local equilibrium concept. Clearly, adsorption only occurs if the isotherm deviates from zero, which is above the $CSAC$ for our case. The difference between the $CSAC$ and the bulk concentration determines the rate of adsorption. However, there is one complicating factor: above the CMC, surfactants form micelles. If it is assumed that all micelles are of the same size at every concentration, and thus that the concentration of individual surfactant molecules (unimers) has the CMC as an upper bound, the adsorption kinetics for our stagnation point flow regime is described by:

$$J_{\text{ads}} = k_{\text{tr,uni}}(CMC - CSAC) + k_{\text{tr,mic}}N(c_{\text{bulk}} - CMC) \qquad (3.2)$$

In Eqn. 3.2, N is the aggregation number, $k_{\text{tr,uni}}$ is the transport coefficient for unimers and $k_{\text{tr,mic}}$ is that for micelles. For our stagnation point setup, we can calculate these coefficients using an equation published by Dabros and van der Ven (see chapter 2.2).[42] Following this equation, k_{tr} scales with the unimer or micelle size according to: $k_{\text{tr}} \sim R^{-2/3}$, where R is the diffusion

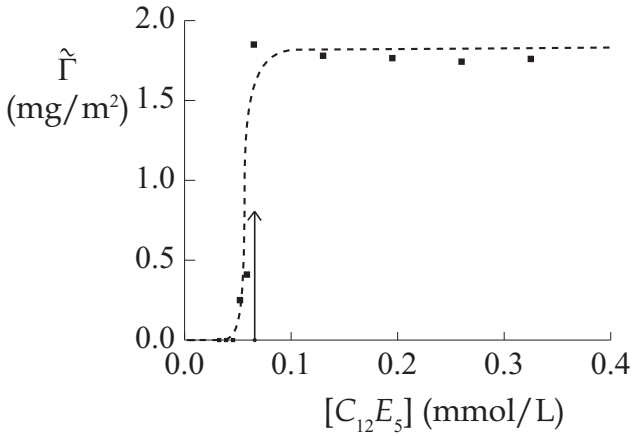

Figure 3.4: *Adsorbed amount in mg/m^2 of $C_{12}E_5$ as a function of the bulk concentration of $C_{12}E_5$ in mmol/l (adsorption isotherm). The arrow denotes the CMC.*

radius of the surfactant unimer or that of the micelle. For our setup $k_{\mathrm{tr,uni}}$ is typically $4 \cdot 10^{-10}$ m s^{-1} and $k_{\mathrm{tr,mic}}$ is in the order of 10^{-11} m s^{-1}, depending on micellar size (see table 3.2).

Using the concept of local equilibrium and the surfactant adsorption isotherm (Fig. 3.4), it is easy to understand that surfactants will desorb upon rinsing with pure solvent. On the basis of this concept and realising $c_{\mathrm{b}} = 0$ and $c_{\mathrm{s}} = CSAC$, the desorption kinetics can be described by:

$$J_{\mathrm{des}} = -k_{\mathrm{tr,uni}} CSAC \tag{3.3}$$

The differences in desorption kinetics between surfactants in Figure 3.3 can be explained by realizing that the CMC, and thus the $CSAC$, decreases strongly with increasing surfactant tail length.

There is a number of different methods to study competitive adsorption. One could, for instance, prepare mixtures of polymers and surfactants, and then try to adsorb both species simultaneously. Another method is to first coat a surface with component A, and then try to displace component A with component B. These two cases we will call respectively simultaneous and sequential adsorption.

In Figure 3.5a, we show the surface excess as a function of time in an experiment where we supply the polymer and the surfactant sequentially. The light gray area corresponds to a non-zero polymer concentration, and the darker gray area to a non-zero surfactant concentration. At $t \approx 2.5$ minutes polymer adsorption starts. At $t \approx 4$ minutes a switch is turned which causes the bulk polymer concentration to drop to zero and the bulk surfactant concentration to rise to 1×10^{-4} M. When the surfactant molecules reach the

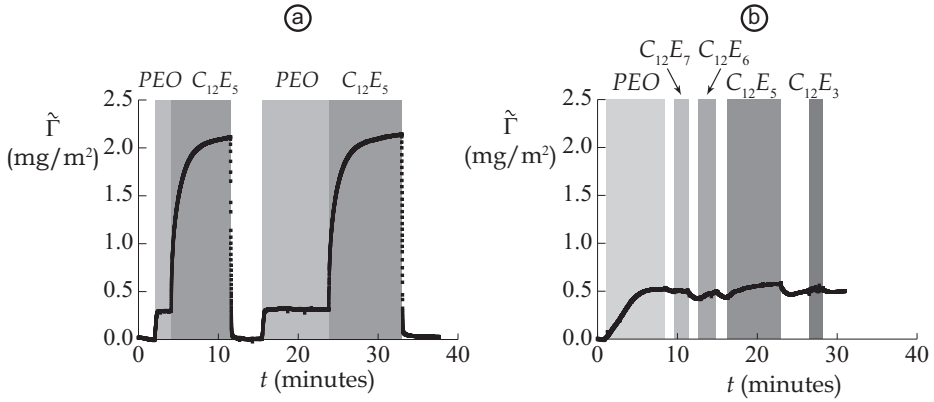

Figure 3.5: *The surface excess versus time in a displacement experiment. In a) PEO M_w = 26840 g/mol, indicated by the dark gray colour, is displaced by $C_{12}E_5$. This cycle is repeated twice. In b) an attempt is made to displace PEO M_w = 167700 g/mol with a four different surfactants.*

surface, the total surface excess increases due to adsorption of surfactant molecules. Since our experiment is sensitive to refractive index effects only, we cannot discriminate between surfactants displacing the adsorbed polymer and surfactants adsorbing on the polymer layer. Hence, at this point we cannot yet decide what the surface composition is. However, at $t \approx 12$ minutes the surfactant solution flowing through the flowcell is replaced by pure solvent. It can be seen that the surface excess drops to zero, which is typical surfactant behaviour. Based on this behaviour, we conclude with certainty that the surface before the rinsing step was covered by surfactants only and thus that the polymer had been displaced by the surfactant. The second adsorption cycle in Figure 3.5a is identical to the first, with the exception that the polymer layer has had more time to relax (500 instead of 150 seconds). The kinetics of displacement is the same for both cases, thus we conclude that polymer relaxation is not an important parameter. We have done experiments where we allowed the polymer to relax for various times up to 17 hours (not shown), and we did not find any change in displacement kinetics. From the lack of difference in displacement kinetics, we conclude that, even at short equilibration times, the polymer layer is in equilibrium.

Figure 3.5b gives another scenario that can occur with sequential adsorption. Here, first *PEO* with a molecular weight of 167700 g/mol is adsorbed onto a silica surface. Next we try to displace the polymer by subsequently using $C_{12}E_7$ ($t \approx 10$ minutes), $C_{12}E_6$ ($t \approx 13$ minutes), $C_{12}E_5$ ($t \approx 16$ minutes) and $C_{12}E_3$ ($t \approx 27$ minutes). Between the surfactant adsorption steps, the flowcell was rinsed with solvent. Although there are some minor disturbances

	Polymer molar mass (g/mol)						
	4250	12600	20360	28640	43520	82250	167700
$C_{12}E_3$	y	n	n	n	n	n	n
$C_{12}E_5$	y	y	y	y	y	n	n
$C_{12}E_6$	y	n	n	n	n	n	n
$C_{12}E_7$	y	n	n	n	n	n	n
$C_{14}E_7$	y	y	y/n	n	n	n	n
$C_{16}E_7$	y	y	y	y	y	y/n	n

Table 3.4: *Systematic overview indicating the displacement capabilities per surfactant. A (y) indicates that the surfactant can displace the polymer, and a (n) indicates that the polymer can displace the surfactant. The two cases, where we could not determine what species preferentially adsorbed, are denoted with (y/n).*

in the adsorbed amount, the surfactant is apparently not able to displace the polymer.

Using the method of sequential adsorption/desorption cycles described above, a set of experiments with different types of surfactants and different polymer lengths has been performed, where we investigated whether the surfactant was capable of displacing the polymer (y) or not (n), or whether the situation would seem intermediate (y/n). For these experiments, we have chosen to use a surfactant concentration of 1.00×10^{-4} M except for the $C_{12}E_3$. For this surfactant a concentration of 6.00×10^{-5} M was chosen because above this concentration we experienced problems with its solubility. The results of this set of experiments can be found in Table 3.4.

Every surfactant can displace PEO up to a certain molar mass, called the critical molar mass. In Table 3.4, we show that all surfactants studied here can displace low molecular weight polymer ($M_w = 4250$ g/mol), and none of the surfactants can displace polymer with a high molar mass ($M_w = 167700$ g/mol). We also show that the critical molar mass is higher for $C_{12}E_5$ and $C_{16}E_7$ than for the other surfactants.

Two special cases, denoted by "y/n", where neither the polymer, nor the surfactant can displace the other, are found. We can identify these special cases by determining that our surfactant does cause an increase of the surface excess if it is allowed to adsorb on a surface covered by the polymer, but the equilibrium adsorbed amount will be lower than the equilibrium adsorbed amount found in single component surfactant experiments. Furthermore, upon subsequent rinsing with solvent, part of the surface excess will desorb, but also a part of the surface excess will remain. We assume that surface excess after rinsing consists only of polymers, and all the adsorbed surfactants have desorbed. Using our experimental setup, it is, however, not possible to

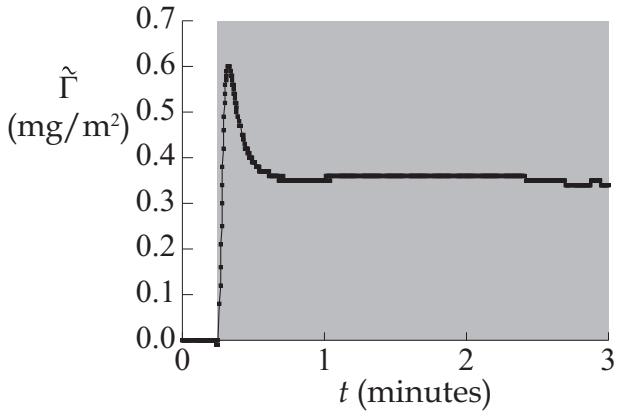

Figure 3.6: *Surface excess of PEO Mw = 28640 g/mol and $C_{14}E_7$ versus time in a displacement experiment.*

determine the composition or structure of the adsorbed layer.

For the two cases where we observed incomplete displacement, we tried to displace the polymer using a surfactant solution with a 30 times higher concentration namely 3.00×10^{-3} M. In both cases this was successful, i.e. the polymer was entirely displaced from the surface by the surfactant, proving not only that the surfactant type, but also that the surfactant concentration is an important parameter.

We have also performed a number of simultaneous adsorption experiments. For this purpose, mixed solutions were prepared and polymer and surfactant were simultaneously adsorbed. An example where the polymer can displace the surfactant is given in Figure 3.6. At $t \approx 0.2$ minutes, flow is switched to a mixture of a polymer and a surfactant, as indicated by the gray shaded area.

In this case, the polymer can displace the surfactant from the surface. However, because the surfactant molecules are smaller than the polymer molecules, the surfactant arrives at the surface first, and starts populating the surface. When the polymer reaches the surface, it sees a surface partially covered with surfactants. Since the polymer can displace the surfactant, the surfactant will desorb as the polymer adsorbs. This causes the overshoot in the $\tilde{\Gamma}(t)$ graph. From this example it is clear that simultaneous adsorption experiments of species with different diffusion coefficients are in fact a special type of sequential adsorption experiments.

For all the simultaneous adsorption experiments, the results were consistent with those from our sequential adsorption experiments. From this we conclude that in this system the order of addition is not important, or that the structure of the adsorbed layer at the end of the experiment is not a

function of the path followed. This can be interpreted as another indication that the adsorbed polymer layer is in equilibrium.

3.4 Discussion

For our system, where polymers and surfactants bind by the same sort of bond, we find that every type of surfactant can displace a polymer up to a certain critical molar mass (see Table 3.4). We expect that surfactants form layers totally different from those of polymers. To understand what species will adsorb favourably from a certain polymer-surfactant mixture, one can use the powerful machinery of thermodynamics to determine what scenario has the lowest energy, and will thus be the equilibrium configuration. The best way to do this is to calculate some key thermodynamic parameter such as the surface pressure due to polymer or surfactant adsorption.

3.4.1 Surfactants

It is instructive to first have a look at surfactants alone, and explain why $C_{12}E_5$ and $C_{16}E_7$ are better displacers than the other surfactants. One could try to displace one surfactant with the other to determine which of the two adsorbs most favourable. However, this is not possible because two-component surfactant solutions form mixed micelles in the bulk and form, after adsorption, a mixed layer on the surface.[52]

In Table 3.2, the hydrodynamic radius, R_h, as measured by DLS, is presented. We neglect $C_{12}E_3$ for now, because it has a very low cloudpoint. Because of the low cloudpoint, we could not determine its micellar size nor could we make transparent solutions of the same concentrations as the other surfactant solutions. We can see that the best displacers, $C_{12}E_5$ and $C_{16}E_7$, form significantly larger micelles, and thus have a significantly higher aggregation number, than the other surfactants. The equilibrium adsorbed amount for bulk concentrations above the CMC, Γ, is also presented in Table 3.2. Both $C_{12}E_5$ and $C_{16}E_7$ adsorb to reasonably high amounts.

AFM studies have shown that $C_{12}E_5$ and $C_{14}E_6$ form continuous layers on hydrophilic silica.[53] We expect that $C_{16}E_7$ also forms sort of a continuous layer on silica. So, we conclude that good displacers form large micelles in bulk, adsorb to relatively high amounts and form homogeneous layers on the surface. This applies to surfactants that have a head group which is relatively small compared to the size of the tail group, but which is large enough to generate the required adsorption energy.

To calculate the surface pressure associated with surfactant adsorption,

we can use the interfacial variant of the Gibbs-Duhem relation called the Gibbs adsorption equation:

$$\mathrm{d}\gamma = \mathrm{S}_a^\sigma \mathrm{d}T - \sum_i \Gamma_i \mathrm{d}\mu_i \tag{3.4}$$

In our case, the temperature is fixed and we only have one type of surfactant. If we use $\mu = \mu_0 + RT\ln c$, we can rewrite Eqn. 3.4 to:

$$\mathrm{d}\gamma = -\Gamma \mathrm{d}\mu = -RT\Gamma \mathrm{d}(\ln c) \tag{3.5}$$

or

$$\pi = -\int_{\gamma(c=0)}^{\gamma(c^*)} \mathrm{d}\gamma = \int_0^{c^*} RT\Gamma \mathrm{d}(\ln c) \tag{3.6}$$

where c^* is the concentration that we are interested in and π is the surface pressure at c^*. To a first approximation, the adsorption isotherm of a nonionic surfactant is a step function. In this analysis, the adsorbed amount is zero for all concentrations smaller than the $CSAC$ and equal to Γ for all concentrations higher than the $CSAC$. Furthermore, also in a first order approximation, the chemical potential of the surfactant is constant for concentrations larger than the CMC. Using these assumptions, we can write Eqn. 3.6 as:

$$\begin{aligned} \pi &= RT\Gamma \int_{CSAC}^{CMC} \mathrm{d}(\ln c) = RT\Gamma \left[\ln CMC - \ln CSAC\right] \\ &= RT\Gamma \ln\left(\frac{CMC}{CSAC}\right) \end{aligned} \tag{3.7}$$

According to Eqn. 3.7, the surface pressure caused by absorbing surfactants is a function of the adsorbed amount, Γ, and of the ratio of the CMC and the $CSAC$. In Table 3.2, we present the adsorbed amount for surfactants at bulk concentrations higher than the CMC. We notice that as a trend, surfactants tend to adsorb less as the head group size increases, or as the surfactant as a whole becomes more hydrophilic. It is more difficult to obtain a precise value for the $CSAC$, because it is very sensitive for small changes in experimental parameters. However, from our experiments, we do know that for our nonionic surfactants $CSAC \approx 0.7\text{-}0.8 \times CMC$.

Because our surfactants bind to the surface with their headgroups, one can easily imagine that a surfactant with a large headgroup has a $CSAC$ that is relatively far from the CMC as compared to a surfactant with a smaller headgroup. So, a surfactant that is a good displacer, has a head group that is small enough to get a high adsorbed amount, but large enough to have ample adsorption energy.

Another way to look at the surface pressure is to consider the number of adsorbed *EO*-groups, instead of the number of adsorbed molecules. This method assumes that π is dominated by interaction energies rather than by the entropy. In Table 3.2, an estimate of the density of adsorbed *EO*-groups is given. To calculate the density, we assumed that the surfactants adsorb in a bilayer, thus that the density of *EO*-groups near the surface is half the total number of adsorbed *E*O-groups. We see that $C_{12}E_5$ and $C_{16}E_7$ have the highest density of *EO*-groups near the surface, which correlates well with our displacement results (see Table 3.4). Hence, π probably correlates with $\rho_{EO,bilayer}$.

In Table 3.4, two special cases were identified (denoted with y/n) where the surfactant and the polymer formed mixed layers. We also found that, if the surfactant concentration was raised 30-fold, the surfactant was able to displace the polymer. We can understand this using the more sophisticated model for the formation of micelles that was introduced in chapter 1.2.1.

In this model, the micelles are in equilibrium with the unimers, and increasing the surfactant concentration will cause the number of micelles to increase. However, the number of unimers will also increase a little, and if the surfactant concentration is raised 30-fold, the unimer concentration will be a bit higher.

So, it is possible to increase the unimer concentration, and thus the chemical potential, by a small amount. In our cases where we found intermediate displacement results, this small increase in surfactant unimer concentration causes a small increment in surfactant surface pressure (Eqn. 3.6), and the surfactant will be able to displace the polymer.

3.4.2 Polymers

Although the nature of the adsorbate/substrate interactions are the same for the polymers and the surfactants, the layers formed on the surface are very different in structure. Polymers generally adsorb in trains, loops and tails, whereas surfactants form a fragmented bilayer (see chapter 1).[17,32]

To understand which polymer binds favourably, we would like to obtain the surface pressure associated with polymer adsorption. To determine the surface pressure from the Gibbs equation (Eqn. 3.4), one needs to know the entire isotherm. This is very hard to measure experimentally because one would need to measure at incredibly low concentrations.

We can use the Gibbs adsorption equation to understand what happens to the surface tension if the bulk concentration of the polymer is raised. This effectively implies that the integration will be over a larger part of a non-negative function, thus the surface pressure is always larger for higher bulk

M_w (g/mol)	$\tilde{\Gamma}_{EO,\text{exp}}$ mg/m^2	$\rho_{EO,\text{exp}}$ EO/nm^2	$\tilde{\Gamma}_{EO,\text{fit}}$ mg/m^2	$\rho_{EO,\text{fit}}$ EO/nm^2
4250	0.17	2.33	0.16	2.19
12600	0.24	3.28	0.25	3.45
20360	0.30	4.10	0.29	4.01
26840	0.35	4.79	0.31	4.33
43520	0.30	4.10	0.35	4.89
82250	0.40	5.47	0.41	5.63
167700	0.50	6.84	0.47	6.46

Table 3.5: *Adsorbed amount Γ and EO density for the polymers evaluated in this chapter. M_w is the molar mass of the polymer, $\tilde{\Gamma}_{EO,exp}$ is the experimentally found adsorbed amount and $\rho_{EO,exp}$ is the corresponding EO density on the surface. Since there is some scatter on the experimental data, we also fitted a smooth line to the data and present the predicted properties of this smoothing procedure as $\tilde{\Gamma}_{EO,fit}$ and $\rho_{EO,fit}$.*

concentrations.

From literature we know that high molar mass PEO can displace low molar mass PEO.[54,55] This can be explained by realizing that a long polymer chain loses less entropy upon adsorption than two chains of half the length would lose upon adsorption. We can also rephrase these results by saying that high molar mass PEO can induce a higher surface pressure than low molar mass PEO. This corresponds with the experimental observation that low molar mass PEO can be displaced by surfactant, and that high molar mass PEO cannot be displaced.

If we assume, for the sake of our argument, that a polymer adsorbs completely in trains, we can calculate the density of EO-groups on the surface by multiplying the amount adsorbed per area in moles with the number of EO-groups per chain. In Table 3.5, we show our experimental adsorption data. We see that this adsorption data has an increasing trend, but it is not strictly increasing. From literature, we know that the adsorbed amount should be a strictly increasing function of the molecular weight.[48,56] Therefore, we smoothed the data and present this smoothed data as $\tilde{\Gamma}_{EO,\text{fit}}$. In the last column of Table 3.5, we calculated EO-group density based upon the smoothed adsorbed amount. We see that long polymers, from which we know that they can induce a high surface pressure, have a higher density of EO-groups on the surface than short polymers. We return to the question of the surface pressure of adsorbing polymers in chapter 5.

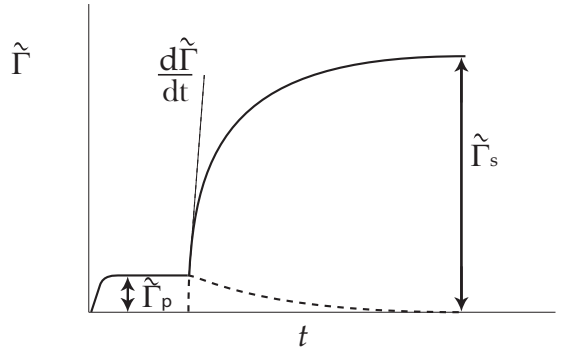

Figure 3.7: *Schematic representation of a surfactant displacing a polymer. The experimentally observed rate of displacement is the sum of the rate of surfactant adsorbing and the rate of polymers desorbing.*

3.4.3 Polymers and surfactants

If a mixture of a polymer and a surfactant is brought into contact with a hydrophilic surface, only one component will adsorb. This will be the component that causes the largest decrease in free energy, which is equivalent to saying that the component that induces the highest surface pressure will adsorb.

For both the polymer and the surfactant it is quite difficult to calculate the surface pressure using the Gibbs adsorption equation. We can however compare the densities of *EO*-groups on the surface, by comparing Table 3.2 and 3.5. Based on this comparison, we can say that PEO with a molecular weight greater than 167700 g/mol can displace $C_{12}E_6$, $C_{12}E_7$ and $C_{14}E_7$. This trend corresponds with our displacement results (Table 3.4). However, the absolute value of the polymer critical molar mass is approximately an order of magnitude too high. From this comparison we can deduce that for our experimental system at the concentrations used, we are in the competitive adsorption regime, where small differences in experimental parameters make a big difference in the experimental results.

3.4.4 Kinetics of displacement

If a surfactant can displace a polymer, there is an associated rate of displacement. Experimentally, this rate is not directly available, because the increase of surface excess in time, is the sum of surfactant and polymer adsorption (see Figure 3.7).

$$\frac{d\tilde{\Gamma}_e}{dt} = \frac{d\tilde{\Gamma}_s}{dt} + \frac{d\tilde{\Gamma}_p}{dt} \tag{3.8}$$

As the surfactant is populating the surface, the polymer is leaving. If it is assumed that the timescale associated with polymer desorption is approximately equal to the timescale associated with the surfactant adsorption, we can write the polymer desorption rate in terms of the experimentally observed adsorption rate.

$$\frac{\mathrm{d}\tilde{\Gamma}_\mathrm{p}}{\mathrm{d}t} = -\frac{\tilde{\Gamma}_\mathrm{p}}{\tilde{\Gamma}_\mathrm{s}}\frac{\mathrm{d}\tilde{\Gamma}_\mathrm{e}}{\mathrm{d}t} \tag{3.9}$$

By combining Eqn. 3.8 with Eqn. 3.9 we can, after rewriting, obtain:

$$\frac{\mathrm{d}\tilde{\Gamma}_\mathrm{s}}{\mathrm{d}t} = \left(1 + \frac{\tilde{\Gamma}_\mathrm{p}}{\tilde{\Gamma}_\mathrm{s}}\right)\frac{\mathrm{d}\tilde{\Gamma}_\mathrm{e}}{\mathrm{d}t} \tag{3.10}$$

Eqn. 3.10 shows that the surfactant adsorption rate, $\frac{\mathrm{d}\tilde{\Gamma}_\mathrm{s}}{\mathrm{d}t}$ is higher than the experimentally observed rate, $\frac{\mathrm{d}\tilde{\Gamma}_\mathrm{e}}{\mathrm{d}t}$, because the polymer is simultaneously desorbing.

In Figure 3.8 we present the desorption kinetics for $C_{12}E_5$ and $C_{16}E_7$. To understand these results, we look at Eqn. 3.2. In this equation, almost all variables are surfactant bulk parameters. The only surface parameter is the $CSAC$. Therefore, it seems naturally to attribute the drop in adsorption kinetics to a shift in the $CSAC$. We can think of the $CSAC$ as a function of the molar mass of the polymer on the surface. As the molar mass of the polymer that is displaced increases, the adsorption rate for the surfactant first drops quickly, but levels off as the $CSAC$ comes close to the CMC. At the point where the $CSAC$ and the CMC are equal, the desorption rate is zero.

Note that the two curves in Figure 3.8 both go to zero at a polymer molar mass of 82250 g/mol. Most likely, the critical molar mass will be somewhat lower for both cases. From our data we can just conclude that the critical molar mass is not higher than 82250 g/mol. Most likely, the critical molar mass for $C_{12}E_5$ and $C_{16}E_7$ are not equal.

In Figure 3.8, we see that the $C_{16}E_7$ curve drops more steeply than the $C_{12}E_5$ curve. We can speculate about the reason for this by considering the adsorption mechanism. In Eqn. 3.2, the rate of surfactant adsorption is split into an unimer and a micellar contribution. The CMCs of $C_{12}E_5$ and $C_{16}E_7$ are quite different (see Table 3.2), but we did all experiments at a concentration of $c = 1{\cdot}10^{-4}$M. Therefore, the relative contribution of micelles to the initial adsorption rate is much larger for $C_{16}E_7$ than for $C_{12}E_5$. We also know that for a surface with adsorbed PEO, the coverage is an increasing function of the molar mass. It seems quite plausible that the adsorption rate of micelles (or in any case aggregates of unimers) is much more sensitive to

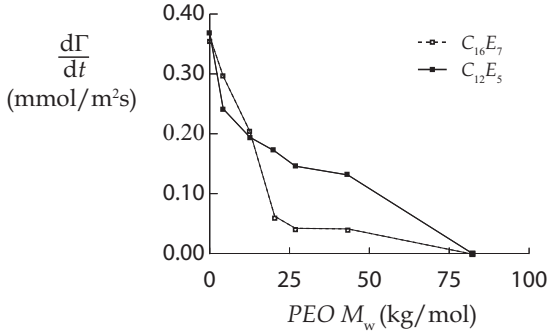

Figure 3.8: *The rate of displacement plotted versus the molar mass of the displaced polymer for $C_{12}E_5$ and $C_{16}E_7$.*

the surface coverage than that of unimers, because micelles need a relatively large 'clean' area to adsorb whereas unimers only need a small clean patch. Therefore, the kinetics of $C_{16}E_7$ is much more sensitive for adsorbed polymer and, hence, its adsorption rate drops more steeply, than that of $C_{12}E_5$.

3.4.5 Kinetics and equilibrium combined

A surfactant can displace polymer up to the critical molecular weight. As the polymer molar mass approaches the critical molecular weight, the rate of adsorption decreases until it becomes zero at the critical molar mass.

We can explain the existence of a critical molar mass by looking at the Gibbs adsorption equation (Eqn. 3.7), and allowing the $CSAC$ to be a function of the molar mass of the polymer that has to be displaced. If a surfactant needs to displace an adsorbed polymer layer in order to adsorb, the surfactant needs to overcome the energy the polymer loses by desorbing. The chemical potential that a surfactant has at the $CSAC$ is just sufficient to let the surfactant adsorb. If, compared to a clean surface, there is an extra barrier in the form of a polymer layer, the surfactant needs a higher chemical potential to adsorb. Hence, the polymer layer causes the $CSAC$ to shift towards a higher concentration, e.g. to the CMC. At some point, a polymer which is long enough causes the $CSAC$ to be higher than the CMC. In this case, the surfactant will not be able to displace the polymer anymore. The polymer molar mass at which the $CSAC$ is equal to the CMC is called the critical molar mass.

The decrease in adsorption kinetics for a surfactant displacing polymer of increasing molar mass can also be understood by a shift in the $CSAC$. The adsorption kinetics for surfactants is described by Eqn. 3.2. If the difference between the $CSAC$ and the CMC decreases, the contribution of unimers to

the adsorption kinetics decreases.

All our measurements have been carried out above the CMC, and thus the micellar contribution is also important. However, we know that the EO-groups repel each other in our system, and therefore we cannot expect an intact micelle to adsorb on a surface which is covered by PEO. Only surfactant unimers are small enough to penetrate into the polymer layer and adsorb onto the surface. Therefore, the contribution of micelles to the kinetics of displacement is small if the surface is covered by PEO. Hence, the kinetics of displacement is mainly governed by the difference between the $CSAC$ and the CMC. In chapter 7.4 we propose a slightly altered model that takes this behaviour into account.

3.5 Conclusions

The nonionic polymer PEO, and the nonionic surfactant C_nE_m, both readily adsorb onto silica from individual solutions. In mixtures, the components do not associate in bulk solution.

When a certain polymer-surfactant mixture is allowed to adsorb onto a hydrophilic silica surface, only one component adsorbs. All surfactants studied here can displace the shortest PEO ($M_\mathrm{w} = 4250$ g/mol), but none can displace the largest PEO ($M_\mathrm{w} = 167700$ g/mol). The largest PEO chain that a certain surfactant can displace is called the critical molecular weight. The location of the critical molar mass varies per surfactant.

Experimentally we have found that $C_{12}E_5$ and $C_{16}E_7$ can displace longer PEO chains than the other surfactants. We know that, in bulk, these two surfactants form larger micelles than the other surfactants, and the surface excess at the CMC at equilibrium is rather high.

To predict what component will adsorb from a mixed solution, one needs to calculate some key thermodynamic parameter in order to establish what configuration will energetically be most favourable. A good choice would be to look at the surface pressure. This quantity is not experimentally accessible for a solid-liquid interface, but can be calculated using the Gibbs adsorption equation.

Differences in surface pressure due to surfactant adsorption are very small between different types of surfactants. Therefore, the Gibbs equation can only be used if the adsorption isotherm is known very precisely. Using our experimental results, it was not possible to calculate the surface pressure using this method. We did find that the density of EO-groups on the surface correlates well with the displacement results. Furthermore, if the surfactant bulk concentration is raised, the surfactant will be able to cause a higher

surface pressure and thus it can displace longer polymers.

To calculate the surface pressure caused by polymer adsorption, one needs to know the entire isotherm. This is nearly impossible, because even at extremely low concentrations, polymers still have a significant surface excess. We can understand from the Gibbs adsorption equation that polymers adsorbing from higher polymer bulk concentrations can cause a higher surface pressure, and are therefore harder to displace. Also, from results published by others, we can deduce that longer polymers can exhibit a higher surface pressure, and are thus harder to displace.

We can understand both the existence of the critical molecular weight and the decrease in kinetics with increasing molecular weight, by allowing the $CSAC$ to be a function of the molecular weight of the polymer that the surfactant needs to displace in order to adsorb. The adsorbing surfactant needs to compensate for the unfavourable polymer desorption. This is an extra adsorption barrier, that the surfactant can only overcome at a higher chemical potential, and thus at a higher concentration. Therefore, the $CSAC$ shifts to a higher concentration. The polymer molar mass that causes the $CSAC$ to become equal to the CMC, is called the critical molar mass.

The Gibbs adsorption equation states that the driving force for adsorption is a function of the logarithm of $(CMC/CSAC)$. At the critical molar mass, this is equal to zero, which implies that there is no driving force for adsorption.

According to the local equilibrium concept, the kinetics of adsorption/ desorption is a function of $CMC-CSAC$. Since this property decreases upon increment of the molar mass of the polymer that is displaced, the kinetics of displacement decrease as the molar mass of the polymer increases.

Chapter 4

Self-Consistent Field Model

This chapter describes the development of a self-consistent field model that can be used to make predictions about the behaviour of a polymer/surfactant mixture. The modelled system is described in a molecular realistic manner and we explicitly account for the pH and the ionic strength. The model can be used to evaluate the bulk behaviour of a system and obtain information such a the phase behaviour of a polymer, the scaling of the polymer coil size as a function of its length, the surfactant micellar concentration (CMC), the surfactant aggregation number, etcetera. It is also possible to use the model for adsorption calculations. We then introduce a flat surface, which has a charge that depends on the pH. In this case, the model can predict the adsorbed amount of a polymer as a function of its length or the bulk concentration, or we can predict the adsorbed amount of a surfactant as a function of the surfactant architecture or the bulk concentration. Since we have taken the pH and the ionic strength explicitly into account, we can also study the response of the system upon changing these variables.

In the next paragraph of this chapter, we present some of the thoughts that we had before we started to develop the model. We then proceed to shed some light on the self-consistent field theory, where we mention the most important equations and its main approximations. Next, we describe our model and mention all parameters involved. To interpret the outcome of the calculations on the behaviour of surfactants, a special extension of thermodynamics called "the thermodynamics of small systems" is needed. The last section of this chapter discusses this extension.

4.1 Introduction

To better understand the experimental results described in Chapter 3, we have modelled aqueous solutions of water-soluble nonionic polymer and nonionic surfactant in contact with a surface that is charged depending on pH and salt concentration. One of the complicating issues with this system is that string-like molecules can take a large number of different conformations that intricately depend on the interactions with the surface and with all the other molecular components. One typically uses computer simulations to predict the relevant interfacial behaviour for such complicated systems. However, in all-atom computer simulations, the vast number of different molecules and corresponding conformations pose a serious problem even for the fastest computers. A pragmatic route to overcome some of these computational difficulties is to drop non-relevant degrees of freedom by describing the system on a course grained level. However, in such a procedure it is hard to describe polymers as well as the charged interface in combination with its electric double layer in sufficient detail.

We have chosen to use a self-consistent field (SCF, also called mean field) approach, to come up with some sort of intermediate model. At the basis of the mean field approximation, the binary interactions between pairs of particles are replaced by an average, so-called self-consistent potential field that is probed by the particles. Unfortunately, also on the SCF-level there are no analytical solutions. However, the computer power needed to solve the equations numerically is orders less compared to simulations. Since for a SCF solution the (mean field) free energy is available, one can directly find a large number of observables, such as the adsorbed amount, molecular distributions, etcetera.

Because of the many repeating units in the polymer chains, it is believed that sufficiently long polymers must feature generic behavior.[21] Polymer solution theory as well as polymer adsorption models have made extensive use of this insight. From an experimental point of view, however, it is known that each new polymer has its own unique features, strongly suggesting that for some of the properties the chemistry matters. At present, little is known about how and when molecular features present themselves and to what extent they disturb (hide) the generic effects. To improve this situation it is necessary to elaborate on statistical thermodynamical theories that can account for the molecular details, but are still coarse enough for universal features to be studied as well. Self-consistent field (SCF) theories have been used extensively to investigate the generic features of polymers at interfaces using simplified models for the polymer chain. However in principle one can introduce extra details in these models to account for some of the chemistry

on a monomeric level. It is also possible to describe systems containing surfactants using SCF theory. Since surfactants are relatively small molecules containing (at least) two different domains, surfactant are described in more detail compared to polymers. Because our surfactants consist of the same atoms as our polymers, it is possible to describe both species with a limited number of segments, and hence a limited number of interaction parameters (some of which can be found in literature.[28] Such a molecularly realistic SCF model is the method of choice to bridge the gap between chemistry and physics in polymer and surfactant adsorption theory.

As stated, generic models pay little attention to the adsorption mechanism. Typically, one introduces an effective adsorption parameter and ignores the details. In this work, we are interested in surfactants and water-soluble polymers adsorbing onto inorganic colloidal particles. Because water has a high diëlectric constant, it is favourable for many colloidal systems to develop some charges on the surface. This also applies to the case of silica. Because PEO and C_nE_m are not charged, one may argue that to first order the fact that the surface is charged is unimportant. However, experimental evidence is mounting that this is a dangerous approximation and that it does matter.[57–59]

The literature data on the effect of salt on the adsorption of PEO, C_nE_m, or comparable molecules on silica seems to be inconsistent. There are reports on the Pluronic F127 and on comb molecules with PEO side chains, that both adsorb by forming H-bonds between EO groups and silanol groups, stating that adsorption on a silica wafer decreases as a function of $NaCl$ concentration.[57,58] However, it has also been reported that a tiny amount of salt ($\approx 1mM$) can actually increase the adsorbed amount of PEO on silica.[59]

In a molecular model, we will need to account for the fact that the surface charge is not fixed but depends on the ionic strength and pH.[47,60] This is particularly important for EO groups that adsorbs by the formation of hydrogen bonds with undissociated silanol groups.[61–63]

At low ionic strength, water is a good solvent for PEO, and hence also for the C_nE_m head groups. However, as the ionic strength increases, the quality of the solvent decreases.[64,65] It was mentioned in chapter 1.1.2 that a decrease in solvent quality promotes high adsorbed amounts.[66] On a silica surface there are groups that dissociate depending on the pH. Because the adsorption mechanism of EO on the silica surface is expected to involve H-bonds with undissociated silanol groups,[62,63] the attraction between the surface and the polymer is pH dependant. Furthermore, the dissociated surface is negatively charged. Because the overall system must remain electroneutral, the charge of the surface must always be balanced by a layer with a positive excess of counter ions and a negative excess of co-ions. Therefore,

the surface charge and the number and type of ions near the surface, also depends on the pH. If we try to adsorb PEO or C_nE_m onto a charged surface, then there will be a competition between the polymer/surfactant and the ions for the space near the surface; therefore, ions can (partly) inhibit polymer/surfactant adsorption as well or vice versa. So, the addition of salt can either promote or inhibit the adsorption of other species. Using our model, we can evaluate the effects of these opposing trends that present themselves as a logical consequence of introducing molecular details into the SCF model.

4.2 Self-Consistent Field Theory

In a self-consistent field calculation, all interactions between the molecules in the system are replaced by the interactions felt by the test-molecule in an external (self-consistent) potential field. In fact, the potential field is chosen in such a way that it represents the vast body of molecules in which our test-molecule is embedded. Typically, we are not so much interested in one particular conformation of the test molecule, but rather in the ensemble averaged (most-likely) conformations. These average conformations result in volume fraction profiles. This means that we have potentials u on the one hand and corresponding volume fractions φ on the other hand. The optimisation of the mean-field free energy uses the potentials u^i of all segments of all molecules as an input to calculate the respective volume fractions φ^o. These volume fractions are now used as an input for another independent free-energy optimisation that has the potentials u^o as output. When the calculated potentials u^o are numerically equal to the starting potentials u^i, the field is called consistent and a solution to the problem has been found, in other words, the free energy is optimised. If these two potentials are not similar, a numerical procedure is started to search for such self-consistent condition. Usually, this takes a number (order 100) of iterations. Details of this procedure are described by Evers et al.[67] This procedure leads typically to very accurate SCF profiles with at least 7 significant digits. In this thesis, we used the method of Scheutjens and Fleer, who suggested to represent the polymers as a linear string of segments. These segments have to be placed on a discrete set of coordinates, also called a lattice. Even though the details can be found in various publications, we will review its basic assumptions in this chapter.[17,68,69]

Again, the SCF calculations require a discretised space also called a lattice. Below we have used two types of lattices. For the adsorption calculations, we have implemented a flat lattice, which consists of a finite number of parallel layers of thickness l bounded on one side by a solid impenetrable

surface. This is implemented by adsorbing boundary conditions. At the solution side, the bulk solution is present and to prevent conformational artifact the system boundary is taken to be reflecting. For a flat lattice, the number of lattice sites in each layer is constant, that is, $L(z) = L^d$, where $d = 0$.

To model the bulk properties of the PEO or C_nE_m, we have used a spherical coordinate system of M layers. In this case, the layers are actually consecutive spherical shells of decreasing curvature, but with a fixed thickness l. The volume of shell $V(z)$ with $z = 1, \ldots, M$ is $V(z) = 4/3\pi[(z+1)^3 - z^3]$ where z is the inner radius of the shell (in units of l). As the volume of one lattice-site is always l^3, the number of lattice sites $L(z)$ within a layer z increases as the layer is further from the center, approximately as $L(z) \propto z^d$, where $d = 2$. The molecules have segments that fit on the lattice. For a given molecule, the segments have ranking numbers $s = 1, \ldots, N$, where N is the number of segments in the molecule. For monomeric species $N = 1$. For each segment in the molecule, the segment type is fixed and specified by the input parameters. Segments can distinguish themselves by a charge, a particular set of interaction parameters and by the diëlectric permittivity. All these properties contribute to the segment potential.

Associated with the lattice, there are the lattice parameters, λ_{-1}, λ_0 and λ_{+1}. These parameters are relevant for computing the segment potentials as well as determining the degeneracy of chain conformations. Taking the chain conformations as an example, the *a priori* chance that segment $s+1$ will be in the same layer as segment s is given by λ_0, the corresponding chance that $s+1$ is in the next layer is λ_{+1}, or when it is in the previous layer it is λ_{-1}. For a cubical isotropic lattice, $\lambda_0 = 4/6$ and $\lambda_{+1} = \lambda_{-1} = 1/6$.[17]

For the spherical coordinate system the λ-parameters are chosen such that they obey the detailed balance equation $L(z)\lambda_{+1}(z) = L(z+1)\lambda_{-1}(z+1)$.

Most calculations in this thesis are using a mean field approximation where there is just one concentration gradient (1G). This means that the potential field, $u(x, y, z)$, which is in its most general form a function of all spatial coordinates, is averaged in the x-y plane such that it only depends on the distance z from the surface, or from the center of the spherical coordinate system. This means that we are doing calculations on a smeared out layer and that we are only investigating the profile perpendicular to the surface. Especially for surfactants that have a tendency to form a fragmented layer, it might pay off to allow for gradients in two directions (2G) and study the inhomogeneous adsorbed state of surfactants at interfaces.[70] The mayor disadvantage of 2G calculations is that they require substantially more computer time.

4.2.1 From volume fractions to potentials

If we assume that, by some method, we know all volume fractions profiles of all segment types in the system, we can calculate the segment potentials in a unique way. Below we will give a brief explanation of how to perform such a calculation.

In the most general case, the potential of a segment A which occurs in (internal) state k in layer z, $u_{Ak}(z)$, consists of an electrostatical component which features the electrostatic potential $\psi(z)$, as in the Poisson-Boltzmann theory. In addition there are several components due to the fact that the segments have volume. The classical PB contribution $u^{\mathrm{PB}}(z)$ is given by

$$u_{Ak}^{\mathrm{PB}}(z) = \nu_{Ak} e \psi(z) \tag{4.1}$$

In this equation, ν_{Ak} is the valence of species A in state k and e is the elementary charge. The electrostatic potential can be calculated using the Poisson equation. We need this equation in either spherical (for which $d = 2$) or in flat (for which $d = 0$) coordinates

$$\frac{1}{z^d}\frac{\partial}{\partial z} z^d \varepsilon(z) \frac{\partial \psi(z)}{\partial z} = -q(z) \tag{4.2}$$

In this equation $\varepsilon(z)$ is the local permittivity and $q(z)$ is the local charge. To calculate the local diëlectric permittivity of a layer, we simply average the permittivities of all species A, weighted by their local volume fractions, $\varphi_A(z)$ ($\varepsilon_{A,k} = \varepsilon_A \forall k$):

$$\varepsilon(z) = \varepsilon_0 \sum_A \varphi_A(z) \varepsilon_A \tag{4.3}$$

where ε_0 is the permittivity of free space and ε_A is the relative permittivity of species A. The local charge is found from the average over the charge of all species, obviously also weighted by their local volume fractions.

$$q(z) = e \sum_A \sum_k \varphi_{A,k}(z) \nu_{A,k} \tag{4.4}$$

Using Eqs. 4.2, 4.3 and 4.4, it is possible to calculate the electrostatic potential in a layer. From the electrostatic potential we find the electric field by $E = -\partial\psi/\partial z$. This electric field is used to compute a polarisation contribution, necessary because we allow for local diëlectric permittivities. The polarisation contribution $U_A^{\mathrm{pol}}(z)$ is assumed not to depend on the state of the segment and is given by

$$U_A^{\mathrm{pol}}(z) = -\frac{\varepsilon_0}{2}(\varepsilon_A - 1) E^2(z) \tag{4.5}$$

This equation shows that the polarisation of segment A is a function of the local field. The gain in energy is also proportional to $\varepsilon_A E$, hence $-\varepsilon_A E^2$. The factor 1/2 corrects for the entropy-loss due to the segment polarisation.

The two remaining contributions to the segment potential also occur for systems that have no electrostatic contributions. These terms may be called the volume terms and are described by Eqn. 4.6.

$$u_{Ak}^{\mathrm{vol}}(z) = k_B T \left(u'(z) + \sum_B \sum_l \chi_{Ak,Bl}(\langle \varphi_{Bl}(z) \rangle - \varphi_{Bl}^b) \right) \tag{4.6}$$

Here $k_B T$ is the thermal energy. In Eqn. 4.6, $u'(z)$ is the contribution that specifies the work needed to generate an empty site at z for the segment to be placed. Alternatively, $u'(z)$ can be seen as a Lagrange multiplier which ensures that the layer z is completely filled, that is $\sum_A \varphi_A(z) = 1$. The second term on the r.h.s. accounts for all the nearest-neighbor interactions of segment A in state k where the type of the neighboring segment is denoted by B and its state by l. The angular brackets denote a 3-layer average over layers $z-1$, z and $z+1$, $\langle \varphi(z) \rangle = \lambda_{-1}(z)\varphi(z-1) + \lambda_0(z)\varphi(z) + \lambda_1(z)\varphi(z+1)$. The contact interactions are specified by the Flory-Huggins parameters $\chi_{Ak,Bl}$ which needs to be specified for each pair of segments and for all states of the segments. When this value is negative this means that the segments attract each other; when it is positive this means repulsion. For similar contacts, i.e. χ_{AA}, the value is zero per definition. This is because the interactions have the pure components as the reference.

Collecting all terms, the total segment potential is found by:

$$u_{Ak}(z) = u_{Ak}^{\mathrm{PB}}(z) + u_A^{\mathrm{pol}}(z) + u_{Ak}^{\mathrm{vol}}(z) \tag{4.7}$$

In summary, we can use Eqn. 4.7 to evaluate the segment potentials. For this we need the volume fractions as an input. All other contributions are derived from these, such as the electrostatic potential, the charge distribution and the local permittivities. As an input, we also need the interaction parameters for all unlike contacts, the segment valence as well as the diëlectric constants for each segment type.

4.2.2 From potentials back to volume fractions

Next we want to show how to calculate the volume fractions corresponding to the potential field using a method independent from the method used in the previous section. It is convenient to introduce a segment weighting factor, $G_{Ak}(z)$, which is a Boltzmann equation that uses the segment potential.

$$G_{Ak}(z) = e^{-u_{Ak}(z)/k_B T} \tag{4.8}$$

For a segment which can occur in just one state, we have $G_{Ak}(z) = G_A(z)$. If it can exist in multiple states we have $G_A(z) = \sum_k \alpha^b_{Ak} G_{Ak}(z)$ where α^b_{Ak} is the *a priori* fraction of A in state k. This fraction is evaluated in the bulk, where there is no segment potential field. This weighting factor is used to relate the volume fraction in layer z to the bulk volume fraction through appropriate normalisation.

$$\varphi_A(z) = \varphi^b_A G_A(z) \tag{4.9}$$

The corresponding equation for chains is more complicated. From the definitions of the molecular architectures, all segment types A of all segments s of molecules i are available. We may introduce the quantity $\delta^A_{i,s}$ which assumes the value unity when segment s of molecule i is of segment type A, and is zero in all other cases. Using this parameter, one can generalise the segment type dependent weighing factors to segment ranking number dependent ones:

$$G_i(z, s) = \sum_A G_A(z) \delta^A_{i,s} \tag{4.10}$$

Here we do not need to specify the internal state k of a segment. To proceed, it is important to understand the difference between a conformation and a configuration. Both terms are used to describe the shape of a chain molecule. If a configuration is used, every segment is assigned a point in 3-D space. A conformation only describes the layer number of every segment. So, every conformation contains a set of configurations, that is, a conformation is degenerated. All configurations within a conformation are equally likely and we can simplify our computations if we use conformations and account for the degeneracy.

Let us next focus on conformation c. This conformation is specified with the set of layer numbers of all its segments, $c : \{z^c_1, z^c_2, ..., z^c_N\}$. The potential felt by this molecule i in conformation c, u^c_i, is given by

$$u^c_i = \sum_{s=1}^{N_i} u_i(z^c_s, s) \tag{4.11}$$

Next we need to compute the degeneracy ω^c_i.

To calculate the number of configurations that belong to a certain conformation c, we first look at the number of ways to place segment $s = 1$ in layer z^c_1. This is equal to the number of lattice sites in this layer, $L(z^c_1)$. Then we need the number of ways that the next segment can be placed in layer z^c_2. This number is given by multiplying the chance of going from layer z^c_1 to layer z^c_2, given by the appropriate lattice parameter λ (note that z^c_1

and z_2^c can represent the same layer), and the lattice coordination number Z. This is repeated for each subsequent bond in the molecule, hence for a conformation c we find the degeneracy

$$\omega_i^c = L(z_1^c) \sum_{s=2}^{N} (\lambda_{z_s^c - z_{s-1}^c}(z_s^c) \cdot Z) \tag{4.12}$$

As a result the weighting factor for the chain i in conformation c is given by

$$G_i^c = \omega_i^c \exp\left[\frac{-u_i^c}{k_B T}\right] \tag{4.13}$$

The following task is to calculate the unnormalised volume fractions of molecule i, $\widetilde{\varphi}_i(z)$. To obtain this quantity, we need to generate the full set of all possible and allowed conformations. This very large set can be calculated by multiplying the statistical weight of conformation c by the number of segments that this conformation has in layer z, $n_i^c(z)$, and sum this for all conformations:

$$\widetilde{\varphi}_i(z) = \sum_c G_i^c n_i^c(z) \tag{4.14}$$

Similarly, we can compute $\widetilde{\varphi}_A(z)$ or $\widetilde{\varphi}_i(z,s)$. If segment A can exists in multiple states, we can calculate the volume fraction of the states from

$$\widetilde{\varphi}_{Ak}(z) = \alpha_{Ak}(z) \widetilde{\varphi}_A(z) \tag{4.15}$$

where $\alpha_{Ak}(z) = \alpha_{A,k}^b G_{Ak}(z)/G_A(z)$. There are several ways to normalise these volume fraction profiles.

$$\varphi_i(z) = C_i \widetilde{\varphi}_i(z) \tag{4.16}$$

In the case of polymer adsorption, the normalisation is given by $C_i = \varphi_i^b / N_i$. But for other cases, different normalisations are needed. For instance, surfactant adsorption isotherms (but also the micellization in the bulk) requires a normalisation constant such that the total amount of component i maintained.

We note that the evaluation of Eqn. 4.13, as discussed so far, is computationally very expensive. There exists a very efficient computational route for the case that the conformations of the chain molecule is not completely self-avoiding, but when it can fold back onto previously occupied sites. Within the mean field approximations, one can not know for certain whether a particular site is not yet occupied by a neighbouring chain. Therefore, it is not a serious new approximation to allow for chain backfolding. As a result we accept this so-called Markov approximation and typically generate all possible

and allowed freely-jointed chains. We do not go into the details of the propagator scheme to evaluate the volume fractions, because the above equations accurately give the result of this. A detailed description of the propagator scheme can be found, for example, in the book by Fleer *et alia*.[17]

Above we have discussed how the volume fractions can be computed from segment potentials as an input. We have also presented how the segment potentials can be computed from the volume fractions as an input. The fixed point of these equations is found routinely by a numerical procedure.

4.3 The model and its parameters

4.3.1 Bulk components

In a molecular model, one only needs two types of monomers to describe PEO or C_nE_m. Here we use a united atom C, mimicking a CH_2 segment, and oxygen, O. We have the segment W, to model the water phase. In addition we have salt ions. We limit ourselves to 1:1 electroyte and give the ions generic names Na and Cl.

Using these monomers, we can describe PEO of length N as $(C-C-O)_N$ and a C_nE_m surfactant as $C_n-O-(C-C-O)_m)$. We used a small cluster of Ws to model water, consisting of a central W with four neighbours. The advantage of using such cluster is that it accounts, in a very rough way, for the self-assembling properties of water. Above, we have stated that we want to study adsorption on a surface with a charge depending on pH and ionic strength. To include the pH in our model, we have defined three different states for the water. It can exist as uncharged H_2O, but it can also occur as positively charged H_3O^+ and negatively charged OH^-. How one of the states can change to another state is described by the water equilibrium

$$2H_2O \rightleftharpoons H_3O^+ + OH^- \tag{4.17}$$

and the associated equilibrium constant p$K = 14$. All states of water have equal interactions (χ-parameters) with the other segments.

The interactions between the EO segments and with water (see Eqn. 4.6) may be borrowed from the modelling of nonionic surfactants in water. Here we have used $\chi_{C,W} = 1.1$, $\chi_{O,W} = -0.6$ and $\chi_{C,O} = 2$, which are equal to the χ-parameters used in reference.[28] Obviously, we need to define also the corresponding Flory-Huggins parameters for the salt ions. From experimental observations, we know that the solubility of PEO deteriorates with increasing ionic strength. Therefore, the interaction between the EO groups and the salt needs to be repulsive. Pragmatically we have chosen the

symmetric values of $\chi_{Na,C} = \chi_{Cl,C} = 2$. All other interaction parameters were set to zero.

We further need to specify the relative permittivity, ε_A, of our species to calculate the permittivity of a layer in Eqn. 4.3. Again for simplicity we have used $\varepsilon_A = 80$ for all segments, except for hydrocarbon, where we used $\varepsilon = 2$.[71]

To evaluate the Poisson equation, we need to specify the unit length, i.e. the size of the lattice sites, l. We have set $l = 0.3$ nm . This is approximately the average size of the segments used in the model.

In this paper, we have chosen to use $\lambda_{-1} = \lambda_0 = \lambda_{+1} = 1/3$. This choice minimises so-called lattice artifacts, as it allows easy placing of a sharp interface onto the lattice. We do note that this corresponds to an anisotropic lattice, and that some results need a trivial rescaling to apply to an isotropic solution. For the calculations presented in this thesis, this issue is of minor importance.

4.3.2 The silica surface

The focus is on a silica surface. The charge of this surface responds to pH and salt concentration. In our model, the aim is to capture this behaviour, but we immediately mention that silica has many intricacies and that the model remains very rough.

Silica generally has two kinds of surface groups, namely silanol and siloxane groups. The silanol groups can lose a proton to the water, which causes a pH dependant surface charge. In line with this we have defined two types of surface groups. The silanol groups in our calculations, called 'SiO_2', can exists in two states, i) a protonated state called 'HA' and ii) a deprotonated state called 'A'. A HA-group can react with water to form an A-group according to

$$H_2O + AH \rightleftharpoons A^- + H_3O^+ \tag{4.18}$$

We have set the equilibrium constant for this equation on p$K = 6$. The siloxane groups in our calculations exist only in a single state, called 'Si'.

We know that the hydrophobic united carbon segments are repelled by the hydrophilic silica. Therefore, we have set a moderate repulsion between the C-groups and all types of surface groups: $\chi_{C,HA} = \chi_{C,A} = \chi_{C,Si} = 2$. We also expect that EO groups bind by H-bonds between the oxygen groups and undissociated silanol groups. This binding mechanism is pH sensitive. That is, at high pH there is an adsoption/desorption transition. We modelled an attractive interaction between the oxygen atoms and all surface groups. For the A-groups and the Si-groups there is a moderate

attraction: $\chi_{O,A} = \chi_{O,Si} = -2.5$. To account for the H-bonds between HA-groups and oxygen, we modelled a strong attraction $\chi_{O,HA} = -6$. In this way, we can change the effective interaction between the EO groups and the surface by changing the pH, and thus introduce the possibility of an adsorption/desorption transition. For simplicity we will assume that between the salt ions and the surface groups, there is a slight repulsion, i.e., $\chi_{Na,Si} = \chi_{Na,A} = \chi_{Na,HA} = \chi_{Cl,Si} = \chi_{Cl,A} = \chi_{Cl,HA} = 1$. We do know that specific ion effects can be very large. Even though this is a very interesting subject, here we keep our focus on PEO/C_nE_m adsorption. Generally, ions are very well hydrated. Most probably, breaking this hydration shell will cost some energy. Therefore, we have chosen a small symmetric repulsion, and haste to mention that the qualitative results do not depend on the exact values chosen.

In all our calculations, we have taken half of the surface groups as silanol, and the other half as siloxane groups. Since we have set the segment size at 0.3 nm, this implies that there are $1/(2 \cdot 0.3^2) = 5.6$ silanol groups per nm^2. This corresponds with literature values.[47]

In the theory described above, all concentrations are expressed in volume fractions. To convert these volume fractions to moles per liter, we use the fact that the concentration of pure water is $1000/18 = 56$ mol/L. Because all molecules are described as (strings of) segments that occupy one lattice space each, we can also use this conversion for other segments types. When we do use it for chains of segments, we also have to divide by the chain length to account for the molecular volume.

4.4 Thermodynamics of small systems

For the interpretation of our results on micellization, we have to use the thermodynamics of small systems, as developed by Hill and later applied to micellar solutions by Pethica and Hall.[28,72,73] The thermodynamics of small systems assumes on generic physical grounds that in the system there is a hidden variable called the number of subdivisions, $\mathcal{N}$, which divides the system in a number of subsystems. In our case, each subsystem contains one micelle, which means that the number of subdivisions is equal to the number of micelles $\mathcal{N}$. The intensive variable that is conjugated to the extensive $\mathcal{N}$ is the subdivision potential $\mathcal{E}$. We can incorporate these variables into thermodynamics by writing down the change of the Gibbs energy as

$$\mathrm{d}G = -S\mathrm{d}T + V\mathrm{d}P + \sum_i \mu_i \mathrm{d}n_i + \mathcal{E}\mathrm{d}\mathcal{N} \tag{4.19}$$

Here S is the total entropy, T is the absolute temperature, V is the volume, P is the pressure, μ_i is the chemical potential of species i, n_i is the total number of molecules of i. In line with classical thermodynamics, equilibrium implies that the system has minimised its free energy with respect to every degree of freedom it has. Therefore, thermodynamics of small systems implies that at equilibrium

$$\left(\frac{\partial G}{\partial \mathcal{N}}\right)_{T,P,n_i} = \mathcal{E} = 0 \tag{4.20}$$

Moreover, to have stable micelles, the Gibbs energy should be minimal. This implies

$$\frac{\partial^2 G}{\partial \mathcal{N}^2} = \frac{\partial \mathcal{E}}{\partial \mathcal{N}} > 0 \tag{4.21}$$

If the system does not comply with Eqn. 4.21, it can lower its free energy by either increasing or decreasing the number of micelles.

In the SCF calculations we effectively fix the center of mass of a micelle to the center of the spherical coordinate system, and predict its properties as a function of the number of unimers in the micelle (aggregation number g). For an accepted SCF solution, we can evaluate the grand potential that is associated with our pinned micelle, $\mathcal{E}_m$. This differs from the 'true' grand potential or subdivision potential $\mathcal{E}$ as the collective degrees of freedom of the micelle as a whole are neglected. This means that the mixing entropy on a micellar level gives the difference between the true $\mathcal{E}$ and the computed $\mathcal{E}_m$. For dilute micellar systems we may write

$$\mathcal{E}_m = \mathcal{E} - kT \ln \varphi_s^m \tag{4.22}$$

where kT is the thermal energy and φ_s^m is the volume fraction of micelles.

Let us assume that there exists some relevant micellar-like structure. The first issue is to compute the aggregation number g. For this we take the excess number of surfactants in the micelle, or mathematically:

$$g = \frac{1}{N_s} \sum_z L(z)(\varphi_s(z) - \varphi_s^b) \tag{4.23}$$

where the subindex refers to the surfactant molecule, N is the number of segments that make up one surfactant molecule and $L(z)$ is the number of lattice sites in layer z. Hence, $\varphi_s(z)$ is the volume fraction of surfactant in layer z, and φ_s^b is the volume fraction of surfactant in the absence of a field (which corresponds with the bulk). As explained, for such a micelle it is possible to compute the translationally-restricted grand potential ($\mathcal{E}_m(g)$).

Combining the equilibrium condition, Eqn. 4.20, with Eqn. 4.22 thus gives the volume fraction of micelles with aggregation numbers g:

$$\varphi_s^m(g) = \exp\left(-\frac{\mathcal{E}_m(g)}{kT}\right) \tag{4.24}$$

As the surfactants in these micelles are densely packed, we can estimate the volume of the micelle by $V^m = gN_s l^3$. Recall that the monomer concentration that is in equilibrium with the micelles with size g, $\varphi_s^b(g)$ is also available from the computations. We can formulate the mass balance for the surfactant as

$$\varphi_s^t = \varphi_s^b + \varphi_s^m = \varphi_s^b + \exp\left(-\frac{\mathcal{E}_m}{kT}\right) \tag{4.25}$$

This equation is used to estimate the critical micelle concentration (CMC). Below the CMC the volume fraction of micelles is very small and $\varphi_s^t \approx \varphi_s^b$. Above the CMC the majority of the surfactants is in micelles and $\varphi_s^t \approx \varphi_s^m$. At the CMC the two terms are of the same magnitude, that is $\varphi_s^b = \varphi_s^m$. However, it is quite elaborate to calculate the CMC according to this definition. Therefore, we have made a more pragmatical choice. Below we will implement an operational CMC by selecting the micellar system that is characterised by a grand potential $\mathcal{E}_m = 10\ kT$. This basically implies that we require a certain concentration of micelles to be present at the CMC. The required concentration of micelles in units of volume fraction is $\varphi_s^m \approx 4.5 \times 10^{-5}$, which is close to the condition $\varphi_s^b = \varphi_s^m$ for most surfactant systems.

Chapter 5

PEO adsorption

In this chapter, we apply the model described in chapter 4 to the case of PEO adsorption. The bulk solution consists of water, PEO, 1:1 electrolyte, protons and hydroxyl-ions. The solvent quality for the PEO is good below and becomes poor above a threshold ionic strength (of around 1 M). The silica surface features a number of silanol groups that have an affinity for PEO (by means of H-bonding) when these groups are not dissociated. In line with experimental data, the surface changes from adsorbing to non-adsorbing at a sufficiently high pH. Even though PEO is uncharged, there is a complex effect of the ionic strength on the interfacial characteristics. For example, we report a non-monotonic behaviour of the adsorbed amount as a function of ionic strength. Going from a low to a high ionic strength at a neutral or slightly basic pH, the adsorbed amount initially decreases as the surface affinity decreases (caused by the reduction of adsorption sites when, as a result of screening, the surface is increasingly charged), but then increases as a result of a reduction in solvent quality. These results indicate that molecularly realistic models can reveal a much richer interfacial behaviour than anticipated from generic models. The predictions follow many experimental findings.

5.1 Polymers in bulk

Recall that to predict the behaviour for PEO adsorption onto a silica surface from an aqueous solution, it is necessary to have the first order behaviour in

Part of this chapter has been published as: Bart R. Postmus, Frans A. M. Leermakers, and Martien A. Cohen Stuart. Self-consistent field modeling of poly(ethylene oxide) adsorption onto silica: The multiple roles of electrolytes. *Langmuir*, 24:1930-1942, 2008.

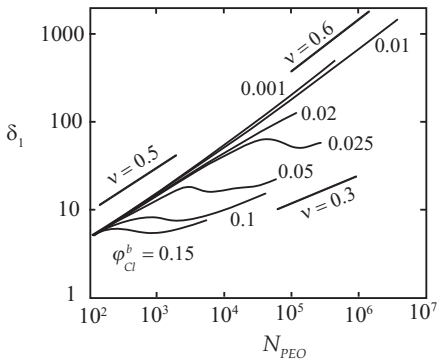

Figure 5.1: *First moment of a PEO chain in units l plotted versus its total number of EO-segments on a log-log-scale for a number of ionic strengths. In the graph, the slopes* $\nu = 0.3$*,* $\nu = 0.5$ *and* $\nu = 0.6$ *are indicated.*

the bulk correct. We therefore pay attention to dilute *PEO* solutions first. The important issue in dilute solutions is the size of the polymer coil as a function of the important variables in the system. Here our interest is in the effect of the ionic strength.

The bulk behaviour of the polymers can be investigated using a spherical coordinate system. The idea is to fix the middle segment of a polymer chain to the center of the coordinate system and measure the size of this chain.[74] This means that we solve the SCF equations for a two-armed star. Here we will be interested in the size of the chain as a function of its length. As all measures of the size scale similarly, we have decided to record the first moment of the free ends of the chain δ_1 (which is segment $s = N$):

$$\delta_1 = \frac{\sum_{z=0}^{M} L(z)\varphi(z,N)z}{\sum_{z=0}^{M} L(z)\varphi(z,N)} \tag{5.1}$$

Using Eqn. 5.1, we calculated the first moment of the chain end. By varying the chain length and the ionic strength, we can determine how the first moment scales with the polymer length as a function of the ionic strength.

From the physics of polymers in solution, it is known that as long as a polymer chain does not have too many internal contacts, it remains Gaussian.[75] As soon as the number of contact in the chain, estimated by Flory by $N^{1/2}$ times the second virial coefficient($\nu_{\mathrm{eff}} = 1 - 2\chi_{\mathrm{eff}}$), exceeds unity, the chain will swell. When it is less than negative unity, it will collapse. Our results closely follow this Flory picture. A quantitative analysis of our predictions is possible. Here it suffices to know under which conditions the chains are in a good, near theta, and poor solvent conditions.

In Figure 5.1, we plotted δ_1 versus N on a log-log scale. In this Figure

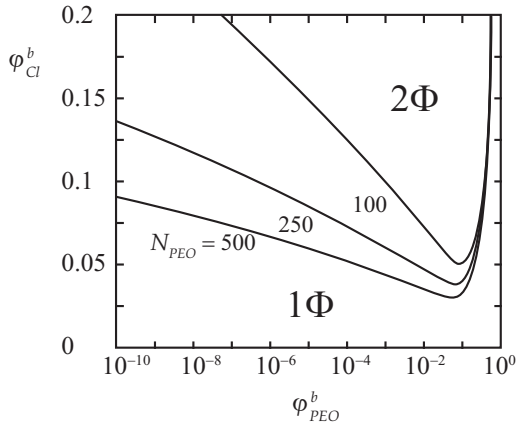

Figure 5.2: *The phase diagram or binodal for three different polymer lengths. Below the curve, one has a one-phase state (1Φ). Above the curve, it is a two-phase state (2Φ); that is, a polymer rich phase coexists (φ^b_{EO} is high) with a solvent rich phase(φ^b_{EO} is low).*

we indicated the slope ν, which gives the scaling $\delta_1 \propto R_g \propto N^\nu$. The slopes $\nu = 0.33$ (for poor solvents), $\nu = 0.5$ (theta solvent) and $\nu = 0.6$ (good solvent) are indicated. By fitting a power law to the $\varphi^b_{Cl} = 0.01$ curve, we found that the slope of the curve is 0.6 for the chain lengths above a million segments. For lower ionic strengths, the solvent quality will be better, and hence there the polymer will reach this scaling at lower lengths. If we increase the salt content, we see that ν decreases and for a sufficiently high salt concentration, we enter the poor solvent regime for which the polymer chain collapses above a critical chain length. When a polymer chain is collapsed, it forms a dense sphere. In this case the scaling coefficient, ν, is 0.33.

In Figure 5.1, we see that for a salt volume fractions of $\varphi^b_{Cl} = 0.01$, ν is higher than 0.5 for all chain lengths and thus that the solvent quality is good. Because our results are most relevant for the case where PEO is in a good solvent, we will use $\varphi^b_{Cl} \leq 0.01$ for most of the calculations in this thesis. When we do use a higher salt concentration, we have to be extra careful when interpreting the results. This is because collapsed chains can easily form two-phase systems, wherein a polymer rich phase coexists with a polymer poor phase.

To illustrate this, we have plotted a binodal for $N_{PEO} = 100$, 250 and 500 in Figure 5.2. We can calculate these by defining a flat lattice with reflecting boundary conditions. After breaking of the symmetry, the SCF machinery leads to two coexisting systems and an interface between them. Here, φ^b_{PEO} of the concentrated and the dilute phase is plotted versus the salt concentration, φ_{Cl}, in the dilute polymer (or water rich) phase on a lin-log-

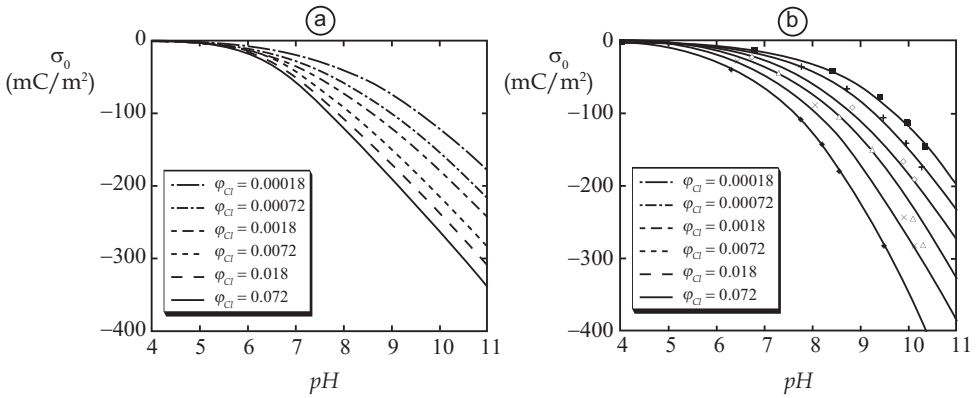

Figure 5.3: *The surface charge, σ_0, as a function of the pH, for a number of different salt concentration. In graph a we present some results of our model calculations. In graph b we show experimental data obtained by Bolt et al.*[60]

scale. We see that there is a volume fraction of salt above which the polymer just starts to phase separate. As we increase the salt concentration from here, we may have a coexisting concentrated polymer phase and a solvent rich phase. Because Figure 5.2 is drawn on a lin-log-scale, we can really see how incredibly dilute in polymer the solvent rich phase is. For longer polymers, the polymer concentration in the solvent rich phase will be even lower, so that, for some polymer length ($N_{PEO} \approx 1000$), it effectively drops to zero.

Figures 5.1 and 5.2 are coupled. They are different ways to present very similar information about one system. When we look at Figure 5.2, we see that the critical point for PEO with $N_{PEO} = 100$ is approximately at $\varphi^b_{Cl} = 0.05$. If we compare this with Figure 5.1, we see that the line corresponding to $\varphi^b_{Cl} = 0.05$ starts to deviate from $\nu = 0.5$ at approximately $N_{PEO} = 100$. Furthermore, from both Figures we can deduce that the solubility of longer polymers is more salt dependant than that of short polymers, e.g. longer polymers phase separate at lower salt concentrations. So, although the curves in Figure 5.2 are for rather short chains, we can still conclude that both Figures present consistent information.

5.2 Titration curves for Silica

In the absence of polymers our model gives the surface charge as a function of pH and ionic strength. This is actually similar to solving a modified Poisson-Boltzmann equation (see Eqns. 4.2 and 4.8) where we also account for the ion volume. To determine the surface charge, we multiplied the volume fraction

of dissociated silanol groups (A segments) with the unit charge and divided this by the square of the segment length ($\sigma(0) = 1.6 \cdot 10^{-19} \varphi_A(0)/(0.3 \cdot 10^{-9})^2$ [C/m^2]).

In Figure 5.3a we plot the surface charge for silica versus pH. The different curves represent a range of ionic strengths conditions. An increase in pH leads to a more negative surface charge. This is due to the higher concentration of OH^--groups in the bulk, which causes the dissociation of silanol groups, and thus more negative charge on the surface. The case with the highest amount of salt in solution can acquire the highest surface charge. This can be explained by screening of the charged surface groups by counterions in solution.

In Figure 5.3b we plot some experimental titration results from literature.[60] These results are obtained by potentiometric titration of a silica sol. For proper comparison, we converted the experimental salt concentrations to volume fractions of salt and used these volume fractions in our calculations. Fig 5.3a and 5.3b show convincingly similar trends. However, the experimental system tends to have a lower surface charge at high pH. We have to choose the amount of silanol groups per surface area in our calculations. As stated above, we have defined half of of the surface groups as silanol groups, and the other half as siloxane groups. By defining a higher density of silanol groups, we can reproduce the experimental curves more precisely. We can also lower the pK of the silanol groups to fit the data at high pH better. However, this would result in a substantial difference between the experiments and the theory at low pH.

Also, the specific adsorption of salt ions is not accounted for. In fact, we have defined a small symmetric repulsion between the surface and the salt ions ($\chi_{surface,Na} = \chi_{surface,Cl} = 1$). By setting an attraction, which can also be asymmetric, between the surface and the salt, it will become more favourable for the ions to be near the surface. The subsequent increase in salt near the surface will allow for a better screening of the charged surface groups which will result in a higher (in our case more negative) surface charge.

However, our interest is to capture the essential properties of the silica surface and the results presented above are definitely doing a good enough job. So, we decided to stick to our original density of silanol groups and not to include any specific salt effects for the time being.

5.3 PEO adsorption onto silica in good solvents

From the introduction, it is clear that there are several regimes for polymer adsorption. Here we focus on the adsorption of PEO onto silica from dilute

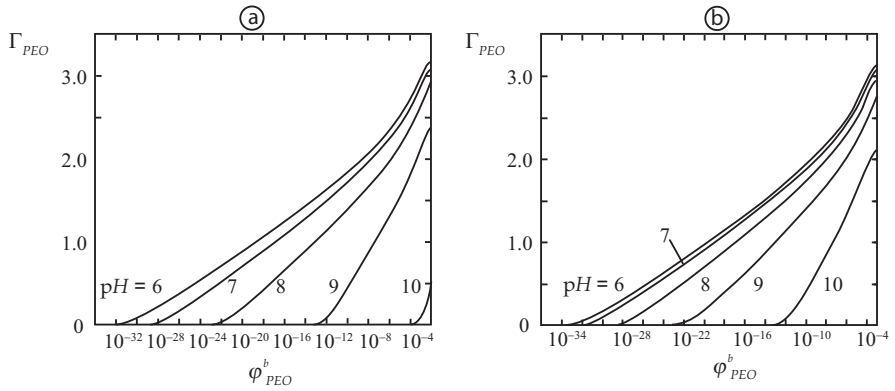

Figure 5.4: *Adsorbed amount of PEO with length $N_{PEO} = 500$ in equivalent monolayers, Γ_{PEO}, plotted versus the bulkconcentrations (adsorption isotherms), in good solvent conditions. In graph a, $\varphi^b_{Cl} = 0.001$ and in b $\varphi^b_{Cl} = 0.0001$. The pH for different curves varies as indicated in the graph.*

solutions. Moreover in this section we will limit ourselves to the case that the polymers are in good solvent condition. This means that we limit ourselves to relatively low ionic strengths.

To study polymer adsorption, we model a flat lattice where the surface is placed on one side and the bulk exists on the other side. As we stated in the introduction, solving such a problem gives accurate profiles of the volume fraction of all species. Using these volume profiles, we can calculate the adsorbed amount of species A, Γ_A:

$$\Gamma_A = \sum_1^M (\varphi_A(z) - \varphi_A^b) \tag{5.2}$$

Polymers typically adsorb according to a so-called high affinity isotherm. We present some typical examples of such isotherms for PEO with $N_{PEO} = 500$ on a lin-log-scale in Figures 5.4a and b. We used $\varphi^b_{Cl} = 0.001$ in Figure 5.4a and in Figure 5.4b we used $\varphi^b_{Cl} = 0.0001$. To calculate the adsorbed amount, Γ_{PEO}, we compute the total amount of PEO in the system and subtract M times the bulk concentration (recall that M is the number of layers). Hence, Γ_{PEO} is a surface excess.

We plotted the adsorbed amount, Γ_{PEO}, versus the bulk volume fraction of PEO. The different curves refer to different values of the pH. If we look at the line corresponding to p$H = 6$ in Figure 5.4a, we can see that the

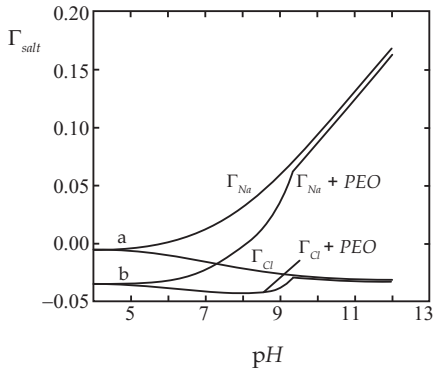

Figure 5.5: *Surface excess of salt as a function of pH. Lines denoted 'a' are taken from a system without any polymer and the lines denoted 'b' are taken from a system where the salt needs to compete with PEO of length* $N_{PEO} = 500$. *For these calculations we used* $\phi^b_{Cl} = 0.01$ *and* $\phi^b_{PEO} = 0.0001$.

polymer starts adsorbing at very low concentrations. For more basic pH, the onset of adsorption shifts to higher concentrations.

The largest part of the concentration range of Figure 5.4 is experimentally inaccessible. In experiments where the total amount of surface is low compared to the volume of the bulk solution, it is very hard, or impossible, to make solutions of a concentration where the polymer just starts adsorbing. Even the smallest impurity will influence the results. However, in the other regime, where the total amount of available surface area is high and the volume of the bulk is low, it is possible to generate starved interface by underdosing the system. The measurement of the equilibrium bulk concentration that results after most of the polymers adsorb, is the difficult task in this case. Furthermore, in these very dilute polymer concentrations, the kinetics of adsorption will be accordingly slow. Therefore, one often finds in experiments that the surface excess is hardly a function of the bulk concentration, that is, one focuses on the (semi) plateau of the adsorption isotherm.

If we compare curves for different values of the pH, we see that polymers adsorb more at low pH than at high pH. This is caused by the dissociation of silanol groups. Dissociated silanol groups cannot form H-bonds with the oxygen atoms in the polymers. In our model we implemented this by defining strong attraction between silanol and oxygen segments, $\chi_{O,HA} = -6$, and defining a higher χ-parameter for the interaction between dissociated silanol groups and oxygen segments, $\chi_{O,A} = -2.5$. Hence, the dissociation of silanol groups leads effectively to a lowering of the adsorption energy for the oxygen segments and thus also for the polymer which must lead to a lower adsorbed amount.

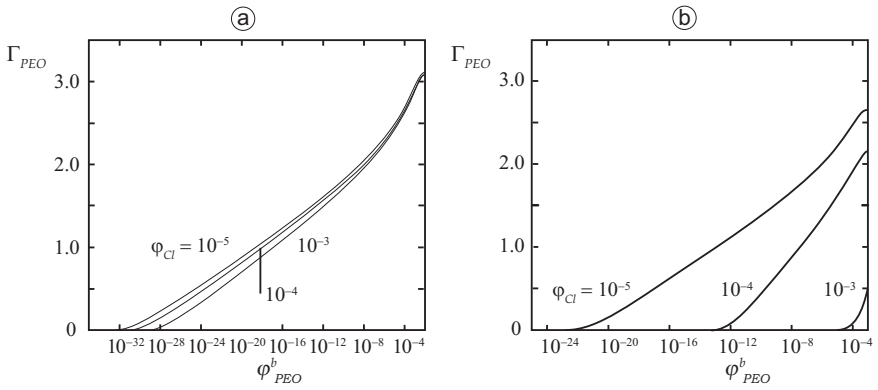

Figure 5.6: *Surface excess of PEO, Γ_{PEO}, of length $N_{PEO} = 500$ plotted versus its bulk concentration. In graph a we used $pH = 7$ and in b we used $pH = 10$.*

There is another reason why polymers adsorb less on silica from a solution with a high pH. In Figure 5.3, we see that at a high pH the surface has a high negative charge. This means that the ions in the solution will arrange themselves into a double layer and that there will be a significant amount of counter-ions near the surface. However, in our calculations, an adsorbed polymer typically likes to occupy half of all sites near the surface (see Figure 5.11 below). Hence, there will be a competition for space in the first layer, and the polymer adsorption is suppressed by this competition.

This competition is illustrated in Figure 5.5, where we present the surface excess of Na and Cl in a system with (curves b) and without polymer (curves a). Because the surface is negatively charged at high pH values, we see a positive excess of the positively charged Na segment (Γ_{Na}) and a negative excess of the negatively charged Cl segment (Γ_{Cl}). As the pH increases, the surface attains more negative charge, and hence Γ_{Na} will increase and Γ_{Cl} will decrease. At p$H = 4$, there are very few charged sites on the surface, and $\Gamma_{Na} \approx \Gamma_{Cl}$. Note that both Γ's are slightly negative. This is due to the slight repulsion that we defined for the surface and the salt molecules ($\chi_{surface,Na} = \chi_{surface,Cl} = 1$). We see that if we introduce an adsorbing polymer in the system (curves b), there is a depletion effect for the salt at low and neutral pH. At pH slightly above 9, there is a fairly abrupt shift in the surface excess of both ions. This due to the polymer that does adsorb at p$H \lesssim 9$, but does not adsorb anymore at p$H \gtrsim 9$ (vide infra). If the polymer does adsorb, there is less available space near the surface for the salt, and hence there is a competition for adsorption.

In Figure 5.6, we present complementary isotherms. Here we fixed the pH and looked at the effect of salt on the adsorption of PEO with length $N_{PEO} = 500$. In Figure 5.6a, we have set p$H = 7$ and in Figure 5.6b we

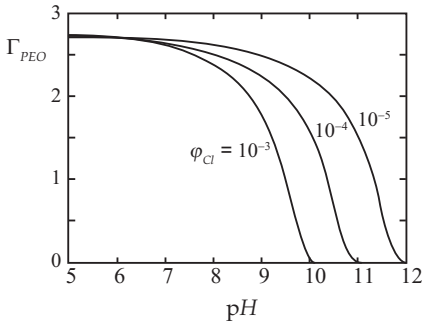

Figure 5.7: *Adsorbed amount of PEO with $N_{PEO} = 500$ plotted versus the pH for a number of ionic strengths. The volume fraction of polymer φ^b_{PEO} was 0.001 for all curves.*

set p$H = 10$. Each curve corresponds with a certain volume fraction of salt, which is indicated in the graph. We see that for p$H = 7$, the volume fraction of salt does not strongly influence the adsorbed amount. There are ample adsorption sites and the surface charge is rather low, so there is not a fierce competition with the salt ions. For p$H = 10$ the situation is entirely different. Here, the adsorption sites are getting scarce. Adding salt will screen existing dissociated silanol groups, allowing more silanol groups to dissociate, and reduce the amount of adsorption sites even more. Because the polymer is just loosely bound to the surface, the competition with salt ions near the surface also causes lower adsorbed amounts. Therefore, the effect of salt on polymer adsorption is large at p$H = 10$.

5.4 The adsorption-desorption transition

The results shown thus far are all for the regime that the polymers are more or less strongly bound to the surface. As the available number of adsorption sites decreases with increasing pH, we eventually should expect an adsorption transition to take place.

In Figure 5.7, we have plotted how Γ changes as a function of pH for three different ionic strengths. We see that for a pH of about 6, the adsorbed amount is not a function of the ionic strength. But as the pH increases, the ionic strength becomes more important. For a salt volume fraction of approximately 10^{-5}, the adsorbed amount starts to drop for pH larger than 9, and at p$H = 13$, the adsorbed amount will be zero. For a volume fraction of 10^{-4}, the adsorbed amount will start to decrease at p$H = 8$ and there will be no PEO adsorption above p$H = 12$. For a ten times higher volume fraction of salt, the curve shifts another pH-unit to the left.

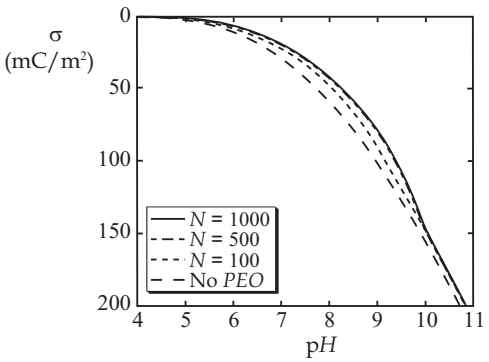

Figure 5.8: *Titration curves, that is the surface charge plotted versus the pH, with and without adsorbed polymer. For these calculations we used* $\varphi^b_{PEO} = 0.001$ *and* $\varphi^b_{Cl} = 0.001$.

5.5 Titration curves with polymer

In our model, if a polymer adsorbs in the regime of strong adsorption, it will roughly occupy half of all surface sites. When the surface is charged, there are also salt ions that want to adsorb onto the surface. So, there is a competition for surface space. If the polymer does adsorb, the local concentration of salt ions near the surface must be lower than it would have been without the polymer (see also Figure 5.5). Since the charge of the surface is a function of the salt concentration, the adsorbing polymer actually lowers the surface charge.

In Figure 5.8, we plotted the surface charge, σ_s, versus the pH for a clean surface and for three surfaces covered with polymer of different lengths. In these calculations $\varphi^b_{PEO} = 10^{-3}$ and $\varphi^b_{Cl} = 10^{-3}$. We found that in the pH range of 6 to 10, the polymer indeed suppresses the surface charge. For lower values of the pH,the surface is hardly charged and for higher pH, the polymer does not adsorb anymore.

In Figure 5.8, we also see that the two long polymers ($N_{PEO} = 500$ and $N_{PEO} = 1000$) suppress the surface charge more than the polymer with $N_{PEO} = 100$. The reason for this is that the shorter polymer occupies approximately 37% of the sites in the layer just next to the surface ($\varphi_{PEO}(1) = 0.37$) ,which is the same as saying that 37% of the surface is covered by polymer train segments. The longer polymers occupy 50% of these surface sites. Therefore the long polymers leave less space for the salt ions to occupy, and the surface charge has to be lower.

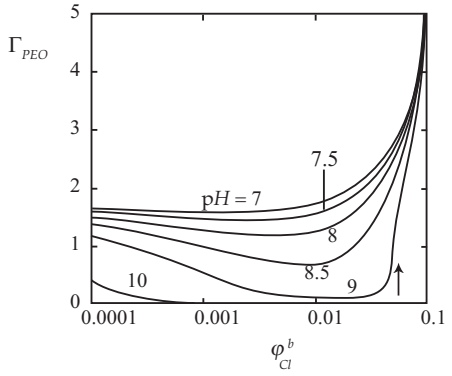

Figure 5.9: *Surface excess of PEO, Γ_{PEO}, plotted versus the volume fraction Cl^- in the bulk for various values of the pH as indicated. For these calculations we used $N_{PEO} = 500$ and $\varphi^b_{PEO} = 0.001$.*

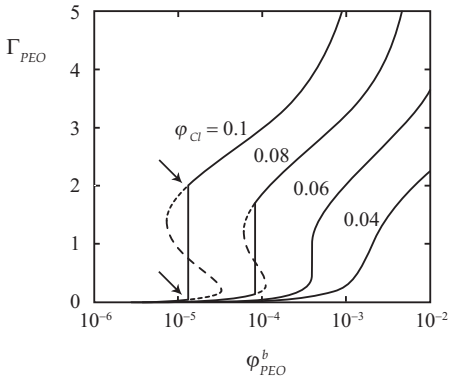

Figure 5.10: *PEO adsorption isotherms taken at $pH = 9$ and salt concentrations that correspond to the location of the arrow in Figure 5.9. The arrows in this Figure correspond with the profiles in Figure 5.11.*

5.5.1 Combining bulk properties with surface properties

In Figures 5.1 and 5.2, we show that as the salt concentration increases, PEO tends to collapse and wants to phase separate. If the polymer rich phase chooses to set on the silica surface (wetting), we may anticipate a strong increase of the surface excess. We also showed, in Figure 5.6, that as the salt concentration increases, the effective interaction between PEO and silica decreases. It is of interest to combine these two opposing effects, and discuss how the adsorbed amount of PEO changes as a function of salt concentration.

The results of these calculations are shown in Figure 5.9. At p$H = 7$, we can see that initially the salt does not influence adsorption very much.

However, at some point the solvent quality has decreased enough to cause the polymer to phase separate. Because the polymer chains have sufficient adsorption energy, the system chooses to develop a polymer rich phase near the surface and the adsorption goes up sharply (complete wetting). At higher pH, most noticeable at p$H = 9$, there clearly is an initial drop in adsorbed amount. This is due to the dissociation of silanol groups on the surface. But as the ionic strength increases, the solvent quality deteriorates and the adsorbed amount starts to increase. Apparently, the polymer rich phase still preferentially forms at the surface. However, at p$H = 10$ this no longer occurs. Now the affinity for the silica is lost before the two-phase state is entered and the system chooses to form the polymer rich phase in solution (the surface is dry).

The part of the graph corresponding to p$H = 9$ that steeply rises, shows a sort of 'wiggle', which is denoted by the arrow. For the salt concentrations where this wiggle occurs, we calculated some adsorption isotherms, which are plotted in Figure 5.10. Some of these isotherms show a jump in the adsorbed amount. In terminology of liquid films, these kind of jumps are known as prewetting steps.[76] Such a prewetting step is a phase transition from a thin film on the surface to a much thicker layer. The PEO bulk concentration, φ^b_{PEO}, where this transition occurs is a strong function of the salt concentration, φ^b_{Cl}. Because the surface has a reasonable amount of charge at p$H = 9$, the local concentration of salt near the surface will be even higher than the bulk concentration. This local increase of the salt concentration, and hence a local decrease of solvent quality, could cause a phase separation near the surface. This phase separation can present itself as a sudden increase in adsorbed amount, like we see in Figure 5.10. However, as soon as the polymer adsorbs, the amount of salt near the surface must decrease (see Figure 5.5), and the solvent quality near the surface increases.

To see what exactly happens when the isotherm jumps from a low to a high surface excess, we show some profiles of two coexisting states in Figure 5.11. These profiles are taken at the conditions denoted by the arrows in Figure 5.10. Figure 5.11 applies for the case where the polymer is not adsorbing strongly (bottom arrow in Figure 5.10) and Figure 5.11b applies for the strong polymer adsorption case (upper arrow). If the polymer adsorbs only weakly, the salt ions arrange themselves into an almost unperturbed double layer. The double layer thickness is rather low due to the high amount of salt in the system. The behaviour of the salt ions in the strongly adsorbing case is quite different. We see that the amount of salt right next to the surface is lowered due to the adsorbing PEO. But PEO also has a lower volume fraction right next to the surface compared to half a nanometre into the solu-

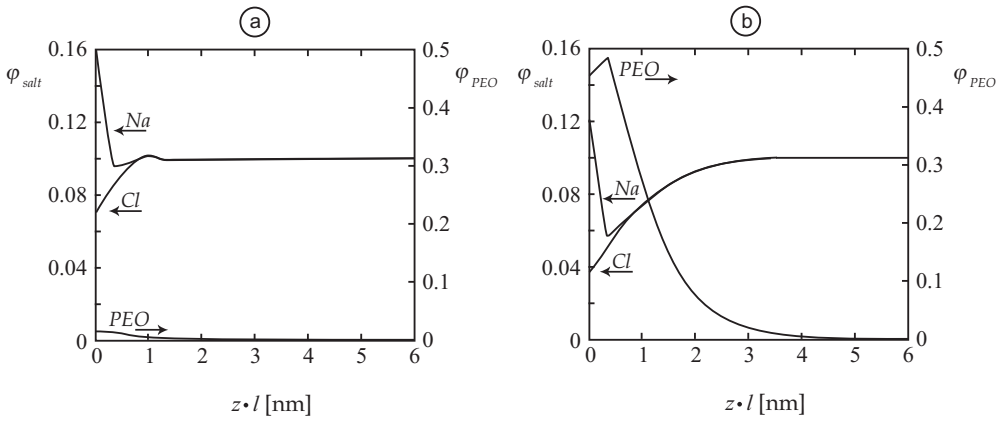

Figure 5.11: *Volume fraction of PEO, Cl and Na plotted as a function of their distance from the surface. Figure a corresponds to the bottom arrow in Figure 5.10, and b correspond to the upper arrow.*

tion. This is due to the competition between PEO and the salt. Right next to the surface, the salt is strongly bound, and is hard to displace. However, at a small distance from the surface, the salt - especially the Na - is strongly displaced. These profiles show that there are many things happening simultaneously at these jumps and that the salt has an important influence on the adsorption of PEO.

These prewetting steps are quite special, because they occur at polymer concentrations, φ_{PEO}, that are two orders of magnitude lower than the polymer concentration where the adsorbed amount diverges. Furthermore, the concentrations where the prewetting step occurs are experimentally accessible. Therefore, these kinds of wetting steps should be experimentally measurable. However, to our knowledge, experimental results like this have not yet been published.

5.5.2 Comparing our model with experiments

The goal is to develop a model that describes the experimental trends as close as possible. To check this, we need to compare the outcome of our model with experimental data. A convenient method to measure PEO adsorption under various conditions onto reflecting surfaces is reflectometry. The details about this technique are described in chapter 2 and information about the chemicals can be found in paragraph 3.1. All experiments presented here are performed with a 1 mg/l solution of PEO with molecular weight $M_w = 43520$ g/mol, which roughly comes down to 1000 EO-segments per PEO-chain.

In Figure 5.12, we plotted the equilibrium adsorbed amount versus the

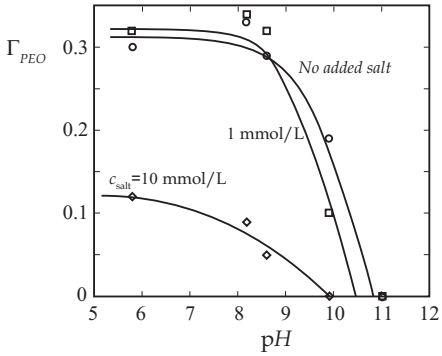

Figure 5.12: *The adsorbed amount of PEO plotted versus the pH as measured by reflectometry. For these experiments we adsorbed from a 1 mg/l solution of PEO with $M_w = 43520$ g/mol onto a silica wafer. The NaCl concentration is indicated.*

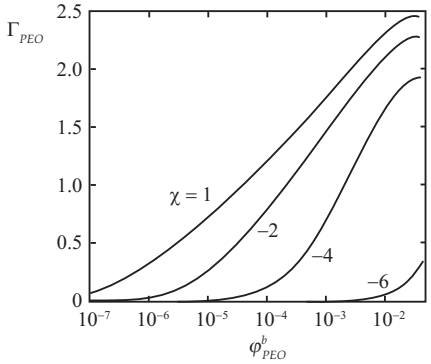

Figure 5.13: *Adsorbed amount of PEO of 100 EO-units plotted versus the PEO bulk concentration. The ionic strength was set at $\varphi_{Cl} = 0.01$ and the pH = 7. Every curve has been calculated with a certain affinity between the surface and the salt as indicated in the Figure. Here, all interactions between the salt and the surface are symmetric ($\chi \equiv \chi_{Na,surface} = \chi_{Cl,surface}$).*

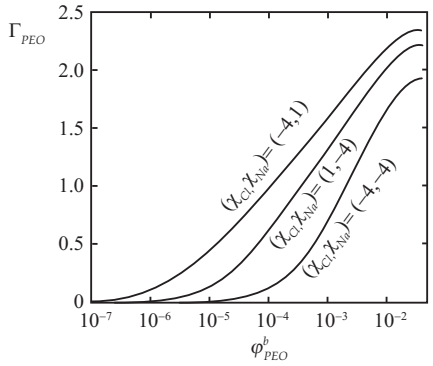

Figure 5.14: *Adsorbed amount of PEO of $N = 100$ EO-units plotted versus the PEO bulk concentration. The ionic strength was set at $\varphi_{Cl} = 0.01$ and the pH = 7. Here we varied the χ's as indicated in the graph ($\chi_{Cl} \equiv \chi_{Cl,surface}$ and $\chi_{Na} \equiv \chi_{Na,surface}$).*

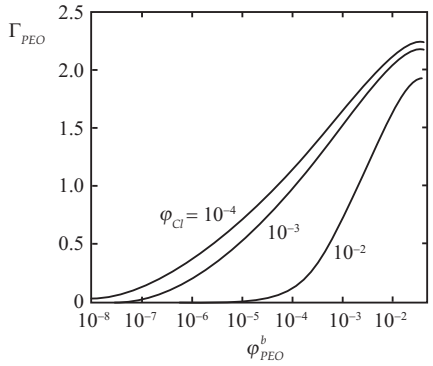

Figure 5.15: *Adsorbed amount of PEO of $N = 100$ EO-units plotted versus the PEO bulk concentration. Here we used pH=7 and $\chi_{Na,surface} = \chi_{Cl,surface} = -4$. We varied the ionic strength as indicated in the graph.*

pH in solution as measured by reflectometry. As expected, the adsorbed amount is a decreasing function of the pH. This type of behaviour has also been reported before by van Beek *et al.* and is in full agreement with our model (see Figure 5.7).[77] Furthermore, we see that by adding salt it is possible to shift the adsorption/desorption transition to a lower pH. This is also predicted by our model (see Figure 5.7).

Due to some scattering in the datapoints, we cannot say if the no salt curve or the 1 mmol/L curve is higher at low pH. However, it is clear that the 10 mmol/L curve is lower that the other two. So, the adsorbed amount seems to be a decreasing function of the ionic strength, even at pH 5 or 6. This latter feature is not predicted by our model. However, this decrease in adsorbed amount as function of ionic strength has also been reported for comparable systems. Iruthayaraj et al. used a low charge polyelectrolyte backbone with PEO side-chains. These molecules also bind to the surface by forming H-bonds with surface silanol groups. They found that adding sodium nitrate, $NaNO_3$, to a polymer solution caused a decrease in the adsorbed amount.[57] Eliseeva *et al.* found that the Pluronic F127, which also adsorbs by means of H-bonds, adsorbs to lower adsorbed amounts as a function of the $NaCl$ concentration.[78]

Because of the similarities between our results and the mentioned literature, we believe that the results in Figure 5.12 are accurate. One possible reason that the drop in adsorbed amount is not captured by our model is that we did not include the specific adsorption of salts in a proper way. We defined a slight symmetric repulsion between the surface and the salt segments ($\chi_{surface,salt} = 1$). To test the influence of specific adsorption of salt on the surface, we now present a selection of results to illustrate these effects.

In Figure 5.13, we vary the interaction between the salt and the surface for a system consisting of PEO chains of $N = 100$ units, $\varphi_{Cl} = 0.01$ and pH = 7. We varied $\chi_{Na,surface}$ and $\chi_{Cl,surface}$ symmetrically from a weak repulsion of 1 to a strong attraction of -6 as indicated in the Figure. Clearly, Γ_{PEO} is a function of the interaction between the salt and the surface. With increasing attraction the tendency of salt to displace the PEO increases for all values of the pH.

In experimental systems, it is most likely that the interactions between the co-ion and the surface are different from the counter-ions and the surface. Figure 5.14 shows some PEO adsorption curves where we changed the χ-parameter of either the co-ion, the counter-ion or both ions to -4. We see that changing the χ-parameter of both ions lowers the adsorbed amount significantly. If we only change one χ-parameter, we see that the counter-ion has a bigger effect than the co-ion. This makes sense because the local concentration of counter-ions near the surface is higher than the local concentration

of co-ions.

Both Figure 5.14 and Figure 5.13 are calculated using a relatively high ionic strength ($\varphi_{Cl} = 0.01$). In Figure 5.15 we test the influence φ_{Cl} on the adsorbed amount of PEO for the case $\chi_{Cl} = \chi_{Na} = -4$. In line with the results of Figure 5.6, we see that at high ionic strength the influence of the salt is larger than at low ionic strength.

We can conclude that it is possible to decrease PEO adsorption at relatively low pH by changing the interaction between the surface and the salt. However, to get a reduction in adsorbed amount of about a factor 3 (similar to the reduction in Figure 5.12), we do need a symmetric attraction between the salt and the surface that is several kT's ($\chi \approx -5$).

Another reason to account for this discrepancy between our model and the experiments might be the occurrence of meta-stable states. In Figure 5.10, we can see that sometimes it is possible to find multiple adsorbed amounts corresponding to one bulk concentration. If this also happens in our experiments, it is possible that we think that the system is in equilibrium, but in reality the system is still in a meta-stable state. We do note that the curves in Figure 5.10 are calculated with a high salt concentration, while our experiments are performed with a fairly low salt concentration.

In summary, we have presented a detailed SCF model on the adsorption of PEO on a silica surface. In this model we were able to explain the main effects of salt and pH on the adsorption. In a previous paper we presented experimental data on the adsorption of PEO of varying molecular weight and a family of nonionic surfactants on silica.[79] In that paper we mainly looked at the competitive adsorption of nonionic surfactants and nonionic polymer. The model described here is a first step towards understanding this experimental data on a molecular level. In a subsequent article we plan to use the model presented here to better understand the adsorption from mixtures.

5.6 Conclusion

In this study we developed a self-consistent field model to describe the adsorption of PEO from a watery solution onto silica. To describe all the features that are seen in experiments in a proper way, it is necessary to model the system in a molecular realistic manner. Therefore we introduced chemical detail into our SCF model. We described the PEO in a manner very close to its chemical structure using an O atom and a united atom for CH_2. Furthermore, we included the effect of salt in our calculations. In the bulk, the addition of salt to the system lowers the solvent quality. We found

that the the system starts to phase separate into a polymer rich phase and solvent rich phase at a certain salt concentration, which depends on the total amount of polymer in the system.

We modelled a surface consisting of silanol and siloxane groups. The silanol groups can dissociate and acquire charge depending on pH and ionic strength. The dissociation of surface groups also changes the effective adsorption strength of the polymer. We have calculated titration curves of the silica surface for different salt concentrations, and we have calculated adsorption isotherms where we varied pH or ionic strength. We found that at high pH (≈ 10) the influence of salt is much bigger than it is at neutral pH (≈ 7).

Because the SCF theory gives the surface excess of all species in at least 7 digits, we can study the competition for surface space between polymer and salt. We can clearly see that a layer of adsorbed polymer causes a lowering of the salt concentration near the surface. This is energetically unfavourable, and therefore the salt causes the polymer adsorption/desortpion transition to shift to a lower pH.

We can also combine the bulk behaviour with the surface behaviour. As the salt concentration in the system increases, the solvent quality decreases, leading to higher adsorbed amounts. But the salt in the system also hinders polymer adsorption at the surface. Combining these two features, we find non monotonic adsorption behaviour. In a saturated system, in the case of complete wetting, we can even find prewetting steps, where there is a first order transition from a very thin surface layer to a much thicker layer.

We have compared the results from our calculation with some appropriate literature data, and with some new measurements in our lab. We can reproduce most of the experimental findings. However, the lowering of the surface excess as a function of the salt concentration at relatively low pH is not captured by our model. The reason is probably that we did not include any specific salt adsorption in our model.

Chapter 6

Surfactant adsorption

The next logical step after introducing our SCF model and subsequently applying it to polymer adsorption, is to apply the model to the case of surfactant adsorption. In this chapter we describe how the model is applied to surfactants in bulk. The quality of the solvent for the surfactant head groups is a function of the ionic strength. Using our model, we can predict the response of the CMC and the aggregation number, g, upon varying the ionic strength. We can also evaluate the adsorption properties of the surfactants. Upon changing the ionic strength, the solvent quality for the head groups decreases, which typically results in higher adsorbed amounts. However, as we have shown in chapter 5.2, the dissociation of the surface also depends on the ionic strength and can cause a lowering of the adsorbed amount upon an increase in the ionic strength. These two opposing effects are carefully evaluated below, where we predict that with increasing ionic strength, the $CSAC$ will first slightly increase, but then drop substantially. We also present some profiles, i. e. the distribution of a species close to the surface, to evaluate the competitive behaviour of the salt and the surfactant. The dissociation of the surface can be controlled by controlling the pH, as we illustrated in chapter 5.2. In this chapter we carefully investigate the effect of the pH on the adsorption characteristics of the surfactant. We show that the $CSAC$ depends on the pH.

Surfactants only adsorb if there is an increase in the free energy of the system, which is an alternative manner of saying that surfactants only adsorb if they have a positive surface pressure, π. We can asses π by looking at the ratio $CSAC/CMC$. When this ratio > 1, (i. e. $CSAC > CMC$) surfactant

Part of this chapter has been published as: Bart R. Postmus, Frans A. M. Leermakers, and Martien A. Cohen Stuart. Self-consistent field modeling of non-ionic surfactants at the silica-water interface: incorporating molecular detail. *Langmuir*, 24:3960-3969, 2008.

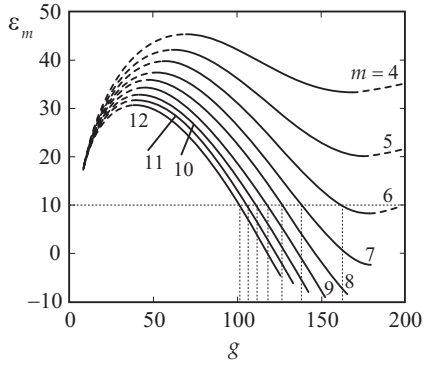

Figure 6.1: *Translationally-restricted grand potential, $\mathcal{E}_m$, plotted versus the aggregation number, g, for $C_{14}E_m$ where $m = 4, 5, ..., 12$. The background electrolyte concentration was set at $\varphi^b_{Cl} = 0.1$. In the graph the line $\mathcal{E}_m = 10$ is exemplified by the horizontal dotted line. The vertical dotted lines point to the corresponding aggregation number g, that are present at the experimentally relevant CMC.*

adsorption will result in an increase in the free energy. Therefore, by evaluation $CSAC/CMC$ one can find adsorption/desorption transitions. It is also possible to investigate the surfactant adsorption kinetics by evaluation the CMC and the $CSAC$.

At the end of this chapter we compare the predictions of our model to some experimental results obtained with a reflectometer as described in chapter 2. We have fount that both the equilibrium predictions as well as the consequences for the kinetics of adsorption follow the experimental findings. Our results show that molecularly realistic models can reveal a much richer interfacial behaviour than anticipated from more generic models.

6.1 Surfactants in bulk: CMC

In figure 6.1 we plot the work of formation of a micelle, or equivalently the translationally-restricted grand potential $\mathcal{E}_m$ as a function of the aggregation number g for $C_{14}E_m$ where $m = 4, 5, ..., 12$. Every curve in this Figure clearly features a maximum. The micelle that exists exactly on this maximum is the smallest thermodynamically stable micelle (according to Eqn. 4.21), which is also referred to as the first micelle. The surfactant bulk concentration where these micelles occur is termed the theoretical CMC. Again, it is often the case that near the first appearance of micelles, the micelle concentration is too low to be noticed in experiments. However, the estimate of the experimentally more relevant CMC given above, is typically very close to the theoretical value. All micelles that are smaller than the first micelle are

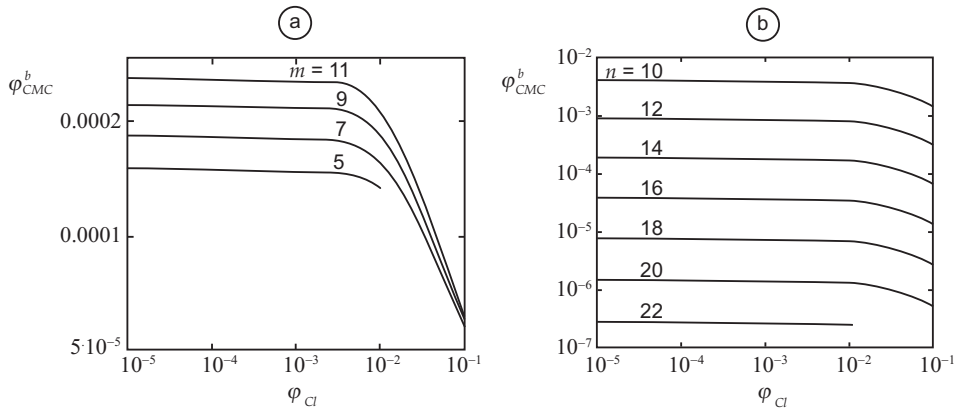

Figure 6.2: *Critical micelle concentration as a function of the ionic strength for eight different C_nE_m surfactants. a) for fixed tail length ($n = 14$) and for a number of head group lengths m as indicated, b) for fixed head group length ($m = 7$) and a number of tail segments n as indicated.*

rejected based on the stability criterium, Eqn. 4.21. This is why we have dashed these parts of the curves in Figure 6.1. Also, at high aggregation numbers there is typically a part of the curve where $\mathcal{E}_m$ starts to increase as g increases. These parts are also dashed since they do not obey Eqn. 4.21. As discussed in chapter 4.4, a pragmatic choice for the CMC is to compute the volume fraction of surfactants in the bulk that is in equilibrium with micelles that have a work of formation $\mathcal{E}_m = 10kT$. In Figure 6.1 we have drawn a dotted horizontal line for this value of $\mathcal{E}_m$ and the vertical lines point to the aggregation numbers g at the CMC.

For some surfactants, $\mathcal{E}_m$ never drops below $10kT$. In such a system the surfactant has a limited solubility, or equivalently, is close to the cloud point. Such systems will also have the tendency to form cylindrical micelles. Indeed this occurs for surfactants with a small head group (data not presented).

In Figure 6.2a we plot the volume fraction of surfactants in the bulk that is present at the experimentally relevant CMC as a function of the ionic strength in the system, for a number of nonionic surfactants. We recall that with increasing ionic strength, the solvent quality for the EO head group deteriorates. So, as the ionic strength increases, the surfactant molecule becomes progressively more 'hydrophobic'. As a result, the molecules have a larger tendency to self-assemble, and the CMC will therefore be lower. This is seen in all curves of Figure 6.2a. Moreover, in line with experimental data it is found that the CMC is a weak function of the head group size. In Figure 6.2a, the head group size was varied from 5 to 11 EO-units, and the CMC changed only by a factor of about two. When we plot the CMC as a

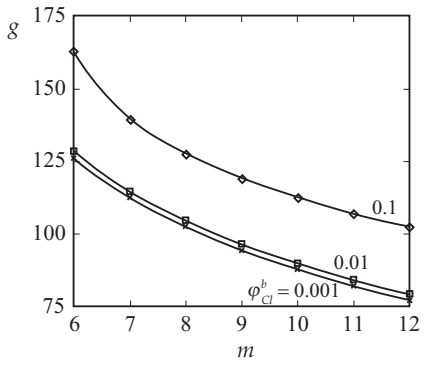

Figure 6.3: *Aggregation number, g, plotted versus the number of EO-groups in the surfactant head group m for surfactants with a C_{14}-tail for three different ionic strengths (ϕ^b_{Cl} = 0.1, 0.01 and 0.001).*

function of the head group size for a fixed tail length and ionic strength, we find a linear dependence (graph not shown).

The effect of the length of the tail on the CMC is much larger, which is illustrated by Figure 6.2b. Varying the tail length from 10 to 22 C atoms, lowers the CMC by four orders of magnitude. Plotting the tail length as a function of the CMC, shows that the CMC varies exponentially as a function of the tail length (graph not shown). This is according to Traube's rule.[80]

The ionic strength not only affects the CMC, but the aggregation number is affected as well. In Figure 6.3 we plot the aggregation numbers for surfactants at the experimentally relevant CMC for three values of the ionic strength as a function of the length of the head group. The lower the ionic strength, the better the solvent quality, and the better the head group can stop the self-assembly process. This means that with increasing ionic strength the stopping force becomes less and the number of surfactants in the micelle g increases. As the ionic strength effects only become important for relatively high ionic strengths, we find very little effects of salt on g in the range of salt volume fractions of 0.001 to 0.01, but much larger effects when the concentration is increased by another factor of 10. The stopping force also increases with increasing length of the head group. A larger head group will oppose to the driving force for aggregation more efficiently which leads to lower aggregation numbers. From Figure 6.3 it can be seen that the increase of ionic strength to the molar range can compensate for a head group size change of two to four ethylene oxide units.

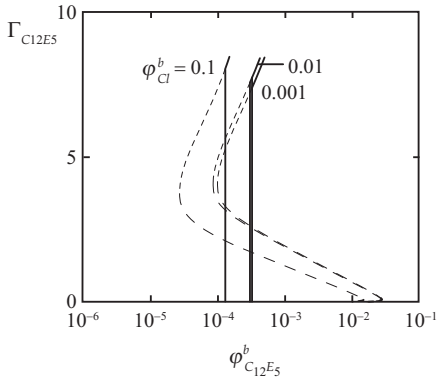

Figure 6.4: *Adsorption isotherms of $C_{12}E_5$, i.e. the adsorbed amount as a function of the logarithm of the equilibrium bulk volume fraction for three values of the ionic strength as indicated. The isotherms feature a van der Waals loop. The transition from the gas to the bilayer state occurs at the $CSAC$ which is indicated by the jump in the isotherm. The meta-stable parts in the isotherm are dashed, the instable parts are dotted. The isotherm terminate at the CMC.*

6.2 Adsorption study: CSAC

For the evaluation of surfactant adsorption we used a flat lattice with a surface positioned at $z = 0$. The presence of the surface implies an adsorbing boundary condition: all conformations that cross this boundary obtain an infinitely small statistical weight. On the other side of the system, i.e. far from the surface we have the bulk solution. In the last lattice layer we implemented reflecting boundary conditions to prevent conformational restrictions and to minimise the effects of a finite system size.

In Figure 6.4 we show a set of three adsorption isotherms of $C_{12}E_5$ on silica for the same three ionic strengths as used in figure 6.3. Due to the mean field approximation, which averages the volume fractions parallel to the surface, one finds surfactant adsorption isotherms that have a so-called van der Waals loop. Such a loop indicates a surface phase transition. In more detail, this means that there is a window of surfactant bulk concentrations for which there exists multiple SCF solutions. Each of these differ with respect to the adsorbed amounts, the structure of the surfactant layer, the charge distribution on the surface, etcetera. Two of these adsorbed states correspond with a (local) minimum of the free energy (meta-stability). The third one is a local maximum (instability). Below the transition point the free energy is lowest for the state of low adsorbed amounts (the so-called 'gas' state because here the surfactants are in low adsorbed amounts far separated

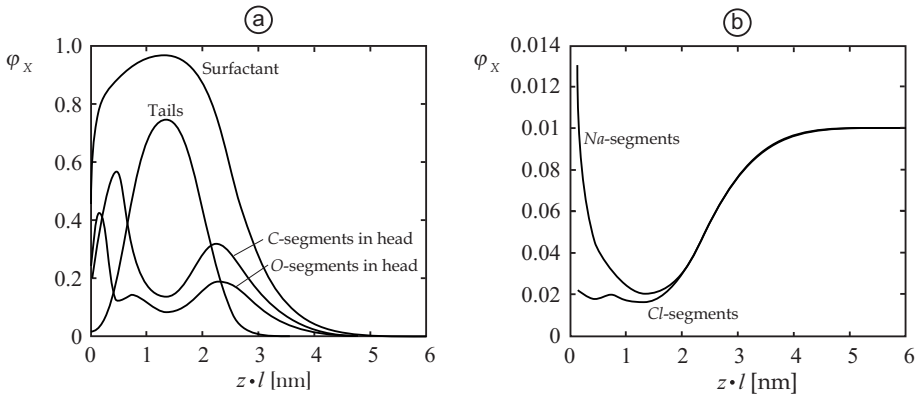

Figure 6.5: *Volume fraction of different segments plotted versus the distance from the surface. In Figure a we show the volume fraction of $C_{12}E_5$ both as a whole and split up in different segments. In Figure b we plot the profile of the salt.*

from each other). Above the transition point the layer with the highest adsorbed amount has the lowest free energy (a well-defined surfactant layer, more specifically a bilayer, is at the surface). At the transition point the two minima of the surface free energy are equally deep and the 'gas' and bilayer phase coexists. The point of the transition can be found by plotting the grand potential as a function of the bulk concentration. This gives a cusped figure. The transition point is at the crossing point because only for this point, the two phases have the same grand potential and the same chemical potentials for all components. We can identify the transition point as the $CSAC$.

On a hydrophilic surface, the nonionic surfactant will adsorb with head groups facing the surface, and an oppositely oriented monolayer is placed on top of this (bilayer configuration). The head groups will shield the tails from the water by closely packing them inside the aggregate. In Figure 6.5 we plotted a volume fraction profile of adsorbed $C_{12}E_5$ at p$H = 7$ and $\varphi_{Cl} = 0.01$. We chose a surfactant concentration just higher than the $CSAC$. Figure 6.5a shows that the surfactant layer is approximately 4 nm thick. We indeed see that all tail groups are found sandwiched between the head groups in a layer that hardly contains any water. However, despite the fact that most head groups are found on the outside of the surfactant layer, there are head groups mixed with the tails in the center. Also, the separation between head groups and tail is not very sharp. This is due to the schizophrenic character of the EO head groups. On the average they are hydrophillic, but they do also contain C-groups that dislike water, and hence like the tails.

Just next to the surface, there is a relatively high amount of O-segments.

This is due to high adsorption energy (i.e. the low χ-parameter between oxygen and the surface). Because every O-segment in the PEO is connected to two C-segments on both sides, there is a low amount of O-segments and a high amount of C-segments at 0.5 nm from the surface. The central part of the bilayer is approximately filled for 75% with tails, 20% with head groups and 5% with water. Since the head groups also contain nonpolar segments, there is no sharp transition between the hydrophobic part and the hydrophillic parts of the bilayer. Furthermore, it is very well possible that there are some head groups mixed in between the tail groups in the hydrophobic domain of the bilayer. However, in our 1G approximation, all lateral surface structures are smeared out.

In Figure 6.5b we plot the volume fraction profiles of the salt. The hydrophobic part of the bilayer has a volume fraction of salt that is approximately five times lower than the bulk volume fraction. This is due to the repulsion between the C-segments and the salt. Near the surface, the concentration of the counter-ion is rather high. The bulk components are either water, surfactant or salt. Because the sum of their volume fractions is unity, and the salt is only 1%, we can say that the part above the surfactant curve in Figure 6.5 corresponds to the local volume fraction of water ($\varphi_W(z)$). Hence, near the surface there is quite a large amount of water. The presence of this water, and the favourable electrostatic potential, causes a rather high amount of counter-ions near the surface. Furthermore, the dielectric constant of the C-groups is rather low, and it is energetically rather costly to have a high potential inside the hydrophobic part of the bilayer. Therefore, it is favourable that the potential drops rather fast and this causes a high concentration of counter-ions near the surface.

We have evaluated the $CSAC$ for a number of different surfactants at varying pH and ionic strength for six surfactants of varying head and tail lengths. In Figure 6.6a we focus on the $CSAC$ as a function of the ionic strength for a given p$H = 7$. In first order, all trends of the CSAC follow those of the CMC. As for the CMC, the effect of the tail length on the $CSAC$ is much larger than the effect of the head group length. Upon a closer inspection however, it is found that the curves in Figure 6.6b all have a small maximum. This maximum is found in the range $10^{-3} < \varphi^b_{Cl} < 10^{-2}$. At ionic strengths lower than that where the maximum is found, the $CSAC$ is suppressed due to the surface charge that increases as the ionic strength increases. As mentioned above, the surfactant layer adsorbed onto the surface is of the bilayer type where the core is densely packed with alkyl chains. However, these hydrophobic cores have a low dielectric constant and thus do not like to be near a charged surface. Hence, charging the surface adds an extra adsorption barrier for the surfactant and the CSAC increases with

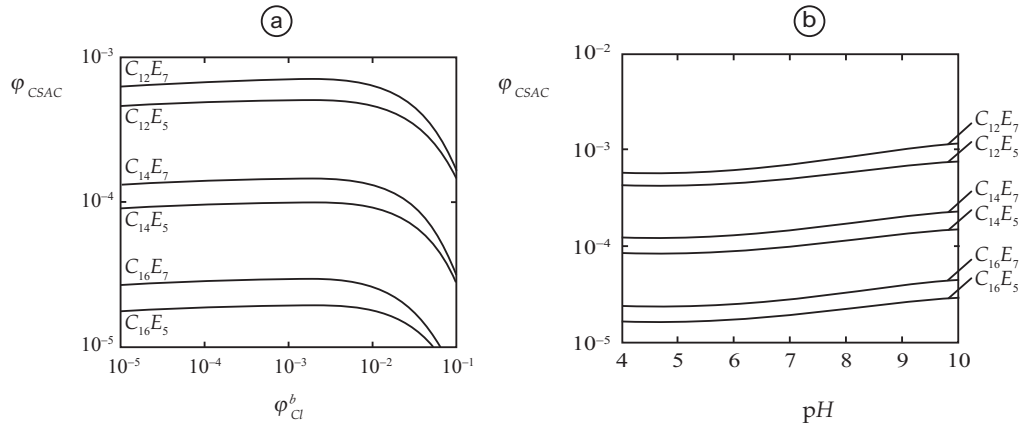

Figure 6.6: *a) CSAC as a function of ionic strength in double logarithmic coordinates at pH = 7. b) The logarithm of the CSAC as a function of the pH for a fixed ionic strength $\varphi^b_{Cl} = 0.001$. The surfactants that are used are indicated.*

increasing ionic strength. At higher salt concentrations - higher than that corresponding to the maximum - we enter the regime where the EO head groups gradually experience a decrease of the solvent quality. This causes the surfactant molecules to become more hydrophobic and this reduced solubility will promote the adhesion of the surfactant to the surface.

In Figure 6.6b we present the predictions on how the $CSAC$ responds to changes of the pH at fixed ionic strength $\varphi_{Cl} = 0.001$. Increasing the pH causes the silanol groups on the surface to dissociate. Since dissociated silanol groups cannot form H-bonds with the EO head groups, the net attraction between these groups decreases. As a result the surfactant only starts adsorbing at higher concentrations and the $CSAC$ increases.

6.3 Combining bulk and surface properties

We present the $CSAC/CMC$ ratio as a function of the ionic strength for a number of surfactants at p$H = 7$ in Figure 6.7a. It is observed that this ratio increases with ionic strength φ^b_{Cl} in the low ionic strength regime 10^{-5} to 10^{-3}. At these ionic strengths, the CMC is almost constant, as we can see in Figure 6.2a,b. This rise is thus entirely due to the rise in the $CSAC$ found in Figure 6.6. In the high ionic strength regime the trend is reversed (Figure 6.7a). From both Figures 6.2a,b, and 6.6a we concluded that in this regime both the CMC and the $CSAC$ decrease. However, the $CSAC$ decreases more rapidly, and hence the ratio also decreases. Part of the reason is that the electrostatic potential generated by the electrified interface drops more

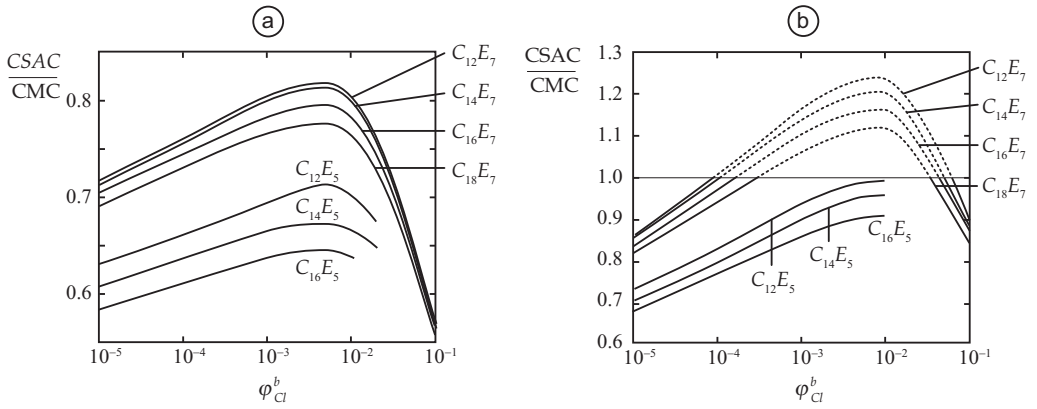

Figure 6.7: *The ratio between the CSAC and the CMC plotted versus the logarithm of the ionic strength φ^b_{Cl} for a number of surfactants. a) at pH = 7, b) at pH=9. The parts of the curve with CSAC > CMC are dotted because experimentally it is difficult to increase the concentration of surfactants above the CMC*

quickly at increasing ionic strength so that the electrostatic potential in the vicinity of the hydrophobic core of the adsorbed bilayer is relatively low. So the penalty to have a hydrophobic region near the interface decreases with increasing ionic strength.

Both the CMC and the $CSAC$ are strong functions of the surfactant tail length. Interestingly though, their ratio is hardly a function of the tail length anymore. Apparently, the shielding of the tails by the hydrophilic head groups is similar in the bulk micelles and near the surface layers. As the adsorption mechanism of the surfactants onto silica involves the affinity of O for the silanol groups, the ratio $CSAC/CMC$ remains a stronger function of the size of the head groups.

Kumar *et al*. considered the adsorption of a number of C_nE_m surfactants on a hydrophobic surface using reflectometry.[81] They found that, on a hydrophobic surface, all adsorption isotherms could be collapsed onto a single curve by scaling the concentration using the CMC and the adsorbed amount Γ by its plateau value, $\Gamma(CMC)$. Based on this observation, they argue that there is a direct relationship between the bulk and surface behaviour of these surfactants. If we compare our predictions with their results, we see that there is a match if we compare surfactants with a fixed head group size. Our predictions do show that there is a head group effect that is not measured by Kumar *et al*.. We attribute this to the different substratum. In our case, the surfactant has to adsorb using its head group, whereas on a hydrophobic surface, the surfactant adsorbs with its tail group. Therefore, the head group

length play a more prominent role in our case.

At p$H = 7$ the $CSAC < CMC$ for all ionic strengths and for all surfactants. This implies that, if the surfactant concentration is high enough, eventually the surface will be covered by a dense surfactant layer irrespective of the ionic strength. This changes when the pH increases. In Figure 6.7b we consider the basic solution p$H = 9$. At this pH the surface is charged more and as a result the number of undissociated silanol groups has decreased. As a result the attraction between the EO groups and the surface decreases with respect to the neutral pH case. The main features of Figure 6.7b are similar to those in Figure 6.7a. However the curves are shifted to ratio's closer to unity. Indeed, parts of some curves show the special situation that the $CSAC > CMC$.

It is well-known that the chemical potential of a surfactant solution has its intricacies. That is, it is a function of the concentration of only the monomers c_s^{mon}[28]

$$\mu_s = \mu_s^0 + kT \ln c_s^{mon} \tag{6.1}$$

In a first order approximation, the monomer concentration is fixed above the CMC. Therefore, the chemical potential of surfactants in solution effectively has the chemical potential at the CMC as its maximum. If the $CSAC$ is higher than the CMC, it actually implies that the surfactant chemical potential needed for the surfactants to adsorb should be larger than the chemical potential at the CMC. Since this is not possible, the surfactant cannot adsorb. The point were $CSAC/CMC = 1$ in Figure 6.7b signals the adsorption/desorption transition. This is the reason why we have dotted these parts in Figure 6.7b. Further inspection of Figure 6.7b shows that it is possible to have an adsorption/desorption transition at relatively low ionic strength, followed by an desorption/adsorption transition at high ionic strength. Such complex behaviour may be of importance for practical applications.

The data shown above points to the possibility to induce an adsorption transition at fixed ionic strength by varying the pH only. Figure 6.8 illustrates this by presenting the $CSAC/CMC$ ratio as a function of the pH at a fixed ionic strength of $\varphi_{Cl} = 0.001$. In this graph we find that the conditions $CSAC > CMC$ is found at a relatively high pH. This is natural because in this limit the driving force force for adsorption vanishes simply because the number of available silanol groups decreases.

6.4 Comparing the model with experiments

As stated above, the idea is to advance molecularly realistic SCF calculations which describe experimental systems accurately, that is at least semi-

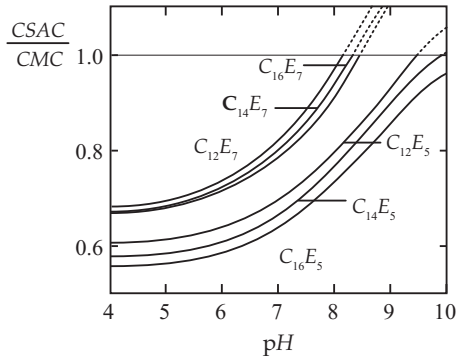

Figure 6.8: *The ratio $CSAC/CMC$ as a function of the pH for a number of surfactants at $\varphi^b_{Cl} = 0.001$.*

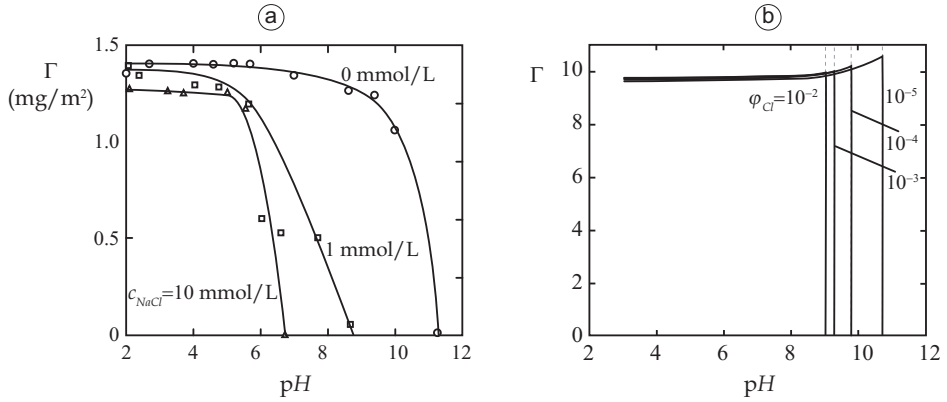

Figure 6.9: *a) Adsorbed amount in mg/m^2 plotted versus the pH for $C_{12}E_5$ as measured by reflectometry for three values of the ionic strength as indicated. b) Adsorbed amount in equivalent monolayers as calculated by our model for a number of ionic strengths as indicated.*

quantitatively. Therefore, it is necessary to critically compare prediction with experimental data. We have studied the adsorption of $C_{12}E_5$ using reflectometry in large detail. As the present paper is mainly theoretical, we can not go into full detail about the experimental conditions, but we may refer to one of our previous papers for this.[79] It suffices to mention that the surfactant $C_{12}E_5$ was dissolved in DI water at a concentration of $6.5 \cdot 10^{-}5$ mol/L (which is near the CMC).[45] When appropriate we adapted the pH using HCl or $NaOH$, and used $NaCl$ to increase the ionic strength. The adsorption of this surfactant was studied using a dynamic reflectometer technique in which the adsorbed amount can be followed quantitatively in real time.

In Figure 6.9a we present three adsorption isotherms of $C_{12}E_5$ at 0, 1 and 10 mmol $NaCl$/L as found by a set of reflectometry experiments. It is seen that the adsorbed amount is rather insensitive for the p$H < 7$. However, at a higher, more basic, pH, the adsorption becomes a strong function of pH. In this regime the adsorption isotherms become a strong function of the salt concentration as well. Indeed in the absence of salt the surfactants adsorb for all p$H < 11$. The addition of only 1 mmol $NaCl$/L causes a shift of the adsorption/desorption transition to p$H \approx 9$, while the transition shifts to even lower p$H \approx 7$ values when the salt concentration is 10 mmol/L.

In Figure 6.9b we tried to reproduce Figure 6.9a using the numerical SCF model. By doing so, we can find significant adsorbed amounts, that is $\Gamma_{C_{12}E_5}$, for a wide range of pH and ionic strengths. However, as we explained above, an adsorption/desorption transition takes places when $CSAC > CMC$. In Figure 6.9b we indicate the occurrence of this transition by the sudden drop of the isotherms. In line with the experimental data, an increase in the ionic strength causes the transition to shift to lower pH values, whereas the adsorbed amount is rather insensitive to pH and ionic strength the remaining part of the isotherm. In the theoretical analysis the drop of the adsorbed amount is jump-like, whereas this is clearly not the case in experiments. This must be attributed to the unrealistic assumption of the mean field model wherein the lateral averaging of the adsorbed layer is implemented. Instead the adsorption, especially near the $CSAC$ is necessarily inhomogeneous and smooth. Therefore also the adsorption/desorption condition taking place at $CSAC = CMC$ is artificial. In reality we must expect a smooth transition similarly as found experimentally.

In a reflectometry experiment we not only have access to the equilibrium adsorbed amount (obtained by waiting long enough for the adsorption to stabilise), but can analyse the kinetics of adsorption and desorption as well. From these experiments we know that the kinetics of adsorption is also influenced by the addition of salt. In Figure 6.10a we plotted the initial rate of

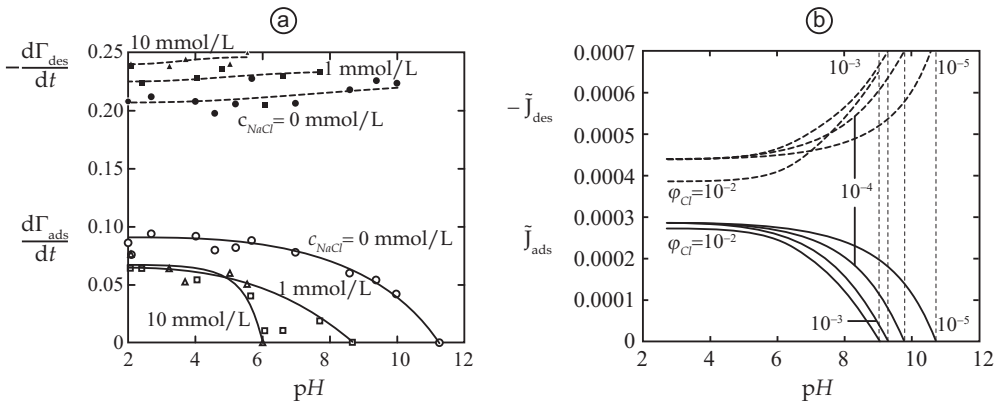

Figure 6.10: *a) The initial rate of adsorption (solid lines) and the initial rate of desorption (dashed lines) of $C_{12}E_5$ as a function of the pH for three different ionic strengths as measured by reflectometry. The surfactant concentration is fixed to be very close to the CMC. b) The corresponding adsorption flux $\bar{J}_{ads}$ and desorption flux $-\bar{J}_{des}$ as a function of pH computed from the theoretical data using the CSAC and CMC, for different values of the ionic strength as indicated. The vertical dotted line presents the adsorption/desorption conditions.*

adsorption (solid curves) and the initial rate of desorption (dashed curves). We see that the kinetics of adsorption slows down when the pH increases. The effect of different ionic strengths is also clear. Without added salt, i.e. for 0 mmol/L salt, the adsorption rate is higher than for the other two curves at all pH-values. For a salt concentration of 1 and 10 mmol/L the adsorption kinetics is the same for low values of the pH, but at higher pH the 10 mmol/L curve drops faster than the other one. The desorption kinetics show the trend that the initial rates increase slightly with increasing pH and the addition of salt seems to increase the rate of desorption even more.

Using the kinetic model by Tiberg *et al.* (see Eqns. 3.2 and 3.3), we may compute the kinetics of adsorption from knowing the position of the $CSAC$ and the CMC.[82] With our model we exactly predict these quantities, but it is not possible to extract a value for the transport coefficient k_{tr}. We therefore introduce two new variables. For adsorption we have $\bar{J}_{ads} = CMC - CSAC \propto J_{ads}$ and for desorption we write $\bar{J}_{des} = -CSAC \propto J_{des}$. Obviously these fluxes are related to the initial adsorption /desorption rates.

In Figure 6.10b we present theoretical predictions for the adsorption and desorption of $C_{12}E_5$ using our model and with Eqn. 3.2. It can be seen that the kinetics of adsorption does not depend on pH at low ionic strength provided that the pH is acidic. At higher pH the adsorption kinetics becomes both a strong function of pH and ionic strength. Similarly as found experimentally (see Figure 6.10a), the speed of adsorption drops to zero above

a threshold pH-value. This value increases strongly with decreasing ionic strength. The desorption-kinetics, which is only a function of the $CSAC$, also follow the experimental trends. With increasing pH the desorption rate increases and the rate is further enhanced by the addition of salt.

The adsorption and desorption curves for the ionic strength of $\varphi = 10^{-2}$ appear to behave exceptionally. Both the adsorption as well as the desorption rates are lower than the other curves at low pH. In Figure 6.6, where the $CSAC$ was plotted as a function of the ionic strength φ_{Cl}, showed that the $CSAC$ started to become significantly influenced by the poorer solvent quality already for $\varphi^b_{Cl} = 10^{-2}$. The rate of adsorption is a function of the CMC and the $CSAC$. In Figures 6.2a and 6.2b we further showed that the CMC also becomes a strong function of the salt strength above $\varphi_{Cl} = 10^{-2}$. The decrease of the adsorption and desorption rates for the rather high ionic strength system must therefore be attributed to these more dramatic solvency effects.

6.5 Conclusion

We have applied the molecularly realistic model that was used previously for the adsorption of PEO onto silica to model the adsorption of nonionic surfactants onto the silica as a function of pH and ionic strength. Using this model we predicted the CMC and the aggregation number of the surfactants, which are a function of the ionic strength. We focused on the sudden adsorption of the nonionic surfactants that occurs above the so-called $CSAC$, and note that the jump-like behaviour is due to the mean-field assumption that we use. In reality the $CSAC$ is a sharp, yet smooth transition. We predicted how the $CSAC$ responds to changes in the pH and ionic strength. By combining the bulk and adsorption results, we find an adsorption/desorption transition as a function of the pH, which depends on the ionic strength. This transition is also found experimentally. By combining results of the theoretical model with a simple kinetic model, we can also predict the initial rate of adsorption and desorption. Again these predictions compare favourably to the rates measured experimentally. In summary, by introducing molecular detail into SCF calculations, we have found rich bulk and interface behaviour that largely follows experimental findings.

Chapter 7

SCF modelling of competitive adsorption

Now that we have thoroughly explored the adsorption properties of solutions containing only PEO or C_nE_m surfactants using our SCF model, it is time to evaluate mixed systems. In this chapter we start by recalling some important PEO adsorption properties, i.e. we look at the effect of chain size on the adsorbed amount and the relation between the bulk concentration and the surface pressure. For the C_nE_m surfactants we recall the relationship between the adsorbed amount and the bulk concentration, and we evaluate the surface pressure as a function of the bulk concentration. We test the validity of the easy-to-use Gibbs approximation for calculating the surface pressure of a surfactant (Eqn. 3.7) by comparing it with our SCF solutions. We find overall a good fit, but there are some details that do not correspond very well.

To predict the behaviour of mixed systems, we use a similar reasoning as we did in chapter 6. We evaluate the behaviour of the $CSAC$ as a function of other system parameters, such as ionic strength, length and concentration of the competing polymer, etcetera. If we find conditions for which $CSAC > CMC$, the surfactant cannot adsorb anymore, and, most probably, the competing species will cover the surface. We also can also make predictions about the adsorption kinetics of the surfactants. However, it turns out the common model is not compatible with our "moving" $CSAC$ idea. Below, we propose a small modification to the model to properly include the behaviour of the $CSAC$. At the end of the chapter, we compare

Part of this chapter will be published in Langmuir as: Bart R. Postmus, Frans A. M. Leermakers, and Martien A. Cohen Stuart. Self-consistent field modeling of adsorption from polymer/surfactant mixtures.

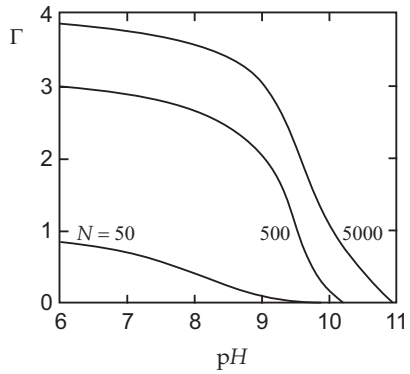

Figure 7.1: *Adsorbed amount, Γ_{PEO}, plotted versus pH for $(EO)_N$ of where N is 50, 500 or 5000 as indicated in the graph. All curves are calculated for $\varphi^b_{PEO} = 10^{-3}$ and $\varphi^b_{Cl} = 10^{-3}$.*

some predicted results with the measured results from chapter 3.

7.1 PEO behaviour

In chapter 5 we carefully looked at the behaviour of PEO. We reported on the scaling of a polymer coil in a aqueous environment, and we determined that for $\varphi^b_{Cl} \leq 0.01 \approx 0.56$ mol/L the solvent quality is good. We also computed a phase diagram to clarify the effect of ionic strength more carefully. In this chapter, we will just make sure that $\varphi^b_{Cl} \leq 0.01$, i.e. that we remain in good solvent conditions. We considered the adsorption of PEO onto a silica surface. As the silanol groups on the surface can dissociate, the surface charge is determined by the pH. The adsorption of a nonionic polymer is influenced by surface charge because it has to compete with charged species - in our case the salt ions - and the polymer has segments with low a diëlectric constant that do not like to be in an environment with a high potential. Furthermore, undissociated surface groups can form H-bonds with the PEO, whereas dissociated surface groups cannot. We have produced a number of adsorption isotherms where we varied pH, salt concentration and some χ-parameters. In Figure 7.1, we present one more result from such calculations. We plotted the adsorbed amount versus the pH for three polymers differing in length only. We see that the longer polymer adsorbs to higher amounts and that the shorter polymer has an adsorption/desorption transition at a lower pH compared to the longer polymer. Both effects are known to occur in experimental cases[54, 83]

As we mentioned before, we want to explain the adsorption behaviour

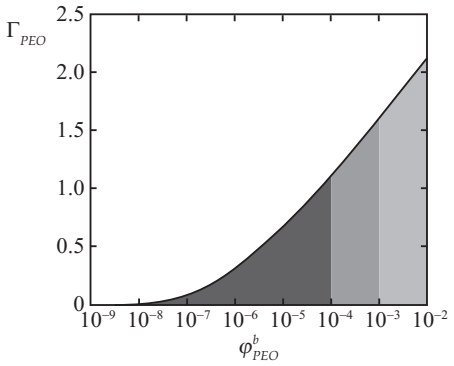

Figure 7.2: *Adsorption isotherm, i.e. surface concentration in equivalent monolayers plotted versus the logarithm of the bulk volume fraction, for the polymer* $(EO)_{100}$.

from a mixture by comparing the surface pressure that individual components can exert. As far as we know, it is not possible to measure the surface pressure at a solid-liquid interface directly. We can, however, use the Gibbs equation to get a feeling for how the surface pressure varies as a function of pH, ionic strength, polymer length, and so forth. In its most general form, the Gibbs equation (for fixed temperature, pH, ionic strength, etcetera) can be written as

$$\pi(\mu) = \int_0^{\mu^b} \Gamma(\mu')\mathrm{d}\mu' \tag{7.1}$$

This equation can be evaluated geometrically by considering the isotherm, i.e. in this case plotting the adsorbed amount of the polymer, Γ_{PEO}, versus the logarithm of the bulk concentration, $\ln(c^b)$. In this case, it is possible to find π at some c^b by evaluating the area under the curve. In Figure 7.2, we present such an isotherm for $(EO)_N$ with $N = 100$. The dark gray area corresponds to the dimensionless surface pressure if $c^b_{PEO} = 10^{-4}$. If the PEO bulk concentration is increased 10 times, the surface pressure will increase with the area which is a slightly lighter grey. Indeed, if we keep increasing the PEO bulk concentration, the surface pressure will also continue to increase.

7.2 C_nE_m behaviour

As mentioned above, we have applied the same SCF model to study surfactant adsorption. Here we used the thermodynamics of small systems to interpret our results. In a previous communication, we have used this model to predict the CMC and the aggregation number of micelles at the CMC.[84]

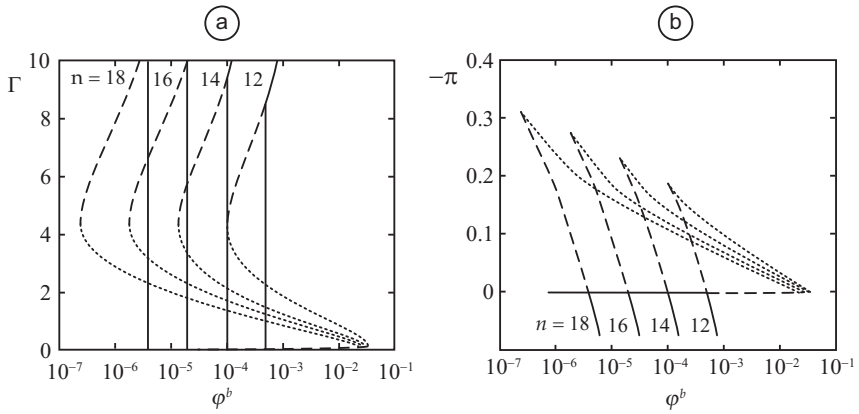

Figure 7.3: *a) Adsorbed amount of surfactant, $\Gamma_{C_nE_5}$, plotted versus the bulk concentration for the surfactants C_nE_5 where we vary n as indicated. b) Negative surface pressure ($-\pi$) plotted versus the logarithm of the surfactant bulk volume fraction. For all curves in Figure a and b we have set $\varphi^b_{Cl} = 10^{-3}$ and $pH = 7$. The stable parts are plotted in a full line, meta-stable sections are dashed and instable parts are dotted.*

We have calculated a large set of adsorption isotherms, where we again varied the pH and the ionic strength. Nonionic surfactants typically start adsorbing strongly to a hydrophillic surface above a certain concentration. This concentration is called the $CSAC$. We predicted how the $CSAC$ changes with the pH and ionic strength.

The chemical potential of surfactants shows the complication that it is only a function of the monomer concentration and effectively independent of the micellar concentration. Therefore, in a first order approximation, the chemical potential is fixed above the CMC. However, the adsorption is a function of the chemical potential. In our calculations, we might find that $CSAC > CMC$, which effectively implies that the surfactant only starts adsorbing at a chemical potential that it cannot obtain. Therefore $CSAC > CMC$ implies that that the surfactant will not adsorb at all.

In Figure 7.3a, we plotted four adsorption isotherms of surfactants differing in tail group length only, as indicated in the graph. Each isotherm displays a typical 'van der Waals loop'. In this loop there are stable, meta-stable and unstable parts. The stable part is plotted as a solid line, the meta-stable part as a dashed line, and the unstable part is dotted. In Figure 7.3b, we plotted the corresponding dimensionless surface pressure - note that it is a negative axis - as a function of the surfactant bulk concentration. The solid lines here correspond to the solid lines in Figure a. They represent those states with the lowest free energy for a given bulk concentration, and thus

they correspond with the most likely states. Unstable states, again denoted with dotted line, can be recognised by noting that it actually costs energy for a surfactant to adsorb, and meta-stable states, denoted by the dashed line, can be recognised by the possibility of choosing a higher surface pressure at the same bulk concentration.

In the article that is the experimental counterpart of this article, we presented the Ansatz that the surface pressure is the leading physical parameter that determines the displacement capabilities of a surfactant.[79] Using our model, we can calculate the surface pressure for a given surfactant at any surfactant bulk concentration. The maximum surface pressure, and hence the maximum displacement capabilities of the surfactant can be found in Figure 7.3 by evaluation π at the CMC. This gives the maximum surface pressure, and hence the maximum displacement capabilities of the surfactant. Figure 7.4a gives $\pi(CMC)$ for a number of surfactants. Clearly, the $\pi(CMC)$ for E_5 surfactants is higher than that for E_7 and E_9 surfactants. In Table 7.1 we listed the ratio of the $CSAC$ and the CMC, and we listed the adsorbed amount at the CMC, because on the basis of Eqn. 3.7, these properties are important. A high surface pressure corresponds to a low value for $CSAC/CMC$ and a high value for $\Gamma(CMC)$. We see that compared to E_7 and E_9 surfactant, the E_5 surfactants have both a low $CSAC/CMC$ and a high $\Gamma(CMC)$. In passing we mention that the increase in the surface excess with a decrease of the head group size has also been found experimentally by Tiberg *et alia*.[32] Hence, the relatively high surface pressure of E_5 surfactants in our model is experimentally validated.

When we consider the influence of the tail group on the surface pressure, we find some remarkable results. For the E_5 surfactants, π is an increasing function of the tail length. However, for the E_9 surfactants, the trend is opposite, and π is a decreasing function of the tail length. The E_7 case seems to be intermediate. This strange tail length dependance is difficult to explain. By carefully looking at Table 7.1 we see that the column $CSAC/CMC$ this column shows the same trend and that $\Gamma(CMC)$ is hardly a function of the tail group length. Hence, for the tail group dependance $CSAC/CMC$ is the leading parameter. In our view on surfactant adsorption, this must have something to do with the packing of the surfactants. Remember that we use a spherical lattice to calculate the CMC, and that we use a flat lattice to calculate the $CSAC$. It might be that some surfactants do not like to form spherical aggregates, and hence the forced geometry might frustrate the packing. For the case of a flat lattice, there might be a similar problem for another surfactant.

The problem with the 1G calculations that we performed, is that the adsorbed surfactant layer must pack lamellar. It cannot form adsorbed micelles

Surfactant type	$CSAC/CMC$	$\Gamma(CMC)$ (molecules/site)
$C_{12}E_5$	0.69	0.349
$C_{12}E_7$	0.81	0.262
$C_{12}E_9$	0.91	0.198
$C_{14}E_5$	0.67	0.353
$C_{14}E_7$	0.82	0.269
$C_{14}E_9$	0.94	0.207
$C_{16}E_5$	0.64	0.347
$C_{16}E_7$	0.79	0.276
$C_{16}E_9$	0.96	0.215

Table 7.1: *Predicted properties of a number of surfactants.*

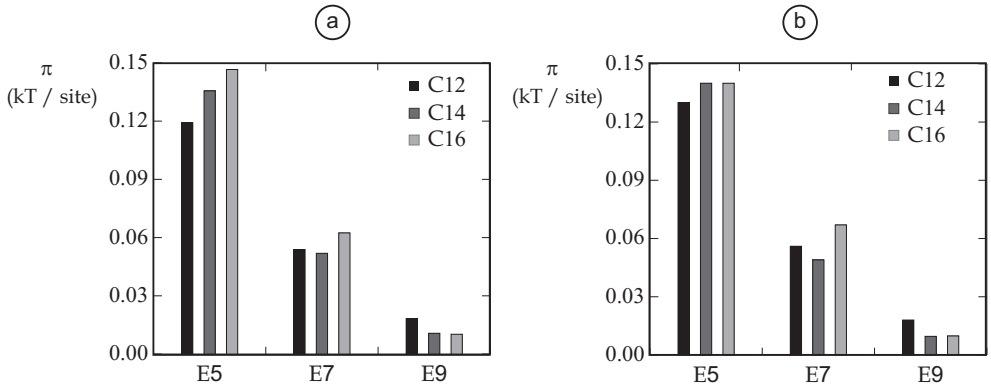

Figure 7.4: *Surface pressure of a number of surfactants a) as predicted directly from our model and b) predicted by taking $CSAC$, CMC and $\Gamma(CMC)$ from the model results and subsequently using Gibbs' adsorption law (Eqn. 3.7).*

or a fragmented bilayer. To get a better idea about the packing of the surfactants, it is necessary to perform 2G calculations. Alternatively, one may do a 1G calculation on a curved interface. In such a system, the volume of a layer is a function of the distance from the surface. One might find an ideal curvature, that corresponds to the most efficient packing. However, these type of calculations fall outside the scope of this article.

By assuming that the surfactant isotherm has the shape of a step function, we can calculate the surface pressure using Eqn. 3.7 and the data from Table 7.1. Of course, the isotherm is not really a step function, and to estimate the error involved, we calculated π using Eqn. 3.7 and we present the outcomes in Figure 7.4b. Since Figure a and b are plotted on an equal scale, we can immediately see that the results are quite similar. However, there are some small discrepancies. When doing the calculations, we fix the chemical

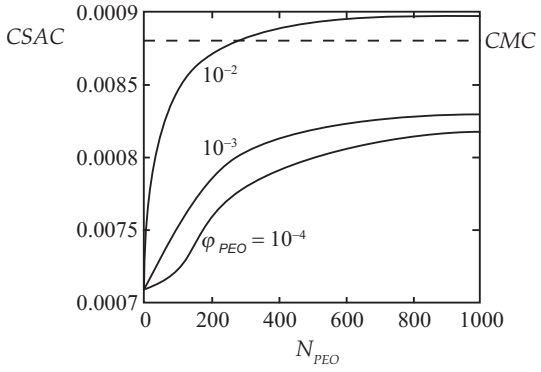

Figure 7.5: *$CSAC$ plotted versus the length of the competing polymer for $C_{12}E_7$. In all these calculations, we set $\varphi^b_{Cl} = 10^{-3}$ and $pH = 7$ and we varied φ^b_{PEO} as indicated.*

potential of all species except for the surfactant. Hence, only the surfactant contributes to π because $\mathrm{d}\mu$ is zero for all other species. Typical, when we perform a calculation, we define a system and we calculate the distribution of all species. Then we add some surfactants, and we do another calculation. We repeat this until we have an entire isotherm. However, when we process these results, the CMC or the $CSAC$ is often not exactly one of the calculated point. Typically, we just draw a straight line between the previous and the next point (linear interpolation), and we estimate the exact value for the CMC or the $CSAC$. Usually this method gives accurate results, however, in the case of a highly curved line, this might give some deviation from the actual value of our calculated result.

7.3 Mixtures of PEO and C_nE_m

As we mentioned above, the results of our experimental observations can be explained if the $CSAC$ would shift towards the CMC due to the competition with other species that also want to adsorb. In our calculations, we define a system that contains PEO, C_nE_m and ions (Na, Cl, H_3O^+ and OH^-). We use the thermodynamics of small systems to calculate the CMC.[72,73] Since the polymer concentration is typically very low, these results are almost equal to the results with only surfactants.[84] Next we can calculate the $CSAC$ where the surfactant has to compete for adsorption with the polymer.

In Figure 7.5 we plot the calculated $CSAC$ for the surfactant $C_{12}E_7$ as a function of the length of the competing EO_N polymer from a bulk solution with a fixed ionic strength and pH, i.e. $\varphi^b_{Cl} = 10^{-3}$ and p$H = 7$.

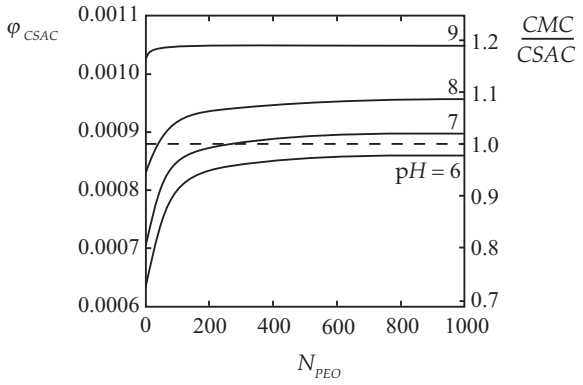

Figure 7.6: *$CSAC$ for $C_{12}E_7$ plotted versus the length of the competing polymer. In all these calculations, we set $\varphi^b_{Cl} = 10^{-3}$ and $\varphi^b_{PEO} = 10^{-2}$ and we varied the pH as indicated. On the right ordinate we normalized the $CSAC$ by the CMC.*

We varied the PEO concentration as indicated in the graph. We see that the addition of PEO causes the $CSAC$ to shift to a higher concentration. The dashed line in Figure 7.5 indicates the CMC ($CMC = 0.00088$). If $CSAC > CMC$, the surfactant cannot displace the polymer anymore. This can be understood from the surface pressure data as well. Since the surface pressure for PEO increases with the concentration (see Figure 7.2), we know that the PEO concentration is an important parameter. This is confirmed in Figure 7.5, where we see that the shift in the $CSAC$ is larger for mixtures with a relatively high PEO concentration.

In Figure 7.6 we plot some results for calculations where we focus on the effect of the pH. Here, we plot the $CSAC$ of $C_{12}E_7$ versus the length of the competing PEO for a number of pHs as indicated. For these calculations, we have set $\varphi^b_{PEO} = 10^{-2}$ and $\varphi^b_{Cl} = 10^{-3}$. The points at $N_{PEO} = 0$ give the variation of the $CSAC$ without any polymer. We see that increasing the pH causes the $CSAC$ to increase. This can be explained by the dissociation of the silanol groups on the surface. More precisely, the number of HA groups on the surface decreases and the number of A groups increases. Since $\chi_{A,O} > \chi_{HA,O}$ - remember that more negative implies more attraction -, the net attraction between the surface and the EO-groups decreases, and hence making it more difficult for the surfactant to adsorb.

In Figure 7.6, the influence of the pH on the displacement behaviour of $C_{12}E_7$ may also be extracted. For p$H = 6$ the shift in the $CSAC$ (for this polymer concentration) will not be large enough to prevent surfactant adsorption at surfactant concentrations equal to or higher than the CMC. However, at p$H = 7$ we see that there is a critical polymer length at which $CMC = CSAC$. Above this length, the $C_{12}E_7$ cannot displace the PEO

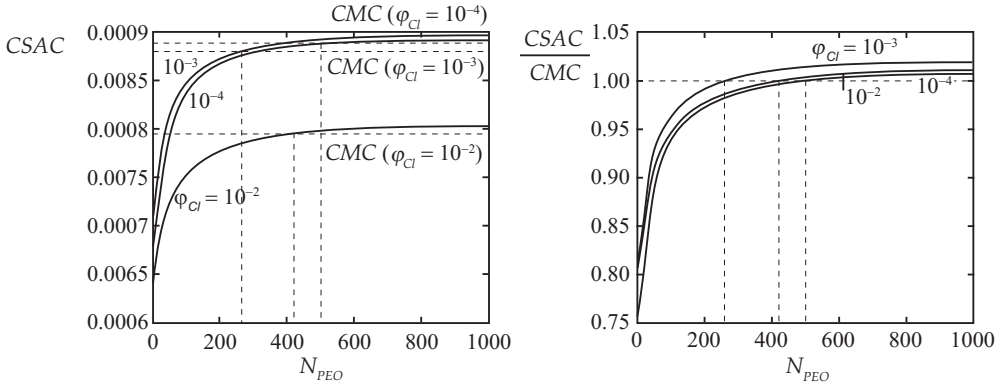

Figure 7.7: *In Figure a we plot the $CSAC$ of $C_{12}E_7$ as a function of the length of the competing polymer for three ionic strengths. The horizontal dashed lines give the CMC. In Figure b we plot $CSAC/CMC$ to emphasise the effect of ionic strength on the adsorption/desorption transition. In these calculations we have set $\varphi^b_{PEO} = 10^{-2}$ and $pH = 7$.*

anymore, and hence the PEO will adsorb. If we go to p$H = 9$, the surfactant cannot adsorb anymore and the surface will be covered by the polymer for all chain lengths (provided it still adsorbs). The PEO might still adsorb. The dependance of PEO adsorption on the pH is described in chapter 5.

Figure 7.7 illustrates the dependance of the $CSAC$ on N_{PEO} for a number of ionic strengths. Here we fixed the pH at 7 and we set $\varphi^b_{PEO} = 10^{-2}$. We know that the salt influences both PEO and C_nE_m adsorption. On the one hand, the salt decreases the adsorption of both species, since it enhances the screening of surface charges and hence facilitates the dissociation of the silanol groups. On the other hand, at high concentrations, the salt decreases the solvent quality of the polymer and the surfactant, and hence their adsorbed amounts may increase.

Obviously, salt will influence the surfactant and polymer adsorption differently. The horizontal dashed line in Figure 7.7a indicates the CMC for the different ionic strengths. Because the CMC is a function of the ionic strength, the Figure looks rather messy. Therefore, we present the ratio $CSAC/CMC$ in Figure 7.7b. In both Figures, we plotted dashed vertical lines that indicate $CSAC = CMC$ or that point where the $C_{12}E_7$ cannot displace the polymer anymore. At very low ionic strength, i.e. $\varphi^b_{Cl} = 10^{-4}$, $C_{12}E_7$ can displace polymer with a length smaller than $N_{PEO} \approx 500$ units. If we go to a 10 times higher ionic strength, the displacement capabilities of the $C_{12}E_7$ decrease. At this ionic strength, it can only displace PEO up to $N_{PEO} = 250$. Apparently, the salt has a stronger influence on $C_{12}E_7$

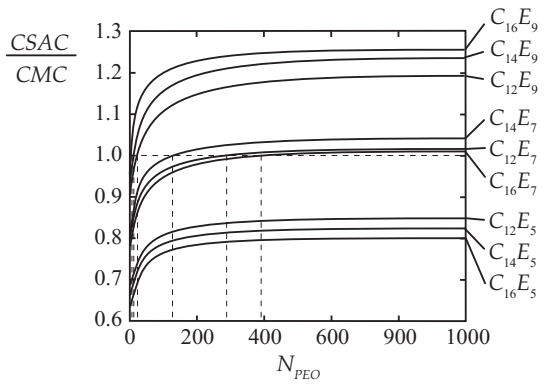

Figure 7.8: *CSAC plotted against the length of the competing polymer for a number of C_nE_m surfactants.*

than it has on the PEO. This can be attributed to the differences in layer structure. The surfactant forms a bilayer-like adsorption layer, where the solution side and the surface side of the layer consist of EO groups, and the interior consists of alkyl tails. The polymer can only adsorb as an EO layer, where the density of the EO is an intricate function of the distance to the surface. If we add salt to our system, the silica surface will respond by increasing its charge. This charge has to be compensated in the solution by the counter-ions. However, the ions tend to avoid the hydrophobic center of the surfactant bilayer. Hence, the ions that are attracted by the charged surface, repel the surfactant layer, which causes a disturbance in the balance between the polymer and the surfactant. Furthermore, the hydrophobic center of the bilayer has a low diëlectric constant, which makes it even more unfavourable to be near a charged surface.

If we increase the ionic strength to $\varphi^b_{Cl} = 10^{-2}$, we see that the displacement capabilities of the surfactant seem to increase again. This effect can be attributed to the bulk effect, or the solvent quality. Apparently, the decrease in solvent quality has a larger effect on the surfactant than it has on the polymer.

So far, we have explored the sensitivity of the system for variations in the salt concentration, PEO concentration and pH. Next we want to compare the displacement behaviour of different surfactants. We have chosen to set $\varphi^b_{Cl} = 0.001$, $\varphi^b_{PEO} = 0.01$ and p$H = 7$. The C_nE_m surfactants that we looked at have $n = 12 \vee 14 \vee 16$ and $m = 5 \vee 7 \vee 9$. The results of these calculations are summarised in Figure 7.8. In this case we can only plot the $CSAC$ normalized by the CMC, because $CSAC$ changes orders of magnitude when the surfactant tail length is varied.

With Figure 7.8 we show that the length of the head group is very impor-

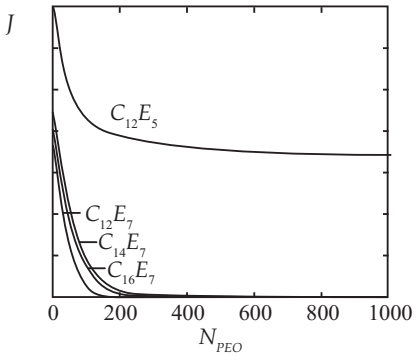

Figure 7.9: *Displacement rate plotted versus the length of the displaced PEO for four surfactants.*

tant for the displacement behaviour. The smaller the head group, the better the displacement capabilities. This is consistent with Figure 7.4, where we saw that surfactants with a small head group can generate a high surface pressure when they are adsorbed from a solution with a surfactant bulk concentration that is equal to or higher than the CMC. As it is reasonable to think that the adsorbing species will be that species that can generate the highest surface pressure, it is only logical that these species are the best displacers.

For the surfactants with a small head group ,E_5 in Figure 7.8, we see that the curve for the C_{12} tail is higher than those curve for the C_{14} and C_{16} tails. This means that for E_5 surfactants, the displacement capabilities increase as the tail length increases. However, for the E_9 surfactants this is exactly opposite. The displacement capabilities decrease as the tail length increases. Interestingly, for the E_7 surfactant the order seems to be some sort of intermediate.

The order of the lines in Figure 7.8 is exactly opposite to the order in Figure 7.4. If the surfactant has a high surface pressure in Figure 7.4, it is difficult for the PEO to compensate this surface pressure. Hence, to increase the $CSAC$ to the point where $CSAC/CMC = 1$, the PEO has to compensate the high surfactant surface pressure, which is only possible at a high N_{PEO}.

7.4 Kinetics of adsorption from mixtures

As mentioned above, we have previously explained the surfactant displacement kinetics using Eqn. 3.2. The r.h.s. of this equation has two terms. One monomer term that assumes a local equilibrium at the surface, and hence,

the adsorption kinetics of the monomers can be calculated from the equilibrium isotherm. The other term describes the micellar transport. Frequently, it is assumed that the micelles fall apart into g monomers near the surface, and that it is only these monomers that adsorb.

Our idea of a $CSAC$ that basically depends on the entire system, and not just on the surface, is not always compatible with Eqn. 3.2. If we start by looking at the case where $c_b < CMC$, i.e. there are no micelles. Since there is no adsorption if $c_b < CSAC$, the corresponding flux should also be zero: $J(c_b < CSAC) = 0$. For the case that $CSAC < c_b < CMC$, the flux is equal to

$$J(CSAC < c_b < CMC) = k_{mon}(CMC - c_b) \tag{7.2}$$

If the $CSAC > CMC$, the adsorption should also be 0 because, according to Eqn. 3.6, it is not energetically favourable to adsorb anymore. Hence, the corresponding flux needs to be zero: $J(CSAC > CMC) = 0$. This is obvious for the case where there are only monomers, but it also has to apply for the regime above the CMC where micelles exist and contribute to the transport.

In Eqn. 3.2, the monomer adsorption rate becomes negative if $CSAC > CMC$. And the micellar adsorption rate is not a function of $CSAC$ at all, which implies a non-zero adsorption rate for the case of no adsorption. To correct such an unphysical prediction, we want to include the $CSAC$ in the micellar contribution to the adsorption rate in some way. This makes sense, since the micelles need to fall apart in order for the monomers to adsorb. We have chosen to keep things phenomenological and simple, and we therefore want to multiply the micellar contribution with a linear function that goes to zero for $CSAC \to CMC$. Hence, we multiply the micellar adsorption rate with $(CMC - CSAC)/CMC$. Suppose that, for some surfactant in a system without any competing polymer, $CSAC = 0.7CMC$. In this case, our function $(CMC - CSAC)/CMC = 0.3$. As the $CSAC$ shifts towards to CMC, the micellar contribution to the adsorption rate goes to zero, which is in line with our physical idea about the system.

$$\begin{aligned} J(c_b > CMC) &= k_{mon}(CMC - CSAC) + k_{mic}(c_b - CMC)\frac{(CMC - CSAC)}{CMC} \\ &= [k_{mon} - k_{mic}(c_b - CMC)/CMC]\,(CMC - CSAC) \\ &= k_t(CMC - CSAC) \end{aligned} \tag{7.3}$$

In Eqn. 7.3, the adsorption is governed by $CSAC - CMC$, which represents the monomer adsorption. The only influence of the micelles is though an

	measured	predicted
$C_{12}E_5$	10^3 - $2 \cdot 10^3$	$\gg 1000$
$C_{12}E_7$	10^2 - $3 \cdot 10^3$	305
$C_{14}E_7$	$3 \cdot 10^2$ - $5 \cdot 10^2$	130
$C_{16}E_7$	10^3 - $2 \cdot 10^3$	425

Table 7.2: *Comparison between experimental and predicted critical polymer length (N^c_{PEO}) for four different surfactants. Because we only tested a number of available PEO lengths in the experiment, we can only give a concentration window for N^c_{PEO}.*

increasing transport coefficient, and not through direct adsorption. This idea is also at the basis of the kinetic model of Tiberg *et al.*, but in their final equation it is obscured.

We calculated the kinetics of displacement using Eqn. 7.3 for a number of surfactants. In Eqn. 7.3 there is a transport coefficient for the monomers, k_{mon}, and for the micelles k_{mic}. Here, we have set $k_{mon} = 1$, and $k_{mic} = g^{-1/3}k_{mon}$ where g is the aggregation number as calculated in our bulk calculations on micellization using the SCF model (recall that the volume of a micelle scales with g, and hence the radius of a spherical micelle scales with $g^{1/3}$). The results of these calculations are plotted in Figure 7.9. We see that for the E_7 surfactants, the adsorption rate J goes to zero as $CMC-CSAC$ goes to zero. For the case of $C_{12}E_5$, we see that J does not go to zero. This makes sense, since we know that PEO cannot displace $C_{12}E_5$ in our model from Figure 7.6, and hence J should not go to zero. Despite of the observation that PEO cannot displace $C_{12}E_5$, it does slow down its adsorption.

7.5 Comparing model predictions with experiments

As mentioned above, we want to use our model to rationalise the experiments that we published before.[79] In table 7.2, we summarised some of the experimental data. In the column "measured", we give a window that encompasses the maximum length of the PEO (the number of EO groups in the polymer) that the surfactant can displace. The column called "predicted" gives the N_{PEO} needed to get $CSAC = CMC$, which can be interpret as the modelled equivalent of the experiment. We see that $C_{12}E_5$ and $C_{16}E_7$, which are experimentally the best displacers, are also the best displacers in our model.

However, in our model, $C_{12}E_5$ is a better displacer than $C_{16}E_7$. Also, the experimental displacement capabilities of $C_{12}E_7$ and $C_{14}E_7$ do not match the predicted ones very precisely.

We attribute these discrepancies to the fact that our model adsorbed layers are smeared out. There is experimental evidence that surfactants adsorb in admicelles, or in a fragmented bilayer.[33,34,85] The shape of the surface aggregates that the surfactants assume probably depends on the surfactant architecture. In our calculations, we do include the excluded volume of a surfactant molecule. However, the existence of discrete aggregates is ruled out in our 1G calculations. This is an oversimplification of the model compared to the experiments. It is possible to improve on this situation, by doing 2G calculations. However, these calculations are very time consuming, and one has thus to be careful in identifying the most relevant calculations.

Despite the observation that our model does not capture the exact displacement capabilities of our experiments, we do feel that we captures the essence of the most important physical phenomena. We can predict that PEO hinders C_nE_m adsorption. Sometimes, this gives an adsorption/desorption transition, and sometimes there is only a decrease in the adsorption kinetics.

7.6 Conclusion

We have used a self-consistent field model to examine the competitive adsorption from aqueous polymer/surfactant mixtures onto a silica surface. The molecules are defined in a detailed molecular model. We have shown before that this model can be used to predict the bulk and adsorption properties of PEO and C_nE_m from solutions only containing the individual components. In this paper we defined mixed solutions and examined the concentration where the surfactant starts to adsorb ($CSAC$). We varied a multitude of parameters, such as polymer length, polymer concentration, surfactant architecture, salt concentration and pH. Our predictions on the pH and salt response of the system can easily be understood in terms of dissociation of the silica surface and shielding of the surface charges.

When we calculate the surface pressure associated with the adsorption of surfactants on the silica/water interface, we find a small tail length dependance. The surface pressure seems to increase with increasing tail group length for surfactants with a small head group, and for surfactants with a bigger head group, the surface pressure decreases with increasing tail group length. When we compare displacement capabilities between different surfactant architectures, we see the same trend as the surface pressure graphs.

This seems logical since we argued that the surface pressure that can be generated by the adsorbing species is the leading parameter that decides what species adsorbs in a competition case.

The ultimate goal of the model described in this paper, is to rationalise experimental data published recently.[79] In this paper, we concluded that a shift in the $CSAC$ in the presence of PEO would explain our experimental results. Using our current model, we can reproduce the shift in the $CSAC$. There are, however, still some discrepancies regarding the experimentally found trends concerning the effect of changing head group size or tail group size. We attribute these discrepancies to the fact that our model assumes a smeared out layer on the surface, whereas in reality, many surfactants adsorb in admicelles or in a fragmented bilayer. These issues can probably be resolved by doing 2G calculations, or maybe even by doing 1G calculations on a curved surface.

Chapter 8

General discussion

The research described in this thesis focusses on the competitive adsorption of nonionic polymers and surfactants on a silica surface. Both species readily adsorb on the silica from single component solutions by forming H-bonds. Adsorbed polymers typically have many adsorbed monomers (train segments), that all contribute to the total adsorption energy. Hence, an adsorbing polymer has intra-chain cooperativity. Surfactants are small molecules, that typically adsorb in surface aggregates. In our case – adsorption on a hydrophilic surface from an aqueous solution – the head groups are attracted to the surface, and the tail groups are attracted by other tail groups. Therefore, adsorbing surfactants show inter-molecular cooperativity.

Our focus is on the battle for adsorption between a polymer and a surfactant. In the previous chapters, we have described a number of reflectometry experiments. We have evaluated the response of an adsorbing polymer or surfactant to changes in the pH and/or the ionic strength. Also, we have used the reflectometer to study the adsorption from mixed systems, i.e. systems containing both surfactants and polymers. To understand our experimental results on a molecular scale, we have modelled our system using SCF theory.

8.1 Molecular competition in technology

All the research described in the previous chapters concerns the $PEO/C_nE_m/SiO_2$ model system. One might think that, after reading through so many pages about a well defined system, the results are only interesting in an academic setting. This is not true. Many technological settings, some of which are mentioned in chapter 1, rely on competitive adsorption. To emphasise the technological importance of our results, I will sketch how competitive

adsorption might be beneficial for life sciences below.

Fouling is the accumulation of proteins, bacteria and other species on surfaces. It is often undesired since it can lead to technology breakdown and downtime. For instance, in the marine industry, thick layers of proteins, bacteria, and algae can form on ship hulls, which has a negative effect on the ships streamline, and hence on its fuel economy.[86] Fouling also occurs in other industrial settings, for instance the formation of biofilms on membranes used in separation steps in the food processing industry. In a biomedical setting, the formation of a biofilm on medical implants can lead to dangerous infections.[87]

The formation of these biofilms is typically described in multiple steps. The first step is always the formation of a conditioning film, which is the accumulation of small species – such as polymers, proteins, etcetera – on a surface. This step is typically followed by bacterial adhesion, and the formation of an extra-cellular matrix. Since the formation of a biofilm starts with the formation of a conditioning film, and this film is in direct contact with the surface, the removal of a biofilm is often focussed on destroying the conditioning film. One of the proposed methods of removing a conditioning film, is the addition of surfactants. Surfactants can remove proteins from interfaces by two mechanisms: i) solubilisation, where the surfactants form a soluble complex with the proteins, and ii) replacement, where the surfactant displaces the protein.[88] Typically, ionic surfactants bind stronger to proteins compared to nonionic surfactants. Therefore, the solubilisation mechanism is often found for ionic surfactants, and the displacement mechanism is regarded prominent in the case of nonionics.[89]

The goal of the research described in this thesis is to study the fundamentals of competitive adsorption from mixtures. We have therefore decided to evaluate a relatively simple system. Our system of choice was the polymer PEO mixed with the surfactant C_nE_m. These species do not form mixed aggregates in solution, which enables us to really focus on the competition on the surface. Also, PEO and C_nE_m are often used for all kinds of technological purposes. We have chosen to use silica as the adsorbent. Both species readily adsorb onto this surface, it is highly reflective which is useful for experimental purposes, and the silica surface is often found in technology.

8.2 Experimental observations

Our method of choice to study the competitive adsorption from mixtures is reflectometry. This optical technique is very sensitive for changes in adsorbed layer density. Of course, this method also has some drawbacks. The

major drawback of using reflectometry to evaluate our system is that it cannot 'sense' what species is adsorbed. In chapter 3 we have used tricks to determine what species was adsorbed, e.g. we could distinguish based on the adsorbed amount and the ability to redissolve the layer. To actually measure how component A desorbs as component B is adsorbing, one should combine two techniques. For example, the combination of TIRF and reflectometry used by Fu and Santore to investigate the competition between PEO chains of different molecular weights.[55] An issue of using this technique is that it requires the addition of a label to one of the components, which might disturb the subtle balance between the competing effects in our system.[90] A method that might be used to distinguish between polymer or surfactant adsorption and that does not require the use of labels is solvent relaxation NMR.[59,61,91] However, this technique can only be used to study equilibrium layers and not the actual displacement process.

The reflectometer that we used was equipped with a stagnation point flow cell connected to a syringe pump to regulate the flow rate. This requires a closed cell, that was specially made for this setup. In this cell, the distance between the adsorbent and the prism (h in Figure 2.4) is fixed. Combined with the precise control over the flow rate, this allows for accurate kinetic studies. Another advantage of our closed flow cell is the use of a round silicon fluid barrier (a silicon O-ring), that is virtually leak prove.

In chapter 3.1 we describe a method to thoroughly clean the silica. This method is certain to remove all organic molecules, and hence, it allows for recycling of the surfaces. This recycling of the surfaces is the method of choice for minimising the error between experiments. The surface of a glass bottle is very similar to a silica surface. Hence, we can use our results on adsorption/desorption transitions to clean our glassware. It is advantageous to always use the same glassware. Bottles containing a surfactant solution can be cleaned by rinsing with copious amounts of solvent. The bottles used to contain a polymer solution can be cleaned by a surfactant solution, or, by a solution with a high pH and some salt.

Our experiments show that surfactants are very effective in probing the properties of a polymer layer. If a surfactant needs to displace a polymer layer in order to adsorb, the surfactant adsorption rate depends on how fast it can displace the polymer. We have found that the time a surfactant needs to displace a polymer layer increases with the length of polymer. This observation gives some unexpected possibilities.

It is thought that a freshly adsorbed polymer layer is not in thermodynamic equilibrium.[20,49] After the polymer chains adsorb, they start rearranging to an energetically more favourable state. This process is often called relaxation. In chapter 3 we argue that the rate of surfactants displacing a

polymer is a function of the polymer surface pressure, e.g. the free energy of adsorption. The only reason for polymers to relax is to somehow find a state that has a lower free energy. Hence, our surfactants should be able to probe the amount of relaxation. We performed measurements where we changed the relaxation time of the polymer layer from 1 minute up to 17 hours. In all these experiments we have found similar displacement rates, and hence we conclude that a layer of adsorbed PEO needs less than 1 minute to relax. Other studies on competitive adsorption of coumarin labelled PEO with unlabelled PEO have found that relaxation takes place in the first 10 h after initial adsorption.[49] However, it has been shown that 'normal' PEO adsorbs favourable on soda-lime glass when it is mixed with Fluorecein labelled PEO.[90] In our view, the influence of the coumarin label on the PEO adsorption behaviour should be a similar. Hence, we attribute the inconsistencies in the relaxation results to the use of the coumarin label, and we claim that our results are accurate.

8.3 On the modelling of complex fluids

Performing and evaluation adsorption experiments typically leads to increased insight in the adsorption or displacement process. Another method of acquiring insight in these processes is to develop a theoretical model. We have made such a model within the framework of the self-consistent field theory. Similar models have been developed to understand the adsorption behaviour of systems containing only polymer[68,69] or containing only surfactants.[92,93] Since polymers are long chains, the modelling of such systems is often focussed on the general behaviour of polymers without introducing much chemical detail. Surfactants consist of (at least) two different groups. Hence surfactants are typically described in more detail compared to polymers.

Systems containing more than one component often feature species specific behaviour. We aimed to include the specific behaviour of our system, such as the salt and pH dependance, in our model. We therefore decided to model the system in a fairly detailed manner. We understand that this implies that the predicted results only apply for relatively few systems, however, we argue that this is the way to evaluate complicated systems theoretically.

8.4 Outlook

In chapter 3.4.1 we concluded that the packing of our nonionic C_nE_m surfactants is important. Surfactants unimers with a cylindrical shape – $CPP \approx 1$

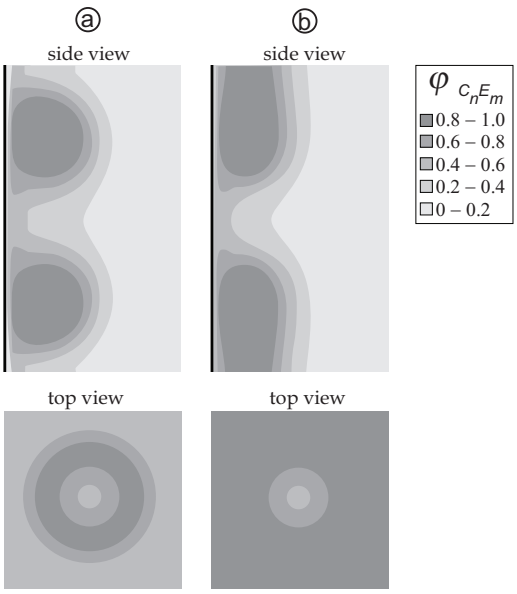

Figure 8.1: *Volume fraction contour plot of a 2G calculation for a) $C_{12}E_7$ and b) $C_{16}E_5$. We are looking at a cross-section perpendicular to the surface and a top view. The gray scale indicates the volume fraction of the surfactant as indicated in the legend. We interpret a) as a torus and b) as a bilayer with a hole.*

– will form large objects in solution and will form bilayers at hydrophilic surfaces. The bilayer configuration is rather efficient, since it covers the whole surface and does not leave much 'empty' space like in the case of admicelles. Hence, surfactants that adsorb in a bilayer-like structure typically adsorb in high amounts (in moles/m^2), and, according to the Gibbs adsorption law (Eqn. 3.7), the surface pressure of these surfactants is high (provided that $CSAC/CMC$ is constant). We argue that high surface pressure implies strong displacing capabilities. Therefore, surfactants that pack efficiently in a bilayer are good displacers, and surfactants that adsorb in admicelles have lower displacement capabilities.

If two nonionic surfactants are mixed, they will form mixed micelles in the bulk,[1,94] and also on the surface they will form mixed aggregates.[52] The preferred curvature, e.g. the degree of fragmentation of the adsorbed layer, of these systems is probably some sort of intermediate depending on both species. By carefully choosing different surfactant architectures and bulk concentrations, it might be possible to make mixtures that can displace very long polymers, i.e. longer than any of the two components can displace without the other. An example of such a system is the mixture of $C_{12}E_3$ with $C_{12}E_7$. In technology, surfactants are typically not homo-disperse, but have

a certain distribution. Hence, knowledge about the displacing capabilities of mixtures of surfactants is relevant for applications.

In chapter 7.5, we concluded that we can capture the experimentally observed adsorption behaviour of PEO/C_nE_m mixtures quite reasonably. However, in our model, the surfactants with small head groups appear to have an unrealistic advantage over surfactants with a slightly bigger head group. We attribute this inconsistency to the fact that we have neglected the fragmentation of an adsorbed layer of surfactants. In our adsorption calculations we force all surfactants to form a bilayer, even if the surfactant might prefer to form a more fragmented layer.

There are a couple of methods to account for fragmented layers in the SCF model. It is possible to do calculations that allow for concentration gradients along the surface (e.g. 2G calculations). Figure 8.1a illustrates such a calculation for $C_{12}E_7$ and 8.1b for $C_{16}E_5$. For these calculations we have set p$H = 7$, $\varphi_{Cl} = 10^{-2}$ and the surfactant bulk calculations is set at the CMC as obtained using an 1G calculation. For both side views, the surface is on the left side, and the bulk solution is on the right. The gray scale gives the amount of surfactant as is indicated in the legend. The top view gives the distribution of surfactants if one would look from the bulk solution side to to surface. Obviously, this 2G method does allow fragmented layers to be formed, and hence, will probably give slightly different results than our 1G approximation. It is also possible to do a 1G calculation on a curved lattice. In this case, the volume of a layer is an increasing function of the distance from the center. By evaluation the (mean field) free energy as a function of the curvature, it is possible to gain insight in the preferred form of the surfactant aggregates.

Summary

The research described in this thesis focusses on the competitive adsorption of nonionic polymer and nonionic surfactant on a silica surface. These type of systems are interesting from both an academical and a technological viewpoint. Our academic interest stems simply from the observation that we had a hard time predicting the (adsorption) behaviour of the system beforehand. The technological relevance of our study can be attributed to the observation that technological applications are often complex mixtures containing a large variety of additives. The interactions between all these different components, such as the formation of mixed aggregates or co-adsorption, are quite complex. For applications, these interactions are very important since the properties of a mixture on a microscopical scale can be used to manipulate the macroscopical behaviour. Or, in the case of undesirable macroscopic behaviour, a detailed knowledge about the microscopic interactions can be used to improve on the situation.

For the research described in this thesis, we restrict ourselves to a relatively simple complex mixtures, i.e. we choose a well-defined model system consisting of homodisperse components. This model system is an aqueous mixture of the nonionic polymer PEO with the nonionic surfactant C_nE_m. To study the adsorption behaviour of this mixture, we have chosen to use a flat silica surface as a model surface.

The C_nE_m surfactants adsorb (on a hydrophilic surface) with their head groups. Because the head groups consist entirely of EO segments, the binding mechanism of the surfactants to the silica is exactly the same as the PEO binding mechanism, namely H-bonding. By evaluating the competitive adsorption of the system, we are effectively investigating the subtle effects of layer structure. By making small changes to the choice of surfactant architecture, polymer length or solvent quality, large changes in layer structure can be induced.

To study the interactions between the PEO and the C_nE_m in the bulk experimentally, we used dynamic light scattering (DLS). Solutions containing only surfactant were prepared and the hydrodynamic radius of the micelles was measured. For these measurements, it was necessary to use quite high surfactant concentrations (3.00×10^{-3} mol/L) in order to get a proper signal. Next, we turned our attention to mixed solutions containing both PEO and surfactants. Typically, a co-assembly of polymers and surfactants, such as the string-of-pearls aggregate, is a rather large structure, and hence, it should be very well observable using DLS. Measurements on these polymer/surfactant mixtures were performed, and it turned out that the micellar size was basically the same with and without the polymer. Hence, we conclude that the polymer and the surfactant do not form mixed aggregates in solution. This result is consistent with the experimental fact that PEO does not phase separate in these single component solutions, from which we can conclude that the EO head groups of the surfactants will not have an attractive interaction with the polymer. It is also consistent with the observation that the the tails of surfactant unimers do not aggregate on the heads of other unimers or on the micellar corona, which would result in phase separation.

Reflectometry was used to investigate the adsorption behaviour of solutions containing either PEO or C_nE_m. In these experiments we have varied the ionic strength and the pH, as well as the polymer length and the surfactant architecture. The results for the experiments with only PEO showed that the adsorbed amount of PEO increases linearly with time until the surface is saturated. For the case of p$H \approx 5.8$ and no added salt, we typically found adsorbed amounts of EO_N ranging from 0.2 mg/m^2 for $N = 100$ to 0.5 mg/m^2 for $N = 4000$. These adsorbed amounts were found almost independently of the PEO bulk concentration. Hence, PEO adsorbs according to a high affinity isotherm. By subsequently rinsing the polymer layer with solvent, it proved impossible to rinse the PEO layer away. We also performed a series of experiments where we varied the pH or the electrolyte concentration. To limit the number of experiments, only EO_N with $N \approx 1000$ ($M_w = 43520$ g/mol) was investigated. To set the electrolyte concentration, $NaCl$ was added, and the pH was adjusted using HCl or $NaOH$. The results show that when the pH of a solution that does not contain any salt is varied, the adsorbed amount is approximately constant (0.3 mg PEO/m^2) between pH = 6 and 9. Further increment of the pH causes the adsorbed amount to decrease until it is zero at pH = 11. Adding some salt (10 mmol/L) to the polymer solution, will result in a lower adsorbed amount for every pH. Also the adsorption/desorption transition shifts to a lower pH due to the salt.

The adsorption behaviour of C_nE_m was also evaluated using reflectometry. Surfactant adsorption behaviour is very different compared to that of

polymers. From an aqueous solution where the surfactant concentration is equal to the CMC (p$H \approx 5.8$ and no added salt), surfactants adsorb to a higher surface excess compared to polymers. Furthermore, it is easy to redissolve the adsorbed surfactant layer by rinsing with solvent. We did a series of measurements where we systematically varied the surfactant type and the bulk concentration to get a number of adsorption isotherms. Typically for surfactants, the adsorbed amount is very low at low bulk concentrations. At a certain concentration, the adsorbed amount increases rapidly to, depending on the surfactant architecture, approximately 2 mg/m^2. That concentration where the surface excess increases rapidly is called the $CSAC$, and typically the adsorbed amount reaches a plateau value at concentrations above the $CSAC$. The adsorbed amount at this plateau (in moles/m2) is mainly a function of the head group size and depends not so much on the tail group size. To study the response of the surfactant system to salt and pH changes, we prepared solutions of $C_{12}E_5$ where we added $NaCl$ to change the ionic strength, and the controlled the pH by adding HCl or $NaOH$. For systems without added salt, the adsorbed amount is at a plateau value in the pH range from 2 to 10. If the pH is increased even more, the adsorbed amount decreases rapidly to zero at the adsorption/desorption transition. By adding salt to this system, we see that at low pH, the adsorbed amount is not a function of the ionic strength. However, the ionic strength does influence the adsorption/desorption transition. This transition shifts from p$H \approx 11$ in the case of no added salt, to p$H \approx 9$ in the 1 mmol/L $NaCl$, to p$H \approx 7$ for the case of 10 mmol/L $NaCl$. Also, the kinetics of adsorption decrease as the system gets closer to its adsorption/desorption transition.

The next step was to use reflectometry to look at the competitive adsorption from mixtures containing PEO and C_nE_m. There are several methods to test this competitive adsorption. In the case of simultaneous adsorption, the polymer and surfactant are allowed to adsorb from a mixture. It is also possible to study adsorption sequentially, i.e. first adsorb component A, and subsequential try to displace component A with component B. We decided to start by doing sequential adsorption experiments, because these are easier to control. In such an experiment, the PEO is allowed to adsorb onto the surface from a solution with 5 mg PEO/L. Care was taken to insure that the layer was in its steady state. Next, the flow of PEO solution was replaced by the background solution, and subsequently by a solution containing only surfactants. The concentration of the surfactant solution was 1×10^{-4} mol/L for all surfactants except for $C_{12}E_3$, where solubility problems demanded the use of a lower concentration $c = 6 \times 10^{-5}$. Still, all surfactant solutions had a concentration higher than the CMC. The results of these experiments can basically be grouped in two categories. Upon changing to the surfactant

	Polymer molar mass (g/mol)						
	4250	12600	20360	28640	43520	82250	167700
$C_{12}E_3$	✓	✗	✗	✗	✗	✗	✗
$C_{12}E_5$	✓	✓	✓	✓	✓	✗	✗
$C_{12}E_6$	✓	✗	✗	✗	✗	✗	✗
$C_{12}E_7$	✓	✗	✗	✗	✗	✗	✗
$C_{14}E_7$	✓	✓	?	✗	✗	✗	✗
$C_{16}E_7$	✓	✓	✓	✓	✓	?	✗

Table 8.1: *Systematic overview indicating the displacement capabilities per surfactant. A ✓ indicates that the surfactant can displace the polymer, and a ✗ indicates that the polymer can displace the surfactant. The two cases, where we could not determine what species preferentially adsorbed, are denoted with "?".*

solution, the adsorbed amount would either increase sharply (Figure 3.5a), or the adsorbed amount would remain constant (Figure 3.5b). In the first case where the adsorbed amount would increase until the amount that the surfactant would also reach from a single component solution. Furthermore, subsequent rinsing of this layer would result in a total dissolution of the layer, and hence, the adsorbed amount would go to zero. Since this is typical surfactant behaviour, we can conclude that the surfactant displaces the polymer as it adsorbs.

A schematic overview of the PEO displacement capability per C_nE_m surfactant is shown in Table 8.1. We present the length of the preadsorbed PEO on the horizontal axis versus the type of C_nE_m surfactant on the vertical axis. The cases where it is possible to displace the PEO layer with a surfactant layer are denoted with a ✓, and the opposite case where the surfactant cannot displace the polymer are marked with a ✗. In two cases, we found that when we would switch to the surfactants solution, the adsorbed amount would go up, but it would not reached the expected adsorbed amount. And, if we would subsequently switch back to the solvent, the adsorbed amount would not go to zero. Hence, these two cases seem to be intermediate. The surfactant is able to displace part of the polymer, but also, some of the polymer resides at the surface despite the competition with the surfactant. For these two polymer/surfactant combinations, we performed another displacement experiment where we increased the surfactant concentration with a factor 30, to $c = 3 \times 10^{-3}$mol/L. In both cases we observed that, at this concentration, the surfactant would entirely displace the polymer.

Table 8.1 shows that all surfactants can displace short polymer, but none of the surfactants can displace the long polymer. It is possible to find a maximum polymer length for every surfactant that it can just displace. This

length is called the critical length, N^c. The rate of displacement is evaluated by looking at the initial rate of increment of the surface excess and correcting this for the desorbing polymer. It turns out that surfactants can displace short polymer rather efficient, but as the polymer length increases, the displacement rate decreases until it hits zero at N^c. So, similar to the case of surfactants and salt, the rate of surfactant adsorption decreases as it comes closer to its adsorption/desorption transition.

In chapter 3 we argue that it is possible to understand the existence of N^c and the reduction in displacement kinetics, by allowing the $CSAC$ vary as a function of the competing polymer. However, measuring the $CSAC$ accurately is not easy and therefore, it is very difficult to measure the shift in the $CSAC$ experimentally.

To better understand the experimental observations, we have developed an SCF model. This model describes the system in a detailed manner. We describe the PEO and the C_nE_m using united carbon groups C and oxygen groups O. Hence, EO_N can be modelled as $(C-C-O)_N$ and C_nE_m as $(C)_n - O - (C-C-O)_m$. The solvent in the model is water, which is described as a small cluster. Compared to a monomeric water, such a compact object has less translational freedom, which is a first order attempt to include the associative behaviour of water. It is known that the solubility of EO groups depends on the ionic strength. To control this, we have defined a 1:1 electrolyte, and we have named the ions Na^+ and Cl^-. For all these segments, it is necessary to define the χ-parameters, that represent the nearest neighbour interactions. For this summary, I have chosen not to mention these parameters, but to refer to chapter 4.3 for their values. Using the species mentioned above, we have performed calculations on the bulk behaviour of our system. The results of these calculates can be used to evaluate the properties of PEO or C_nE_m, such as those conditions where the PEO starts to phase separate, or that concentration where the surfactant starts forming micelles (CMC) and the corresponding micellar size.

To evaluate the adsorption behaviour of the PEO/C_nE_m, it is necessary to define a surface. All our adsorption experiments are performed on a silica surface. Therefore, we have chosen to model a silica-like surface, and, to some extent, to include molecular detail. Inorganic oxides, such as silica, have a charge that depends on the pH. To include this in the model, the pH must be explicitly taken into account. We have chosen to define three internal states for the water: i) OH^-, ii) H_2O, and iii) H_3O^+. The concentrations of these states is controlled by the water equilibrium, and the pK of this reaction is set at 14. The surface consists of two types of segments, that model siloxane and silanol groups. However, in principle they can also be used to model other types of surfaces. The silanol groups are allowed to change their state,

i.e. a silanol group can dissociate into a dissociated silanol group and a proton. Hence, the amount of dissociated silanol groups is related to the number of protons in solution (the pH). The pK for this reaction is set at 6. Because the dissociated silanol groups carry a single negative charge and we have defined a separate set of χ-parameters for dissociated and undissociated silanol groups, the surface changes as a function of the pH.

It is possible to calculate the charge on the silica surface as a function of the pH and the ionic strength. This yields titration curves that can be compared with experimental titration curves. Our calculated results correspond quite well with literature data. One can also use the model to make predictions about the adsorption of PEO on our silica surface. It is possible to go to concentrations much lower than those that are experimentally accessible. We have made predictions about the response of the adsorbed polymer layer upon changes in ionic strength and pH. The results show that PEO adsorption is relatively insensitive for the ionic strength at p$H \approx 7$, but at p$H \approx 10$, the ions can displace the polymer quite well. This type of behaviour is also found experimentally. Every time that we perform a calculation (and we do find a solution), we obtain the mean field free energy and the most likely conformation of the system. By looking at the profiles of the most likely conformation, i.e. plotting the volume fraction of a species versus the distance from the surface, we can see that the adsorbed polymer inhibits the adsorption of salt. Hence, the polymer and the salt are in competition for adsorption.

The behaviour of C_nE_m surfactants can also be evaluated. Here we use exactly the same parameters that we used for the PEO. Again, we started by evaluating the surfactant bulk behaviour. Instead of investigating the first occurrence of a micelle, we have defined a more experimentally relevant CMC. We have evaluated that concentration where $\mathcal{E} = 10kT$, e.g. that concentration where the volume fraction of micelles is approximately equal to the volume fraction of unimers. Based upon this criterium we have calculated the CMC and the corresponding micellar size for a number of surfactant architectures and for a number of ionic strengths. We have also evaluated surfactant adsorption isotherms. These calculated adsorption isotherms feature a first order transition at the $CSAC$. By evaluating the behaviour of the $CSAC$, we have found that the $CSAC$ shifts to a higher concentration when the pH or the ionic strength is increased. We identified conditions for which the $CSAC > CMC$, which effectively implies that the surfactant does not adsorb anymore (Eqn. 3.7). We compared these predicted results to data measured using a reflectometer, and we find that the model predicts the experimental results quite well.

The next step is to use the model to try and reproduce the displacement

results. We have defined systems that include both PEO and C_nE_m, at some pH and ionic strength. To determine which component adsorbs from a mixture, we evaluate the response of the C_nE_m to the competing polymer. The surfactant starts adsorbing at some concentration ($CSAC$). If the surfactant concentration is lower than the $CSAC$, then the PEO will adsorb (we assume that the pH and ionic strength are such that the PEO is capable of adsorbing). For surfactant concentrations higher than the $CSAC$ but lower than the CMC, the surfactant will preferentially adsorb. In the case of $CSAC > CMC$, the surfactant will not adsorb. Typically, the polymer will adsorb in this case, however, one can think of situations (high pH and high ionic strength) where the polymer will also stay in solution.

Using the method described above, we can model the competitive adsorption of PEO and C_nE_m. We can evaluate the response of the surfactant to competing species, such as PEO of length N. By identifying for every surfactant architecture that polymer length N where $CSAC = CMC$, we can make a predicted equivalent of Table 8.1. It turns out that, although we do predict an adsorption/desorption transition upon changing the polymer length, the location of the transition does not strictly follow the experimental findings. We attribute this discrepancy to the neglect of layer fragmentation. A useful follow-up study would be to perform 2G calculations, where lateral inhomogeneities are allowed.

Although this is (almost) the end of this thesis, the story about the competition between polymers and surfactants is not finished yet. Even our simple system still holds unrevealed behaviour. Experimentally, one can evaluate the displacement capabilities of mixtures of (nonionic) surfactants, or investigate other parameters such as the temperature. The SCF model is capable of predicting many properties of the system. However, the important property of layer fragmentation is neglected. Including this in the model will probably result in more accurate predictions.

Samenvatting

Dit proefschrift beschrijft een systematisch onderzoek naar de competitieve adsorptie van ongeladen surfactanten en ongeladen polymeren op een geladen hydrofiel oppervlak. Vanuit een academisch standpunt is dit onderwerp interessant omdat we eenvoudigweg het gedrag van dergelijke systemen in de regel (nog) niet kunnen voorspellen. Vanuit een meer technologisch oogpunt is dit onderwerp ook zeer belangrijk, omdat een meer gedegen kennis van dergelijke systemen kan leiden tot betere producten.
We hebben ervoor gekozen om dit onderzoek te beperken tot een goed gedefinieerd waterig systeem. Dit systeem bevat het oplosmiddel water, een silica-oppervlak, het polymeer PEO en de surfactant C_nE_m. Het ongeladen polymeer PEO kan dusdanig gemaakt worden dat alle moleculen nagenoeg even lang zijn. Dit is belangrijk omdat in het hier beschreven onderzoek de polymeerlengte een essentiële parameter is. De lengte van de hier gebruikte polymeren varieert van circa 100 tot 4000 EO eenheden. De ongeladen surfactant C_nE_m bestaat uit een hydrofiele voorkant en een hydrofobe achterkant. Het hydrofiele stuk (ook wel de kop genoemd) is identiek aan PEO maar wel veel korter (typisch 3 tot 9 EO eenheden). De hydrofobe achterkant (meestal staart genoemd) is typisch 10 tot 18 koolstofsegmenten lang. In de formule C_nE_m geeft n de lengte van de staart aan, en m de lengte van de kop (zie ook Figuur 1.1). Surfactanten zijn dus korter dan polymeren. Verder, hebben ze een aantal speciale eigenschappen. Als de concentratie hoog genoeg is, vormen ze aggregaten van circa 100 moleculen. Deze aggregaten worden micellen genoemd en de concentratie waar de vorming van micellen begint, heet 'critical micelle concentration' of CMC. Binnenin een micel zitten de hydrofobe staarten en de buitenkant bestaat uit hydrofiele koppen. Op deze manier worden de staarten afgeschermd van het water door de koppen.
Zowel PEO als C_nE_m adsorbeert vanuit een waterige oplossing op een silica-oppervlak. Als een PEO-molecuul dicht bij een silica-oppervlak komt, kan er

een fysische verbinding gevormd worden welke ervoor zorgt dat het molecuul dicht bij het oppervlak blijft. Hierdoor is de polymeerconcentratie bij het oppervlak hoger dan in de oplossing. Deze aantrekkende kracht tussen een zuurstofatoom van het PEO en een silanol oppervlaktegroep wordt ook wel waterstofbrug genoemd (H-brug). Omdat een polymeer een lang molecuul is, worden direct aan het oppervlak gebonden stukken afgewisseld met stukken die niet direct aan het oppervlak gebonden zijn. Stukken welke direct gebonden zijn aan het oppervlak worden 'treinen' genoemd. Een 'lus' is een stuk polymeer dat niet gebonden is aan het oppervlak maar wel aan beide kanten begrenst wordt door een trein, en losse uiteinden worden staarten[a] genoemd. De voorkant van dit proefschrift en Figuur 1.2 illustreren deze indeling.
De surfactant C_nE_m kan ook adsorberen aan een silica-oppervlak. Omdat silica hydrofiel is, zal de surfactant adsorberen met zijn kopgroep. Aangezien de kopgroep van C_nE_m identiek is aan het PEO, is het bindingsmechanisme tussen het surfactant en het oppervlak gelijk aan dat van het polymeer met het oppervlak. De surfactant zal dus adsorberen met zijn kop richting het silica. Dit betekent automatisch dat de hydrofobe staarten richting de (waterige) oplossing wijzen. Omdat staarten niet graag omgeven willen zijn door een waterig medium, adsorbeert er een tweede surfactantlaag. Op een hydrofiel oppervlak adsorberen surfactanten dus in twee lagen, oftewel een bilaag. Dit wordt geïllustreerd op de achterkant van dit proefschrift en in de Figuren 1.4 en 6.5.
Zoals hierboven al genoemd, gaat dit proefschrift over de competitieve adsorptie van PEO en C_nE_m op silica. Om dit te onderzoeken is het belangrijk om eerst te kijken naar hoe een dergelijk mengsel zich in oplossing gedraagt. In hoofdstuk 3.2 hebben we aangetoond dat PEO en C_nE_m geen gemengde aggregaten vormen binnen het voor ons relevante concentratiegebied. Vervolgens zijn we met een reflectometer (zie hoofdstuk 2) gaan kijken naar de laag die gevormd wordt op een silica-oppervlak indien PEO en C_nE_m beide kunnen adsorberen. Het blijkt dat er bijna altijd één soort aan te wijzen is die zal adsorberen, en de andere soort dus verhindert om te adsorberen. Welke soort de adsorberende soort is, hangt subtiel af van de lengte van het polymeer en van de grootte van de kop- en staartgroep van de surfactant. Tabel 3.4 geeft een overzicht van deze experimenten. Bij iedere surfactant is een kritische polymeerlengte te vinden. De surfactant kan alle polymeren korter dan de kritische polymeerlengte verdringen en kan geen enkel polymeer langer dan de kritische lengte verdringen. Bij het vergelijken van de verschillende surfactanten lijkt het erop dat de relatieve grootte van de kop-

[a] In tegenstelling tot de staart van een surfactant molecuul, is bij deze indeling de staart chemisch niet anders dan de rest van het polymeer.

en staartgroep belangrijk is. Verder hebben we ook gekeken naar de adsorptiesnelheid van de surfactanten in aanwezigheid van het polymeer. Het blijkt dat het polymeer de surfactantadsorptiesnelheid verlaagd. Hoe langer het polymeer is, hoe meer de adsorptiesnelheid wordt verlaagd totdat het polymeer de kritische lengte bereikt en de surfactant niet meer adsorbeert.
Om de verdringingsexperimenten beter te begrijpen hebben we het systeem gemodelleerd met een zelf-consistent veld model. Dit betekent dat we het systeem gedetailleerd hebben beschreven en vervolgens met behulp van een computer de meest waarschijnlijke toestand uitgerekend hebben (zie hoofdstuk 4). Op deze manier hebben we steeds het effect van bijvoorbeeld de ketenlengte, het type surfactant, de zoutconcentratie, de pH, enzovoort kunnen bepalen.
In hoofdstuk 5 hebben we het model toegepast op het geval van polymeeradsorptie. We hebben gekeken naar het effect van de ketenlengte, zoutconcentratie en pH op het gedrag van PEO in oplossing en op een oppervlak. Het blijkt dat het in ons model mogelijk is om de adsorptie van PEO te verhinderen door de juiste pH en zoutconcentratie te kiezen. Om het model te valideren, hebben we de voorspellingen vergeleken met een set experimentele reflectometrieresultaten. Het blijkt dat ons model het geval van PEO-adsorptie heel redelijk beschrijft.
De volgende stap was om het model toe te passen op surfactantadsorptie. In hoofdstuk 6 kijken we naar de invloed van kop- en staartlengte en, net als in het geval van de polymeren, naar het effect van zout en pH. Surfactanten beginnen pas met adsorberen bij een bepaalde concentratie. Deze concentratie wordt de 'critical surface aggregation concentration' of $CSAC$ genoemd. Als de $CSAC$ en de CMC bekend zijn voor een gegeven surfactant is het mogelijk om uit te rekenen hoeveel "energie" een systeem wint door de surfactant te laten adsorberen. Als de $CSAC < CMC$ dan is het energetisch gunstig om de surfactant te laten adsorberen. Echter, het is energetisch juist ongunstig als $CSAC > CMC$. In hoofdstuk 6 hebben we voor een reeks surfactanten de $CSAC$ en de CMC uitgerekend. Hiermee hebben we voorspellingen gedaan over het adsorptiegedrag van deze surfactanten. De voorspellingen zijn wederom vergeleken met experimentele resultaten. Het blijkt dat de experimentele trends goed overeenkomen met onze voorspellingen. Verder is het ook mogelijk om de adsorptiesnelheid van een surfactant uit te rekenen als de $CSAC$ en de CMC bekend zijn. Het blijkt dat onze kinetische voorspellingen ook goed overeenkomen met de experimenteel gevonden kinetiek.
Toen we ervan overtuigd waren dat we het gedrag van oplossingen met PEO of C_nE_m goed konden modelleren, wilden we de stap naar gemengde oplossingen maken. We hebben gekeken naar het adsorptiegedrag van de surfactanten als functie van de concentratie en de lengte van PEO waarmee de

surfactant concurreert voor oppervlaktebezetting. Het blijkt dat het polymeer ervoor zorgt dat het surfactant minder makkelijk kan adsorberen. Dit komt doordat het surfactant er eerst voor moet zorgen dat het polymeer niet meer adsorbeert. Deze adsorptiehindernis zorgt ervoor dat het surfactant pas begint met adsorberen bij hogere concentraties vergeleken met het geval van alleen surfactant in oplossing. Het is dus zo dat de $CSAC$ schuift naar hogere concentraties. We kunnen de $CSAC$ weer met de CMC vergelijken en voorspellingen doen over de kritische polymeerlengte en de snelheid van adsorptie van de surfactanten. Als we deze voorspellingen vergelijken met de experimentele resultaten uit hoofdstuk 3 zien we dat zowel de evenwichtstrends als de kinetische trends redelijk overeenkomen. Echter in absolute zin wijken de voorspellingen wel af van de gemeten resultaten. In hoofdstuk 8.4 bespreek ik dit kort en stel ik mogelijke verbeterpunten van het model voor.

References

[1] B. Jönsson, B. Lindman, K. Holmberg, and B. Kronberg. *Surfactants and polymers in aqueous solution*. John wiley & sons, Chichester, 1998.

[2] S. M. Moghimi and A. C. Hunter. Poloxamers and poloxamines in nanoparticle engineering and experimental medicine. *Trends in Biotechnology*, 18:412 – 420, 2000.

[3] B. S. Murray. Stabilization of bubbles and foams. *Curr. Opin. Colloid Interface Sci.*, 12:232 – 241, 2007.

[4] S. Damodaran. Protein stabilization of emulsions and foams. *J. food Sci.*, 70:R54 – R66, 2005.

[5] R. Lambourne and T. A. Strivens. *Paint and surface coatings - theory and practice*. Woodhead Publishing, Norwich, 1999.

[6] M. M. Rieger and L. D. Rhein. *Surfactants in cosmetics*. Marcel Dekker, New York, 1997.

[7] C. L. Foy and D. W. Pritchard. *Pesticide formulation and adjuvant technology*. CRC press, London, 1996.

[8] R. M. Ottenbrite and E. Chiellini. *Frontiers in biomedical polymer applications*. CRC press, London, 1997.

[9] D. J. F. Taylor, R. K. Thomas, and J. Penfold. Polymer/surfactant interactions at the air/water interface. *Adv. Colloid Interface Sci.*, 132:69–110, 2007.

[10] J. Penfold, R. K. Thomas, and D. J. F. Taylor. Polyelectrolyte/surfactant mixtures at the air-solution interface. *Curr. Opin. Colloid Interface Sci.*, 11:337 – 344, 2006.

[11] R. Zhang and P. Somasundaran. Advances in adsorption of surfactants and their mixtures at solid/solution interfaces. *Adv. Colloid Interface Sci.*, 121 - 123:213 – 229, 2006.

[12] S. K. Parida, S. Dash, S. Patel, and B. K. Mishra. Adsorption of organic molecules on silica surface. *Curr. Opin. Colloid Interface Sci.*, 121:77 – 110, 2006.

[13] C. La Mesa. Polymer-surfactant and protein-surfactant interactions. *J. Colloid Interface Sci.*, 286:148–157, 2005.

[14] R. Miller, V. B. Fainerman, M. E. Leser, and M. Michel. Kinetics of adsorption of proteins and surfactants. *Curr. Opin. Colloid Interface Sci.*, 9:350 – 356, 2004.

[15] E. Papirer. *Adsorption on silica surfaces*. CRC press, London, 2000.

[16] J. C. Dijt, M. A. Cohen Stuart, and G. J. Fleer. Reflectometry as a tool for adsorption studies. *Adv. Colloid Interface Sci.*, 50:79–101, 1994.

[17] G. J. Fleer, M. A. Cohen Stuart, J. M. H. M. Scheutjens, T. Cosgrove, and B. Vincent. *Polymers at interfaces*. Chapman & Hall, London, 1993.

[18] N. A. Plate and I. M. Papisov. Nomenclature of regular single-strand organic polymers. *Pure Appl. Chem.*, 61:243 – 254, 1989.

[19] F. E. Bailey and J. V. Koleske. *Alkylene oxides and their polymers*. CRC press, London, 1991.

[20] P. G. de Gennes. Polymers at an interface: a simplified view. *Adv. Colloid Interface Sci.*, 27:189 – 209, 1987.

[21] P. G. de Gennes. *Scaling concepts in polymer physics*. Cornell university press, Ithaca and London, 1979.

[22] J. R. Lu, R. K. Thomas, and J. Penfold. Surfactant layers at the air/water interface: structure and composition. *Adv. Colloid Interface Sci.*, 84:143–304, 2000.

[23] S. Paria and K. C. Khilar. A review on experimental studies of surfactant adsorption at the hydrophilic solid-water interface. *Adv. Colloid Interface Sci.*, 110:75–95, 2004.

[24] J. W. McBain. Colloids and their viscosity (discussion). *Trans. Faraday Soc.*, 9:99 – 101, 1913.

[25] D. Daninoa, Y. Talmona, and R. Zanab. Aggregation and microstructure in aqueous solutions of the nonionic surfactant $c_{12}e_8$. *J. Coll. Interface Sci.*, 186:170 – 179, 1997.

[26] J. N. Israelachvili, D. J. Mitchell, and B. W. Ninham. Theory of self-assembly of hydrocarbon amphiphiles into micelles and bilayers. *J. Chem. Soc. Faraday Trans II*, 72:1525–1568, 1976.

[27] J. N. Israelachvili. *Intermolecular & surface forces*. Academic Press, New York, 1991.

[28] J. Lyklema, editor. *Fundamentals of interface and colloid science, Volume V: Soft colloids*. Elsevier Academic press, Amsterdam, 2004.

[29] S. Partyka, S. Zaini, M. Lindheimer, and B. Brun. The adsorption of non-ionic surfactants on a silica gel. *Colloids and Surfaces*, 12:255 – 270, 1984.

[30] S. Partyka, M. Lindheimer, and B. Faucompre. Aggregate formation at the solid-liquid interface: the calorimetric evidence. *Coll. Surf. A*, 76:267 – 281, 1993.

[31] D. M. Nevskaia, A. Guerrero-Ruíz, and J. de D. López-Gonzólez. Adsorption of polyoxyethylenic nonionic and ionic surfactants from aqueous solution: Effects induced by the addition of nacl and $cacl_2$. *J. Colloid Interface Sci.*, 205:97 – 105, 1998.

[32] F. Tiberg, B. Jönsson, J. Tang, and B. Lindman. Ellipsometry studies of the self-assembly of nonionic surfactants at the silica-water interface: Equilibrium aspects. *Langmuir*, 10:2294–2300, 1994.

[33] E. M. Lee, R. K. Thomas, P. G. Cummins, E. J. Staples, J. Penfold, and A. R. Rennie. Determination of the structure of a surfactant layer adsorbed at the siica/water interface by neutron reflection. *Chem. Phys. Letters*, 162:196–202, 1989.

[34] M. Böhmer, L. K. Koopal, R. Jannsen, E. M. Lee, R. K. Thomas, and A. R. Rennie. Adsorption of nonionic surfactants on hydrophillic surfaces. an experimental and theoretical study on association in the adsorbed layer. *Langmuir*, 8:2228–2239, 1992.

[35] A. D. Braem, D. C. Prieve, and R. D. Tilton. Electrostatically tunable coadsorption of sodium dodecyl sulfate and poly(ethylene oxide)-b-poly(propylene oxide)-b-poly(ethylene oxide) triblock copolymer to silica. *Langmuir*, 17:883–890, 2001.

[36] J. Ghodbane and R. Denoyel. Competative adsorption between nonionic polymers and surfactants on silica. *Colloids Surf. A Physicochem. Eng. Aspects*, 127:97–104, 1997.

[37] E. S. Pagac, D. C. Prieve, and R. D. Tilton. Kinetics and mechanism of cationic surfactant adsorption and coadsorption with cationic polyelectrolytes at the silica-water interface. *Langmuir*, 14:2333–2342, 1998.

[38] S. B. Velegol and R. D. Tilton. A connection between interfacial self-assembly and the inhibition of hexadecyltrimethylammonium bromide adsorption on silica by poly-L-pysine. *Langmuir*, 17:219–227, 2001.

[39] H. Hommel and H. van Damme. Displacement of poly(ethylene oxide) adsorbed on silica by a nonionic surfactant studied by spin labeling. *J. Surfactants Deterg.*, 5:375 – 380, 2002.

[40] R. M. A. Azzam and N. M. Bashara. *Ellipsometry and polarized light*. Elsevier, Amsterdam, 1996.

[41] J. A. de Feijter, J. Benjamins, and F. A. Veer. Ellipsometry as a tool to study the adsorption behaviour of synthetic and biopolymers at the air-water interface. *Biopolymers*, 17:1759 – 1772, 1978.

[42] T. Dabros and T. G. M. van de Ven. A direct method for studying particle deposition onto solid surfaces. *Colloid & Polymer Sci.*, 261:694 – 707, 1983.

[43] M. Elimelech, J. Gregory, X. Jia, and R. A. Williams. *Particle deposition & aggregation - Measurement, modelling and simulation*. Butterworth-Heinemann, Woburn, 1995.

[44] T. G. M. van de Ven. *Colloidal hydrodynamics*. Academic Press, New York, 1989.

[45] N. M. van Os, J. R. Haak, and L. A. M. Rupert. *Physico-chemical properties of selected anionic, cationic and nonionic surfactants*. Elsevier, Amsterdam, 1993.

[46] Y. C. Chiu and L. J. Chen. Refractive index of nonionic surfactant solutions sontaining polyoxyethylene mono-n-alkylether. *Coll. Surf.*, 41:239–244, 1989.

[47] R. K. Iler. *The chemistry of silica*. John Wiley & sons, New York, 1979.

[48] J. C. Dijt, M. A. Cohen Stuart, J. E. Hofman, and G. J. Fleer. Kinetics of polymer adsorption in stagnation point flow. *Colloids Surf.*, 51:141–158, 1990.

[49] Z. Fu and M. M. Santore. Effect of layer age and interfacial relaxations on the self-exchange kinetics of poly(ethylene oxide) adsorbed on silica. *Macromolecules*, 32(6):1939 – 1948, 1999.

[50] J. C. Dijt, M. A. Cohen Stuart, and G. J. Fleer. Kinetics of polymer adsorption and desorption in capillary flow. *Macromolecules*, 25:5416–5423, 1992.

[51] F. Tiberg, B. Jönsson, and B. Lindman. Ellipsometry studies of the self-assembly of nonionic surfactants at the silica-water interface: kinetic aspects. *Langmuir*, 10:3714–3722, 1994.

[52] J. Brinck and F. Tiberg. Adsorption behaviour of two binary nonionic surfactant systems at the silica-water interface. *Langmuir*, 12:5042 – 5047, 1996.

[53] L. M. Grant, F. Tiberg, and W. A. Ducker. Nanometer-scale organization of ethylene oxide surfactants on graphite, hydrophillic silica, and hydrophobic silica. *J. Phys. Chem. B*, 102:4288–4294, 1998.

[54] J. C. Dijt, M. A. Cohen Stuart, and G. J. Fleer. Competitive adsorption kinetics of polymers differing in length only. *Macromolecules*, 27:3219–3228, 1994.

[55] Z. Fu and M. M. Santore. Kinetics of competative adsorption of *peo* chains with different molecular weights. *Macromolecules*, 31:7014 – 7022, 1998.

[56] J. Lyklema. *Fundamentals of interface and colloid science, Volume II: Solid-Liquid interfaces*. Amsterdam Academic press, Amsterdam, 1995.

[57] J. Iruthayaraj, E. Poptoshev, A. Vareikis, R. Makuka, A. van der Wal, and P. M. Claesson. Adsorption of low charge density polyelectrolyte containing poly(ethylene oxide) side chains on silica: effects of ionic strength and ph. *Macromolecules*, 28:6152–6160, 2005.

[58] O. Eliseeva. *Wetting films stabilized by block-copolymers*. PhD thesis, Wageningen University, 2006.

[59] C. Flood, T. Cosgrove, I. Howell, and P. Revel. Effects of electrolytes on adsorbed polymer layers: poly(ethylene oxide) - silica system. *Langmuir*, 22:6923 – 6930, 2006.

[60] G. H. Bolt. Determination of the charge density of silica sols. *J. Phys. Chem.*, 31:1166 – 1169, 1957.

[61] G. P. van der Beek, M. A. Cohen Stuart, and T Cosgrove. Polymer adsorption and desorption studies via proton nmr relaxation of the solvent. *Langmuir*, 7:327 – 334, 1991.

[62] S. Mathur and B. M. Moudgil. Adsorption mechanism(s) of poly(ethylene oxide) on oxide surfaces. *J. Coll. Interface Sci.*, 196:92 – 98, 1997.

[63] J. Rubio and J. A. Kitchener. The mechanism of adsorption of poly(ethylene oxide) flocculant on silica. *J. Coll. Interface Sci.*, 57:132 – 142, 1976.

[64] E. Florin, R. Kjellander, and J. C. Eriksson. Salt effects on the cloud point of the poly (ethylene oxide) + water-system. *Journal of the chemical society - Faraday transactions I*, 80:2889 – 2910, 1980.

[65] M. Ataman. Properties of aqueous salt solutions of poly (ethylene oxide): Cloud points, θ-temperatures. *Colloid & polymer science*, 265:19 – 25, 1987.

[66] M. Malmsten, F. Tiberg, B. Lindman, and K. Holmberg. Effects of solvency on the interfacial behaviour in aqueous non-ionic polymer systems. *Coll. Surf. A: Physicochemical and Engineering Aspects*, 77:91 – 100, 1993.

[67] O. A. Evers, J. M. H. M. Scheutjens, and G. J. Fleer. Statistical thermodynamics of block copolymer adsorption. 1. formulation of the model and results for the adsorbed layer structure. *Macromolecules*, 23:5221–5233, 1990.

[68] J. M. H. M. Scheutjens and G. J. Fleer. Statistical theory of the adsorption of interacting chain molecules. 1. partition functions, segment density distribution, and adsorption isotherms. *J. Phys. Chem.*, 83:1619–1635, 1979.

[69] J. M. H. M. Scheutjens and G. J. Fleer. Statistical theory of the adsorption of interacting chain molecules. 2. train, loop, and tail size distribution. *J. Phys. Chem.*, 84:178–190, 1980.

[70] A. B. Jódar-Reyes, J. L. Ortega-Vinuesa, A. Martin-Rodriguez, and F. A. M. Leermakers. Self-consistent field model of inhomogeneous adsorption of nonionic surfactants onto polystyrene latex. *Langmuir*, 19:878–887, 2003.

[71] N. V. Sastry, A. George, N. J. Jain, and P. Bahadur. Densities, relative permittivities, excess volumes, and excess molar polarizations for alkyl ester (methyl propanoate, methyl butanoate, ethyl propanoate, and ethyl butanoate) + hydrocarbons (n-heptane, benzene, chlorobenzene, and 1,1,2,2-tetrachloroethane) at 308.15 k and 318.15 k. *Chem. Eng. Data*, 44:456 – 464, 1999.

[72] T. L. Hill, editor. *Thermodynamics of small systems*. Dover publications inc., New York, 1991.

[73] D. G. Hall and B. A. Pethica. *Thermodynamics of micelle formation*, chapter 15, pages 516 – 557. Surfactant science series. Marcel Dekker, New York, 1967.

[74] J. van Male. *Self-consistent-field theory for chain molecules: extensions, computational aspects, and applications*. PhD thesis, Wageningen University, 2003.

[75] P. Flory. *Principles of polymer chemistry*. Cornell university press, Ithaca, 1971.

[76] M. Schick. *Les Houches 1998 - Session XLVIII*, chapter 9 - Introduction to wetting phenomena, pages 419 – 497. North-Holland, Amsterdam, 1998.

[77] G. P. van der Beek and M. A. Cohen Stuart. The hydrodynamic thickness of adsorbed polymer layers measured by dynamic light-scattering – effects of polymer concentration and segmental binding strength. *J. physique*, 49:1449 – 1454, 1988.

[78] O. V. Eliseeva, N. A. M. Besseling, L. K. Koopal, and M.A. Cohen Stuart. Influence of *nacl* on the behaviour of $peo - ppo - peo$ triblock copolymers in solution, at interfaces, and in asymmetric liquid films. *Langmuir*, 21:4954 – 4963, 2005.

[79] B. R. Postmus, F. A. M. Leermakers, L. K. Koopal, and M. A. Cohen Stuart. Competitive adsorption of nonionic surfactant and nonionic polymer on silica. *Langmuir*, 23:5532–5540, 2007.

[80] C. Tanford. *The hydrophobic effect*. John wiley & sons, New York, 1973.

[81] N. Kumar, S. Garoff, and R. D. Tilton. Experimental observations on the scaling of adsorption isotherms fo nonionic surfactants at a hydrophobic solid-water interface. *Langmuir*, 20:4446–4451, 2004.

[82] F. Tiberg. Physical characterization of non-ionic surfactant layers adsorbed at hydrophilic and hydrophobic solid surfaces by time-resolved ellipsometry. *J. Chem. Soc., Faraday Trans.*, 92(4):531–538, 1996.

[83] B. R. Postmus, F. A. M. Leermakers, and M. A. Cohen Stuart. Self-consistent field modeling of poly(ethylene oxide) adsorption onto silica: The multiple roles of electrolytes. *Langmuir*, 24:1930 – 1942, 2008.

[84] B. R. Postmus, F. A. M. Leermakers, and M. A. Cohen Stuart. Self-consistent field modeling of nonionic surfactants at the silica-water interface: Incorporating molecular detail. *Langmuir*, in press, 2008.

[85] L. Grant, T. Ederth, and F. Tiberg. Influence of surface hydrophobicity on the layer properties of adsorbed nonionic surfactants. *Langmuir*, 16:2285 – 2291, 2000.

[86] D. P. Bakker. *Bacterial adhesion to modified polyurethanes*. PhD thesis, Rijksuniversiteit Groningen, 2004.

[87] H. M. Lappin-Scott and J. W. osterton. *Microbial Biofilms*. Cambridge University Press, Cambridge, 1995.

[88] M. Bos, T. Nylander, T. Arnebrant, and D. C. Clarck. *Food emulsifiers and their applications*. Chapmann & Hall, New York, 1997.

[89] E. Dickinson. Adsorbed protein layers at fluid interfaces: interactions, structure and surface rheology. *Coll. Surf. B*, 15:161 – 176, 1999.

[90] Z. Fu and Maria M. M. Santore. Competitive adsorption of poly(ethylene oxide) chains with and without charged end groups. *Macromolecules*, 14:4300 – 4307, 1998.

[91] C. Flood, T. Cosgrove, D. Qiu, Y. Espidel, I. Howell, and P. Revell. Influence of a surfactant and electrolytes on adsorbed polymer layers. *Langmuir*, 23:2408 – 2413, 2007.

[92] F. A. M. Leermakers and J. M. H. M. Scheutjens. Statistical thermodynamics of association colloids. 5. critical micelle concentration, micellar size and shape. *J. Colloid Interface Science*, 136:231 – 241, 1990.

[93] A. B. Jódar-Reyes, J. L. Ortega-Vinuesa, A. Martin-Rodriguez, and F. A. M. Leermakers. Modeling the effect of structual details of nonionic surfactants on micellization in solution and adsorption onto hydrophobic surfaces. *langmuir*, 18:8706 – 8713, 2002.

[94] J. H. Clint. *Surfactant aggregation*. Blacky & Son Ltd, London, 1992.

List of publications

→ Dewi P. Bakker, Bart R. Postmus, Henk J. Busscher, and Henny C. van der Mei. Bacterial strains isolated from different niches can exhibit different patterns of adhesion to substrata. *Appl. Environ. Microbiol.*, 70:3758-3760, 2004.

→ Bart R. Postmus, Frans A. M. Leermakers, Luuk K. Koopal, and Martien A. Cohen Stuart. Competitive adsorption of nonionic surfactant and nonionic polymer on silica. *Langmuir*, 23:5532-5540, 2007.

→ Bart R. Postmus, Frans A. M. Leermakers, and Martien A. Cohen Stuart. Self-consistent field modeling of poly(ethylene oxide) adsorption onto silica: The multiple roles of electrolytes. *Langmuir*, 24:1930-1942, 2008.

→ Bart R. Postmus, Frans A. M. Leermakers, and Martien A. Cohen Stuart. Self-consistent field modeling of non-ionic surfactants at the silica-water interface: incorporating molecular detail. *Langmuir*, 24:3960-3969, 2008.

→ Bart R. Postmus, Frans A. M. Leermakers, and Martien A. Cohen Stuart. Self-consistent field modeling of adsorption from polymer/ surfactant mixtures. *Langmuir*, in press.

→ Philip M. Karlsson, Bart R. Postmus, and Anders E. C. Palmqvist. Dissolution and protection of aluminium oxide in corrosive aqueous media an ellipsometry and reflectometry study. *J. Disp. Sci. Technol.*, in press.

Levensloop

Bart Postmus is op 9 september 1980 geboren in het mooie Groningse dorp Leek, maar bracht het grootste deel van zijn jeugd door in het mogelijk nog mooiere Drentse dorpje Peize. In 1998 haalde hij zijn VWO diploma aan het Nienoord college te Leek, om datzelfde jaar nog te beginnen aan een studie Technische natuurkunde aan de Rijksuniversiteit Groningen. Na drie jaar studeren heeft Bart de mogelijkheid gegrepen om zich te specialiseren in de biomedische technologie. Binnen deze specialisatie heeft hij stage gelopen bij Philips medical systems in Best, waar hij gekeken heeft naar mogelijkheid om atherosclerose (bloedvatvernauwingen) op te sporen met röntgenstraling. Verder heeft hij onderzoek gedaan bij de leerstoelgroep Biomedical engineering van de faculteit Geneeskunde van de Rijsuniversiteit Groningen, en bij de Environmental engineering group van de School of engineering & applied science van Yale university in New Haven (U.S.A.). In dit onderzoek heeft hij gekeken naar de adhesie van medisch relevante bacteriën onder verschillende massatransport condities. Na zijn afstuderen in 2003 is Bart afgezwaaid naar Accenture om te gaan werken als consultant binnen de nutsindustie, om na een half jaar weer terug te gaan naar de wetenschap en als promovendus bij de leerstoelgroep Fysische chemie en kolloïdkunde van Wageningen universiteit te beginnen. Dit proefschrift markeert het einde van Bart zijn promotietijd. Vanaf 1 juni is hij werkzaam als product development manager bij Unilever research and development te Vlaardingen.

Education programme

Discipline specific activities		
Interfacial chemistry course	Wageningen	2004
Caput college	Wageningen	2004 & 2005
DPI review meetings	Eindhoven	2004 - 2008
Winterschool	Han-sur-Lesse, Belgium	2005
RPK-B Polymer Physics	Utrecht	2005
Soft matter conference	Schiermonnikoog	2005
Liquid Matter Conference	Utrecht	2005
ECIS Student conference	Biezenmortel	2005
Annual Ecis conference	Budapest, Hungary	2006
ECIS Student conference	Ven, Sweden	2007
Annual ECIS conference	Geneva, Switserland	2007
Gordon Conference	France	2007
General courses		
English writing	Wageningen	2007
Personal assessment	Wageningen	2007
Optionals		
Preparation PhD proposal	Wageningen	2004
Work group meetings	Wageningen	2004 - 2008
Colloquiua	Wageningen	2004 - 2008
Excursion BASF	Ludwigshaven, Germany	2005
PhD trip	Sweden and Denmark	2007

This research forms part of the research programme of the Dutch Polymer Institute (DPI), technology area Coating Technology, DPI project #292.